THERMO ANALYSIS OF COMBINED CYCLE POWER PLANT

Thesis Submitted
in partial fulfilment of the requirements for the Degree of

DOCTOR OF PHILOSOPHY

in

Mechanical Engineering

by

ASHUTOSH MISHRA
(Roll No. 2K18/PHD/ME/506)

Under the Supervision of

PROF. B. B. ARORA
Delhi Technological University

PROF. AKHILESH ARORA
Delhi Technological University

To the
Department of Mechanical Engineering
DELHI TECHNOLOGICAL UNIVERSITY
Shahbad Daulatpur, Main Bawana Road, Delhi-110042. India

December, 2024

CERTIFICATE

Certified that **Ashutosh Mishra (**2K18/PHD/ME/506) has carried out their research work presented in this thesis entitled **"Thermo Analysis of Combined Cycle Power Plant"** for the award of **Doctor of Philosophy** from Delhi Technological University, New Delhi, under our supervision. The thesis embodies results of original work, and studies are carried out by the student himself and the contents of the thesis do not form the basis for the award of any other degree to the candidate or to anybody else from this or any other University/Institution.

Prof. B. B. Arora
Professor
Department of Mechanical Engg.
DTU, New Delhi

Prof. Akhilesh Arora
Professor
Department of Mechanical Engg.
DTU, New Delhi

Date:

CANDIDATE'S DECLARATION

I hereby declare that the thesis entitled "**Thermo Analysis of Combined Cycle Power Plant**" submitted by me, for the award of the degree of **Doctor of Philosophy** to the Delhi Technological University (Formerly Delhi College of Engineering) is a record of bona fide work carried out by me under the guidance of **Prof. B. B. Arora & Prof. Akhilesh Arora**.

I further declare that the work reported in this thesis has not been submitted and will not be submitted, either in part or in full, for the award of any other degree or diploma in this Institute or any other Institute or University.

Place: Delhi

Date:

ASHUTOSH MISHRA
Roll No. 2K18/PHD/ME/506
Department of Mechanical Engg.
Delhi Technological University,
Bawana Road, New Delhi

ACKNOWLEDGEMENT

First and foremost, I would like to express my deep and sincere gratitude to my supervisor, Prof. B. B. Arora, and my co-supervisor, Prof. Akhilesh Arora, for their valuable guidance and never-ending support. Their enthusiasm and passion have been constant sources of inspiration and encouragement.

I wish to record my thanks and gratitude to Prof. S. Maji, Prof. Vipin, and Prof. S. K. Valluru for their invaluable suggestions and constructive discussion during this research work.

Moreover, I would like to thank my friends and colleagues, Mr. Rashin Khera, Dr. Saket Kumar, Dr. Sunil Kumar Gupta, Mr. Siddharth Arora, Mr. Neeraj Kumar, and Mr. Sandeep Kumar for their support throughout my time at the University.

Last, I would like to thank my parents, wife, and brother for their understanding and encouragement throughout my education.

Ashutosh Mishra

ABSTRACT

Combined cycle power plants (CCPPs) are crucial in satisfying the increasing energy needs because of their superior efficiency and flexibility in comparison to single-cycle thermal power plants. However, achieving more improvements in thermal efficiency remains a key challenge. CCPPs are designed to run on specific operating conditions to fetch their maximum efficiency. Ambient temperature is one of those significant operating conditions. As the ambient air temperature rises, the performance of gas turbine power plants decreases. It is essential to mitigate the adverse effects of high ambient air temperature by cooling it before intake to the air compressor.

Therefore, this research addresses this challenge by integrating an inlet air cooler based on a double-effect vapour absorption refrigeration system (VARS). The VARS utilizes the waste heat of CCPP exhaust gas as the heat input to cool the air at the compressor's inlet. The improvements are seen in terms of energy, exergy, and sustainability aspects of an integrated CCPP as compared to the standalone CCPP. The energy analysis reveals the maximum improvements in work output and thermal efficiency of 5.04% and 1.64%, respectively. Furthermore, the results show that as the ambient temperature rises, the work output of the standalone CCPP system decreases faster than that of the integrated CCPP system. Also, the maximum yield in exergetic efficiency and total work output is observed at the degrees of cooling of 8K and 18K, respectively. Therefore, this system can be operated suitably within this range of degrees of cooling. Besides, the exergy-based sustainability indicators are found to be improved. The environmental sustainability index has increased by up to 3.52%, showing improved fuel utilization. This also indicates that, for the same amount of emissions, the integrated CCPP plant generates more power.

The performance of CCPP is further investigated as the effect of various input parameters, such as the compressor pressure ratio, and gas turbine inlet temperature. The effect is obtained on the exergetic performance of the CCPP system as a whole and its components. After the most influential operating parameters have been identified, the mathematical model is then subjected to multi-objective optimization using a genetic algorithm. According to the Pareto set of optimal solutions, cooling the inlet air by 16.5K results in the highest net specific work output, but, increased exergy

destruction. Increased exergy destruction, on the other hand, is undesirable. However, if the cost of power per unit is high, this could be economically advantageous.

Exergy analysis is then advanced in a subsequent section by splitting the exergy destruction into avoidable and unavoidable components so that the amount of avoidable exergy destruction in each component can be obtained. Results show that under the standard settings, the avoidable exergy destruction accounts for 25.02% of the overall exergy destruction. Additionally, the heat recovery steam generator exhibits the highest potential to mitigate irreversibility generation, accounting for 91.53% of its overall irreversibility. In contrast, the combustion chamber has the lowest potential, contributing only 6.94% of its total irreversibility.

Furthermore, the synergistic combination of advanced exergy and exergy costing methods extends analysis to advanced exergoeconomic analysis, and the resulting optimization is referred to as advanced exergoeconomic optimization. Using auxiliary equations and cost equations for capital costs, the cost functions for each stream are then derived and solved to determine the cost parameters of each component of the CCPP. Investigation subsequently yields the total capital cost and the total cost rate of exergy destruction. Each of these cost factors is also split into avoidable and unavoidable parts. The suggested set of optimal solutions approximates the pressure ratio of 13, 10K degree of cooling, and turbine inlet temperature of 1564K when the operational parameters are optimized to achieve improved modified exergetic efficiency and minimized unavoidable cost per unit of power generation.

The outcomes of this research contribute to advancing the state-of-the-art in CCPP technology, offering practical solutions for enhancing energy efficiency and sustainability in power generation.

TABLE OF CONTENTS

LIST OF FIGURES

LIST OF TABLES

LIST OF SYMBOLS

Abbreviations

CCPP	Combined cycle power plant
CCPPV	Combined cycle power plant with inlet air cooler
CIT	Compressor inlet temperature
GTC	Gas turbine cycle
STC	Steam turbine cycle
HRSG	Heat recovery steam generator
IAC	Inlet air cooling
TIT	Turbine inlet temperature
VARS	Vapor absorption refrigeration system
HPG	High-pressure generator
LPG	Low-pressure generator
COP	Co-efficient of performance
HPST	High-pressure steam turbine
LPST	Low-pressure steam turbine
HPD	High-pressure drum
LPD	Low-pressure drum
RH	Relative humidity
LHV	Lower heating value
BFP	Boiler feed pump
CEP	Condensate extraction pump
SP	Solution pump

Nomenclature

m	Mass flow rate (kg/s)
h	Specific enthalpy (kJ/kg)
v	Specific volume (m3/kg)
s	Specific entropy(kJ/kg.k)

T	Temperature (K)
P	Pressure (bar)
E	Exergy
C	Specific heat (kJ/kg.k)
W	Work (kW)
Q	Heat (kW)
X	Concentration (%)

Subscripts

a	Air
f	Fuel
m	Mechanical
s	Steam
g	Gas
AC	Air Compressor
CC	Combustion Chamber
GT	Gas Turbine
hp	High Pressure
lp	Low Pressure
isen	Isentropic
sh	Superheated
cond	Condenser
cw	Cooling Water
in/i	Entry
out/ex	Exit
cv	Control Volume
ph	Physical
ch	Chemical
ss	Strong Solution
ws	Weak Solution
ms	Medium Solution
evap	Evaporator
de	Double Effect
ex	Exergy
fw	Feed Water
0	Dead State
D	Destruction

CHAPTER 1

INTRODUCTION

1.1 Overview

The utilization of energy is familiarly correlated with the state of well-being and prosperity on a global scale. Addressing the increasing demand for energy in a manner that emphasizes safety and environmental responsibility is a significant problem. One significant factor that influences the need for energy is the inherent human need to maintain and enhance our own well-being, as well as that of our families and communities. The global population currently stands at approximately eight billion people, and the anticipated growth in population is expected to result in a corresponding rise in the demand for energy. This demand is contingent upon the sufficiency of available energy supplies. Moreover, the escalating population and economic progress in several nations carry significant ramifications for the environment, since the energy production procedures discharge pollutants, a considerable portion of which pose harm to ecosystems.

Fossil fuels are a long-standing major source of electricity generation worldwide. The combustion of fossil fuels leads to the emission of substantial quantities of greenhouse gases, specifically CO_2. Coal, the fossil fuel with the highest carbon intensity, continues to contribute one-third of electricity generation [1]. On the contrary, natural gas-based generation exhibits the benefit of producing reduced man-made carbon emissions in comparison to coal. Power generation shifted from coal to natural gas would emit 30–55% lesser CO_2 equivalent greenhouse emissions per unit of electricity generation, according to a study [2]. According to the International Energy Agency (IEA), gas-based power generation has emerged as a significant source of energy, accounting for about a quarter of global electricity production [3].

1.2 Prime Movers

A prime mover is a machine that transforms primary energy into mechanical energy. Choosing an appropriate prime mover is crucial for meeting demand requirements. Therefore, engineers and designers are particularly concerned with the selection of this component. Internal combustion engines, gas turbines, micro turbines, and fuel cells are all examples of prime mover types [4]. Listed below are the prime movers associated with the CCPP.

1.2.1 Gas Turbine

A gas turbine (GT) is one of the most suitable prime movers fired by natural gas-based combustion. The gas turbine is an internal combustion engine that consists of an upstream compressor, a downstream turbine, and a combustor housed between them. The combustion chamber gets an energy input, where fuel is combined with heated air and subsequently ignites in the gas stream. Within the intense conditions of the combustor, the burning of the fuel leads to a rise in temperature. The by-products of the combustion process are directed into the turbine part in order to generate mechanical energy. At that location, the gas flow exhibits a significant speed and quantity, which is channelled through a nozzle towards the turbine blades. This rotation of the turbine generates power for the compressor and, in general cases, thrusts their mechanical output. The turbine receives energy from the reduction in temperature and pressure of the exhaust gas known as exhaust expansion. In a realistic gas turbine, gases are initially augmented using either a centrifugal or radial compressor [5].

Subsequently, the gases are decelerated by the use of a diverging nozzle, commonly referred to as a diffuser. These procedures result in an increase in both the pressure and temperature of the fluid. In an ideal system, it is an isentropic process. Nevertheless, in practical use, energy dissipates as heat as a result of friction and turbulence [6].

The gases are consequently transported from the diffuser to the combustion chamber, where they undergo thermal expansion. This occurs in an ideal system under constant pressure. An increase in the specific volume of the gases results from the absence of a change in pressure. In real-world scenarios, this process often involves a slight decrease in pressure caused by friction. Ultimately, the greater amount of gases is expanded and propelled by nozzle guide vanes, leading to the production of energy by a turbine [7].

Gas turbines usually operate on an open cycle. Fig. 1. 1 represents the schematic diagram of open cycle gas turbine plant.

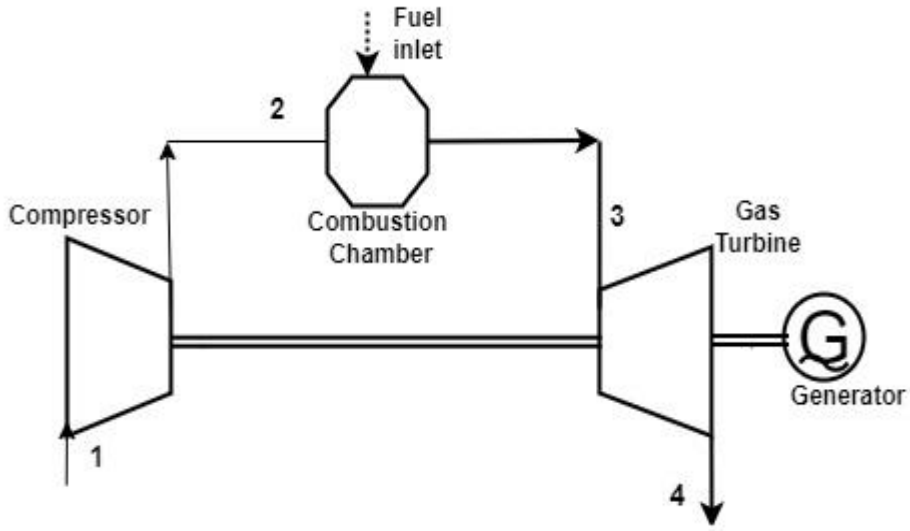

Fig. 1. 1 Schematic diagram of gas turbine plant

The thermodynamic cycle for gas turbines is referred to as the Brayton cycle. Fig. 1. 2 illustrates the Brayton cycle, showcasing the thermodynamic processes occurring in each component of the gas turbine cycle. The air undergoes compression in the compressor, as it is taken from the surrounding environment into the compressor intake. The compressor increases both the pressure and temperature of the air by utilizing compression work, which is provided by the turbine. The pressurized air enters the combustion chamber, where the fuel undergoes burning under continuous pressure. This additional heat elevates the temperature to the turbine inlet temperature, which is the highest temperature in the cycle. Subsequently, the elevated temperature gases go into the turbine, where they undergo expansion to reach atmospheric pressure, generating sufficient power to operate the compressor and generate net shaft work. Ultimately, heat is expelled into the atmosphere [8]. The exhaust exiting the gas turbine are released to the environment (not recirculated), known as the classification of the cycle as an open cycle. The majority of turbines utilized in power generation have axial flow compressors [9].

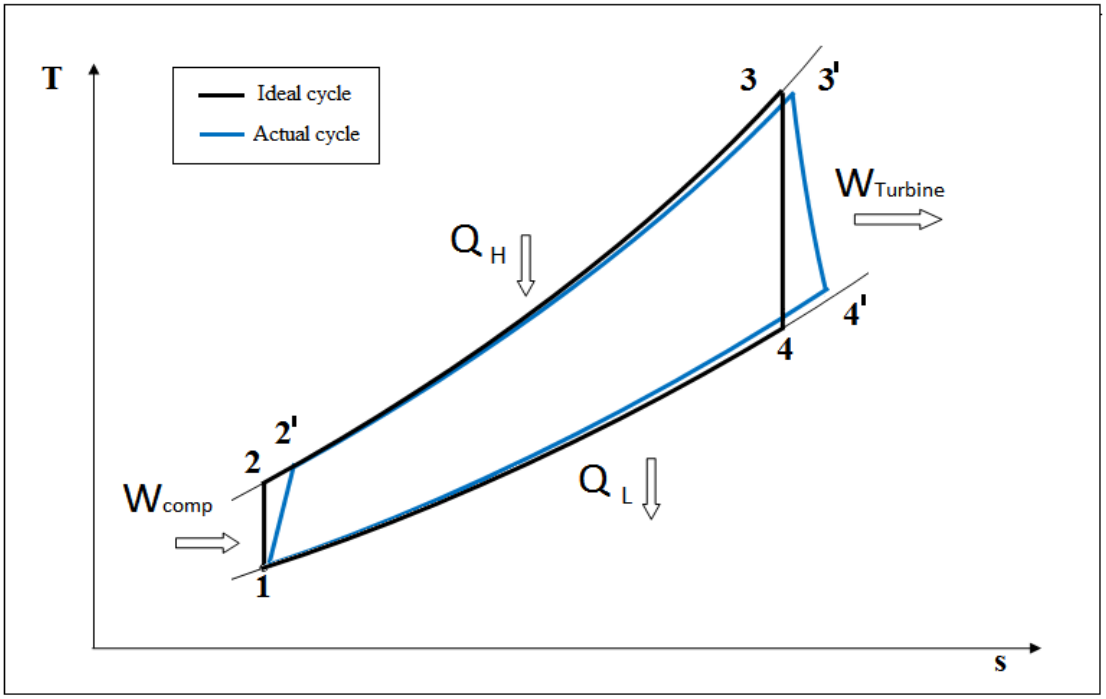

Fig. 1. 2 T-s diagram of Brayton cycle

1.2.2 Steam Turbine

The steam turbine is a highly efficient prime mover used to transform the thermal energy of steam into mechanical energy. Irrespective of their classification as turbines or not, steam engines are purpose-designed to convert the energy present in steam at a high pressure into motion through the expansion of the steam. In turbine designs, the slow expansion of steam via many sets of blades allows for significantly better efficiency compared to a single-step expansion. The steam undergoes expansion as it passes through a series of rotating blades on a shaft and stationary blades in a casing, resulting in the creation of entirely rotational motion. The steam turbine, when combined with an electric generator, is a highly significant method for generating large quantities of electric power globally [10]. A contemporary steam turbine typically consists of three stages. The high-pressure segment is equipped with small blades. Their small size is a result of the tremendous energy and temperature of the entering steam. Once the steam has passed through the high-pressure portion, it is returned to the boiler for the purpose of being warmed. Following this, the steam is directed towards the intermediate pressure section, which is the subsequent part of the steam turbine. The blades in this location possess greater dimensions compared to the blades found in the high-pressure area.

Upon traversing this portion, the steam is directed toward the low-pressure segment of the turbine [11]. Due to the prior extraction of a significant amount of energy from the steam, the blades in this section of the turbine are the largest. The steam is discharged from the turbine through the lower section, where it undergoes condensation and returns to its liquid state as water. Subsequently, it is returned to the boiler in order to be converted back into steam. The steam turbine is commonly employed in a combined heat and power system [12]. The thermodynamic cycle utilized for the steam turbine plant is the Rankine cycle. Fig. 1. *3* illustrates the T-s diagram of the Rankine cycle, depicting the process of pumping water from the condenser pressure at point '7' to the boiler pressure at point '8'. Boiling occurs in three distinct stages: water preheating, evaporating (steam production), and superheating. Subsequently, it undergoes expansion via several turbine stages until it reaches the condenser pressure at point '6' and is then condensed to return to point '7'.

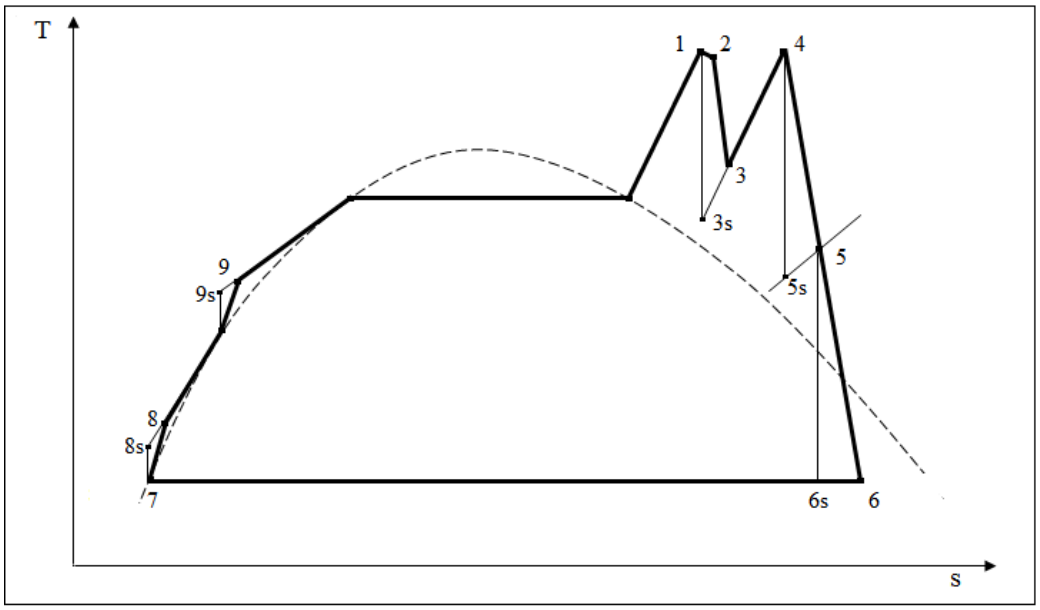

Fig. 1. 3 Rankine cycle on T-s diagram

Gas turbine and steam turbine facilities operating in an isolated mode provide electricity, albeit with significantly lower energy efficiency. The energy efficiency of a basic gas turbine cycle ranges from 25% to 35%, whereas for steam turbines it may reach up to 47% (in the case of large Steam Turbines) [13]. Nevertheless, the integration of a gas turbine cycle with a steam turbine in a combined arrangement enhances both

the efficiency and the total work production. The arrangement is well recognized as a combined cycle power plant.

1.3 Combined cycle power plant

The superiority of a combined cycle power plant (CCPP) over standalone gas turbine and steam turbine plants lies in its enhanced efficiency and overall performance. The primary benefit resides in its capacity for maximizing fuel utilization by sequentially operating both gas and steam turbines. Within a CCPP, the high-temperature waste gases emitted by the gas turbine are harnessed to make steam. This steam is subsequently utilized to power a steam turbine, so generating supplementary electrical energy. The use of this dual-cycle architecture greatly enhances the total efficiency by harnessing and using the waste heat that would otherwise be dissipated in an independent gas turbine facility. The integration of gas and steam cycles enables increased thermal efficiency, leading to increased power production from a given fuel quantity. The increase in efficiency leads to less fuel consumption, decreased pollutants, and eventually decreased operational costs. Furthermore, the CCPP has the capability to adapt to varying power requirements with high efficiency, making them a dependable and economically viable option for electricity production [14].

It has three major components i.e. gas turbine, Heat recovery steam generator, and steam turbine [15]. The performance of gas turbines significantly contributes to the overall performance of power plants, so Gas turbine is considered a foremost influencer in CCPP [16]. Further improvements in Gas turbines resulted in higher thermal efficiency of the CCPP. Mainly four potential Gas Turbine cycles namely simple cycle, intercooled cycle, reheat cycle, and intercooled and reheated cycle are optimized and analyzed. One of these enhancements is the reheated gas turbine cycle, which causes higher exhaust temperature which ultimately improves the thermal efficiency of the steam turbine cycle hence the overall cycle [17].

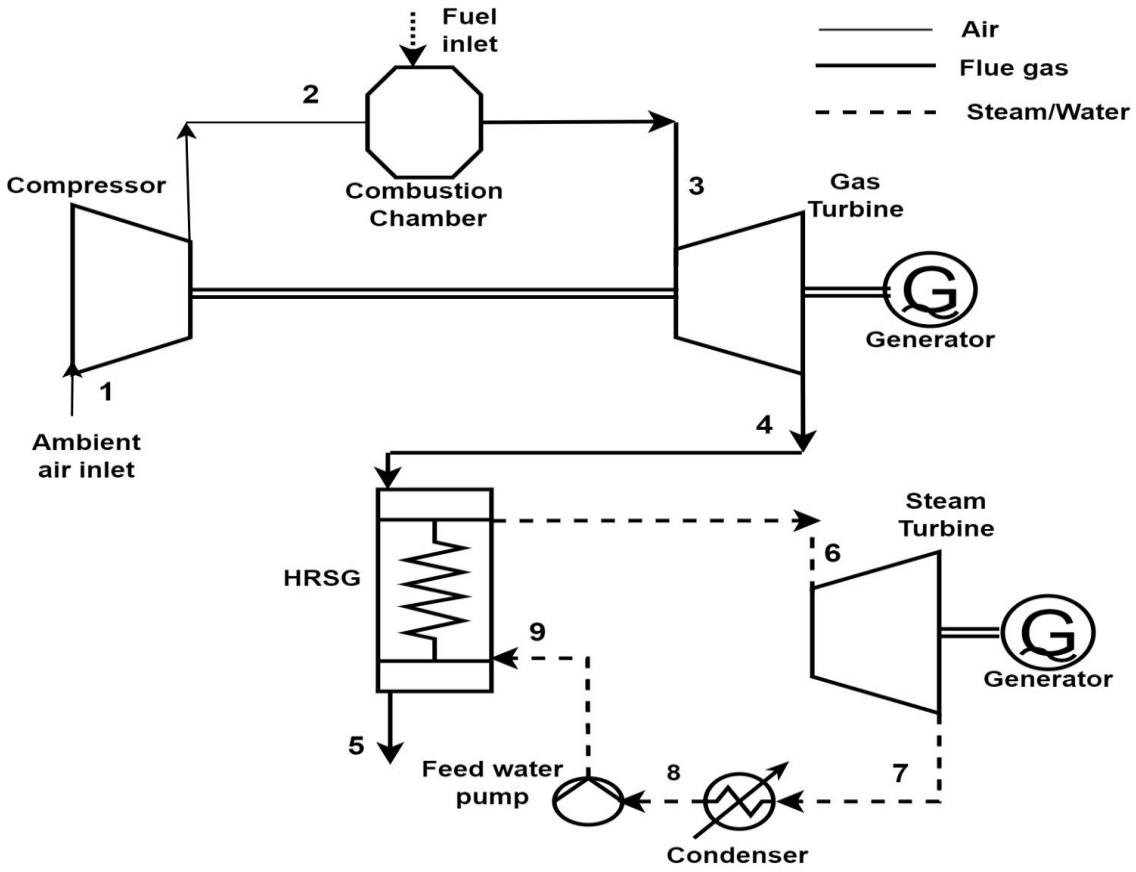

Fig. 1. 4 Schematic of a typical CCPP system

1.4 Heat Recovery Steam Generator

In a CCPP, a heat recovery steam generator (HRSG) recovers the waste heat from the gas turbine to generate steam for the steam cycle. The performance of the HRSG significantly affects the overall performance of a combined-cycle power plant. The steam produced in the HRSG varies in pressure levels depending on the design [18]. Three discrete heat exchanger components comprise the HRSG: the economizer, evaporator, and superheater. In that order, the combustion gases pass through the economizer package, superheater, and evaporator package. The process of heat transfer from the gas side to the water-steam comprises three discrete stages. In the economizer, the input water is heated to a temperature close to its saturation point. When water evaporates within the evaporator at a constant temperature and pressure, saturated steam is generated. The superheater utilizes the high-temperature heat from the exhaust to

raise the temperature of the steam produced in the evaporator. The steam turbine is supplied with superheated steam [19].

To enhance heat recovery in the HRSG, multiple pressure levels are employed. Approximately 30% of the overall power generated in the plant is produced by the steam turbine in a single-pressure HRSG system. Implementing a dual-pressure configuration has the potential to enhance the power generation of the steam cycle by as much as 10%. Furthermore, including a triple-pressure configuration can yield an additional 3% improvement in power production [20]. However, the increment in cost of developing triple-pressure HRSG is significantly higher as compared to the improvement in power production. Fig. 1. 5 and Fig. 1. 6 represent the schematic of single-pressure and double-pressure HRSG with their intrinsic components followed by the paths of water/steam and exhaust gas.

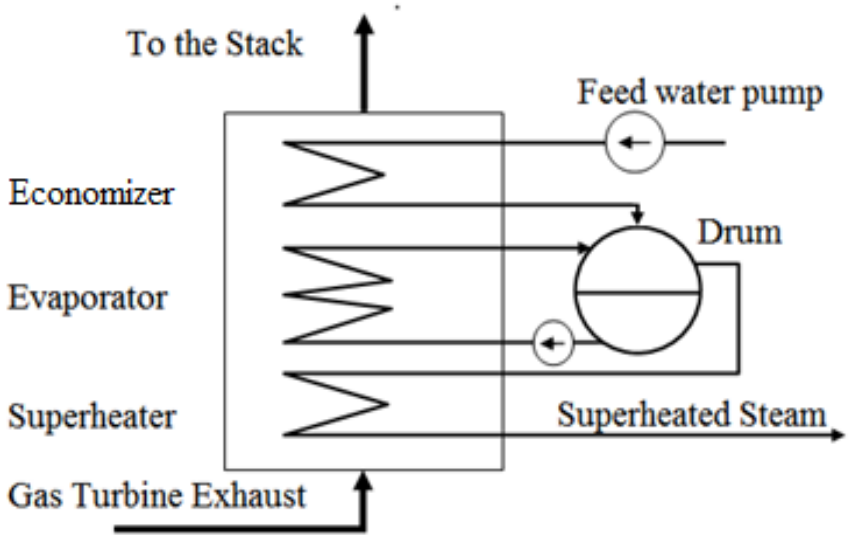

Fig. 1. 5 Single pressure HRSG

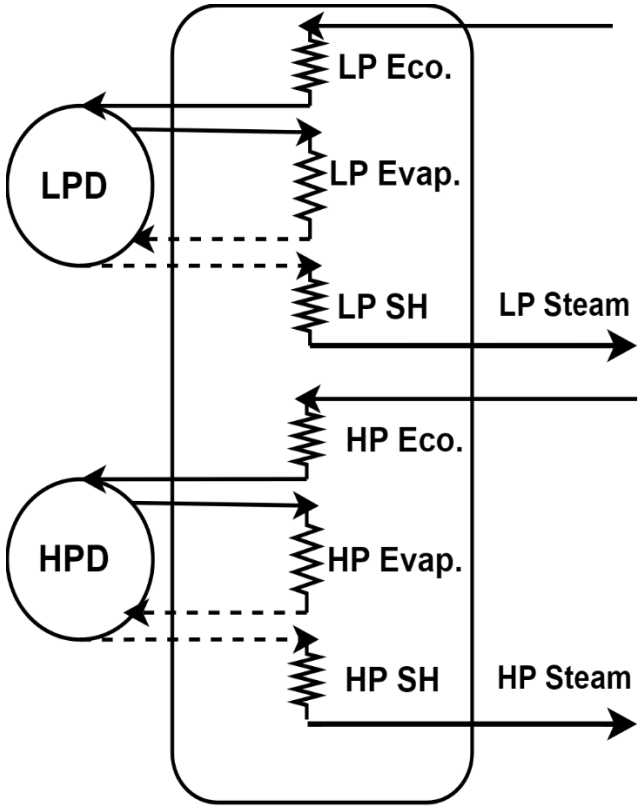

Fig. 1. 6 Dual Pressure HRSG

1.5 Advantages of Combined cycle power plant

CCPP systems offer several advantages, including enhanced plant efficiency, lower heat losses, and wastes, decreased operating costs, lower greenhouse gas emissions, optimized resource utilization, various generating capabilities, and heightened dependability [21]. The subsequent sections elaborate on these advantages.

Implementing the CCPP system enhances the overall efficiency of the plant and diminishes operating expenses. The total efficiency of traditional coal-based steam power plants that utilize a solitary prime mover and rely on fossil fuels (i.e., Coal) often falls below 40%. In other words, about 60% of the heat energy of the fuel that enters a traditional power plant is wasted [22].

By harnessing the waste heat generated by the primary mover, the efficiency of CCPP electricity generation facilities may potentially exceed 64% [23]. In a CCPP system, the waste heat produced by the exhaust of the gas turbine unit is utilized to power the steam generation, followed by steam turbine power generation by eliminating the need for additional fuel. This distinguishes it from a traditional coal-based power plant, which

relies on external energy supplies. Therefore, a CCPP system consumes less energy to achieve the same level of production compared to a traditional plant, resulting in reduced operating expenses.

CCPP also decreases emissions of greenhouse gases. Due to its higher efficiency in converting fuel into power, a CCPP emits a lower amount of greenhouse gases compared to a typical power plant. While the emissions of greenhouse gases from combined cycle plants are lower than those of typical standalone plants, there are restrictions to deploying CCPP in a dispersed way because of the on-site gas emissions they produce [24]. Another significant advantage of employing CCPP systems is their ability to save expenses and energy wastage by requiring fewer power transmission lines and distribution units. Electricity is often generated through a centralized facility, which is typically situated at a considerable distance from the end consumer. The deficiencies incurred during the transmission and distribution of power from the central facility to the end consumer might amount to around 9% [22].

Because of these advantages, CCPP systems have drawn the attention of academics and designers. The enhancement in efficiency is frequently the paramount element in implementing a CCPP system. Prior to selecting the CCPP system, additional assessments of the initial capital and operational expenses are necessary to confirm the efficient and cost-effective assembly and performance of the CCPP.

1.6 3E Analyses

3E analysis includes the energy, exergy, and exergoeconomics methods of assessment of any thermal system [25]. Energy analysis forms the fundamental basis upon which the performance evaluation of an energy conversion system is built. Energy analysis begins with the presumption that the components of the system are contained within an imaginary control volume. The energy interaction is subsequently ascertained within the control volume by applying the principles of mass and energy conservation. The energy analysis is conducted in order to derive an approximation of the system's performance. In energy analysis, thermal efficiency is a prevalent performance parameter utilized in power cycles, while COP is applied to cooling cycles. Nevertheless, an inherent limitation of energy analysis is its inability to quantify the

difference in the system's performance from the ideal conditions that can be attained under reversible conditions [26].

Exergy analysis [27], derived from the second law of thermodynamics, is frequently employed to overcome the constraints of energy analysis. Exergy refers to the largest amount of work that may be extracted from a system when it transitions from an initial state to a reference state.

Whenever the characteristics of the system differ from those of the surrounding environment, there is a possibility for productive activity. However, when the system reaches a state of equilibrium with its environment, the amount of work required to extract potential or exergy becomes zero. At that moment, the system is said to be in a state of complete idleness, sometimes referred to as a "dead state." Exergy is considered to be the combined characteristic of both the system and its surroundings [28].

By identifying the source, location, and actual magnitude of energy loss, exergy analysis facilitates more efficient energy utilization. Consequently, exergy analysis is an exceptionally valuable method for upgrading an existing thermal system or devising and developing a new energy-efficient thermal system. In contrast to energy analysis, which assumes the conservation of energy, exergy analysis posits that exergy is inherently destructive. Exergy destruction occurs when irreversibilities are present in a system, such as heat transfer facilitated by a finite difference in temperature, fluid friction, chemical reactions, and so forth. An established method for improving the performance of a thermal system, exergy analysis identifies the primary locations of irreversibilities before modifying the operating and design parameters to reduce the irreversibilities [29].

Although exergy analysis is adequate for examining and enhancing the efficacy of a thermal system, it fails to consider economic considerations. An optimal thermal system should possess both high efficiency and cost-effectiveness. Although exergy analysis can improve the efficiency of a thermal system, it does not ensure that the system will remain cost-effective [30]. Exergoeconomic analysis, a composite of exergy analysis and economic principles, is utilized to address this limitation of exergy analysis. It offers a comprehensive assessment of the performance of a system. Exergoeconomic analysis furnishes financial data pertaining to a thermal system, encompassing expenses for fuel,

equipment, operation and maintenance, and the ultimate product. Additionally, it discloses costs associated with inefficiencies such as exergy degradation and losses, which are crucial details for optimizing the efficiency of a thermal system and reducing the ultimate product cost. Exergoeconomic analysis assumes particular significance in the context of multi-generation systems, which produce electricity, process heat, and chilled water, among other things, due to its ability to enable cost estimation of each individual product [31].

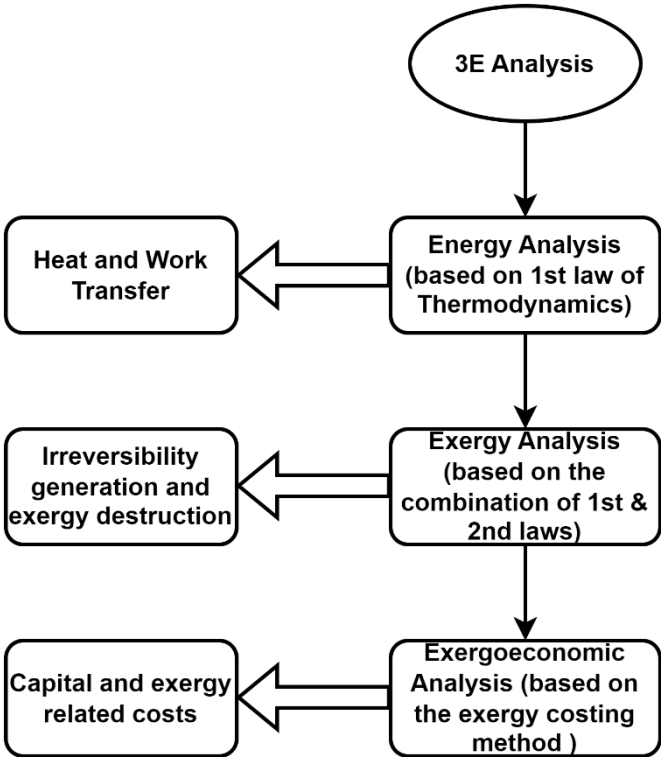

Fig. 1. 7 A flow chart showing the steps of the 3E analysis

1.7 Outline of this Thesis

The thesis has six chapters, which are outlined as follows:

Chapter 1: Introduction

This chapter commences with a concise overview of the current worldwide energy situation and its environmental implications. It then proceeds to explore the application of heat recovery steam generation technologies for harnessing the waste heat from gas

turbine exhaust. This discussion proceeds with an overview of the advancement of the combined cycle power plant system and its several configurations, followed by a summary of 3E analyses, which encompass Energy, Exergy, and Exergoeconomic assessments. Finally, this chapter finishes by providing an overview of the thesis.

Chapter 2: Literature Review

This chapter focuses on conducting a thorough review of the existing literature on combined cycle power plants, specifically exploring the concepts of energy, exergy, and exergoeconomics, followed by Multi-objective optimization. This chapter also explores the new methodology of advanced exergy analysis and its associated research. Furthermore, numerous literary works have also examined the performance-based parametric investigation to analyze the impact of different operating factors. Data and pertinent information were taken from various research papers in international journals and related theses. The findings from multiple Proceedings were also reviewed.

Chapter 3: System Description and Mathematical Modelling

This chapter discusses the description of various configurations of combined cycle power along with inlet air cooling integration. Moreover, the theoretical background of energy, exergy, and exergoeconomic analyses along with their equations are also discussed. Also, the results based on an advanced exergy-based splitting of exergy destruction, and multi-objective optimization using a Genetic Algorithm (GA) are presented in this chapter.

Chapter 4: Model Validation

This chapter presents an overview of the significance of model validation in research or practical applications. The text discusses the need to validate models to ensure their reliability and effectiveness in addressing real-world issues. The mathematical models for the combined cycle power plant system and the double-effect VARS intake cooling system have been validated by experimental data from various investigations.

Chapter 5: Results and Discussion

This chapter provides a comprehensive overview of the results achieved at each stage of the process. Furthermore, it examines the impact of inlet air cooling on the current combined cycle power plant system, as well as the various operational parameters on its performance. The comparisons of the different scenarios are also presented. It also

discusses the findings of exergoeconomic analysis, advanced exergy analysis, and multi-objective optimization.

Chapter 6: Conclusions and scope of future research

This chapter concludes the findings derived from the results gained through the various analyses conducted. Additionally, potential areas for further research have been suggested.

CHAPTER 2

LITERATURE REVIEW

2.1 Background

Due to growing environmental concerns and advancements in technology over the past decade, there has been a significant increase in both the need for and the potential to provide versatile energy solutions. In order to gain an understanding of the most recent developments in the optimisation and performance of the CCPP, a succinct literature review was undertaken. This chapter presents the associated publications and research work, including their objectives, analytical methods, and concise findings. However, this chapter focuses on a comprehensive investigation of existing literature on the inlet air cooling techniques and optimization conducted on different CCPP configurations. Some researchers/authors concentrate on the operational parameters like ambient air temperature, compressor inlet temperature (CIT), compressor pressure ratio, and Turbine inlet temperature (TIT) of the gas turbine (topping cycle), while others optimize the steam plant (bottoming cycle).

The literature in this chapter is categorized into three primary sections: the impact of various operational factors on energy and exergy analysis, exergoeconomic analysis, as well as multi-objective optimization. The main objective of this chapter is to pinpoint the research deficiency and concentrate on the specific domains of CCPP systems.

2.2 Review based on energy and exergy analysis

2.2.1 Effect of Ambient Air conditions

De Sa and Al Zubaidy [32] revealed a direct relationship between ambient temperature and the rating of gas turbine power output. It suggests that for every K increase in ambient temperature above ISO conditions, a gas turbine loses 0.1% in thermal efficiency and 1.47 MW of its gross power output. This relationship can help assess local power generation for installation planning and forecasting, particularly in Middle-

eastern countries that are rapidly developing the application of Gas Turbine Inlet Air Cooling (GTIAC) technologies. The study was conducted on specific turbines SGT 94.2 and SGT 94.3 installed at the DEWA Power Station in Dubai, UAE. The findings can help in assessing the potential of gas turbines in these regions.

Egware and Ighodaro [33] investigated the impact of ambient air temperature on the exergy sustainability and ecological function of a 153 MW gas turbine power plant using MATLAB software. The results show that the combustor has the least improvement potential, relative irreversibility, and lack of productivity compared to other components. For a 1°C increase in ambient air temperature, the fuel depletion number, waste exergy ratio, exergy destruction factor, environmental effect factor, and ecological function increased by 1.51%, 0.693%, 1.505%, 1.924%, and 9.102%, respectively. Thus, the power plant's exergy sustainability performance has a negative impact at high ambient air temperatures.

The greatest influence on gas turbine performance, as demonstrated by Zhang, et al. [34] is the ambient temperature, which results in increased output power, efficiency, and load control capacity at both base load and part load. The efficiency and the power rise by 2.1% and 13.9%, respectively, at base-load when the ambient temperature decreases from 15°C to -15°C, while the efficiency increases from 46.4% to 51.4%.

Hosseini, et al. [35] showed that the gas turbine compressor which is designed for constant volume flow rate of air, making its electric power output dependent on ambient temperature. An increase in ambient temperature decreases the compressor's output pressure, reducing cycle efficiency. Conversely, an increase in air density reduces the heat rate and increases specific fuel consumption. For each 1°C increase in ambient air temperature, the gas turbine's electric power output decreases by 0.5% to 0.9%, and by 0.27% for a combined cycle.

This study by Şen, et al. [36] investigated the impact of ambient temperature change on electric production in a natural gas CCPP plant in İzmir, Turkey. The plant, which had been producing electricity for 14 years, has 240 MW of capacity. Data from gas turbines, steam turbines, and combined cycle blocks were collected during the 8-23°C ambient temperature range. The study found that temperature increases led to a decrease in the efficiency of GTs and indirectly affected STs. The study recommends additional

precautions to ensure optimal air conditions in the combustion chamber and the installation of air cooling systems.

González-Díaz, et al. [37] examined the impact of environmental situations on a CCPP with CO_2 capture in Mexico. It made recommendations for off-design operation and efficient integration. The investigation reveals that the effectiveness of the NGCC decreases from 50.95% to 48.01% as the temperature increases from 15°C to 45°C, and from 50.95% to 50.78% as the temperature decreases. The power output drops from 676.3 MW at a temperature of 15°C to 530 MW at a temperature of 45°C. In order to offset this, the heat recovery steam generator can employ supplementary firing to provide extra power, thereby restoring the power output to 640 MW at a temperature of 45°C. However, this resulted in increased fuel costs and a drop in efficiency.

Barigozzi, et al. [38] analysed the techno-economical parametric analysis of an inlet air cooling system for an aero-derivative Gas Turbine in a CCPP. The system used chilled water thermal storage charged by mechanical chillers to cool inlet air during the hottest day hours. The study considered three cases operating in Phoenix, New Orleans, and Abu Dhabi, each with different climatic conditions. The study found that operational hours and power output augmentation were higher in hotter climates, and wet climates required large thermal storages, increasing investment costs. The best techno-economic performance was achieved in sites with high temperatures and low relative humidity.

Mohapatra and Sanjay [39] analysed a 3-pressure level HRSG integrated CCPP power plant equipped with an Aqua Ammonia VARS. Also, the ambient temperature and relative humidity were considered operational parameters for analysing the performance of CCPP. The effect of ambient relative humidity was reported to be negligible on the performance of several components of the CCPP.

Mishra, et al. [40] examined the impact of inlet air cooling on the exergetic performance of CCPP. The use of an inlet air cooler mitigates high ambient temperature effects. The analysis shows a maximum increase in net specific work, efficiency, and exergetic efficiency of 14.16%, 3.93%, and 5.65% under specific input parameters.

Elberry, et al. [41] examined how to include a cooled gas turbine-based combined cycle with a single-stage Lithium Bromide-Water absorption inlet air cooling method. The waste heat energy from the exhaust gas from the waste heat recovery system was

employed in the investigation. The Nubaria Power Station, located 120km south of Alexandria, was used as a reference plant. A thermodynamic model was introduced, and a parametric study of operational conditions was conducted. The model indicated an 11% growth in electricity generated when inlet air is cooled from 30°C to 10°C.

2.2.2 Inlet Air Cooling Techniques

Dabwan, et al. [42] proposed a new inlet air cooling (IAC) technique to improve CCPP in hot locations. This system used absorption chillers to cool compressor incoming air with intercooler waste heat. This system was tested against four prominent IAC technologies: evaporative cooling, solar-powered absorption cooling, steam-operated absorption cooling, and vapour compression cooling. Estimates included annual profit and payback period. This IAC method solved CCPP's problems in hot climates, improving power output by 19% and efficiency by 2.3%. The suggested inlet air cooling system might boost plant efficiency by 8–18% and increase annual profits by 66% and 10% over steam and mechanical cooling systems, respectively. It was also cost-effective because the payback period of 1.74 years was 3%, 67%, and 85% shorter than mechanical, steam, and solar cooling systems.

Espinosa-Cristia, et al. [43] proposed a new technique to reduce air temperature entering the gas turbine by recovering waste heat from exhaust gas. The heat content of the exhaust gas was used as a heat source for an ejector refrigeration cycle (ERC), cooling the air entering the gas turbine. Exergy and environmental analyses were conducted to investigate the method's impact on exergy efficiency, environmental factors, and sustainability index. The proposed method increased the CCPP's power production by 6.26%.

The study by Majdi Yazdi, et al. [44] examined the use of absorption chiller, heat pump, and inlet fogging systems for cooling gas turbine inlet air in four Iranian cities: Yazd, Bandar Abbas, Ardabil, and Sari. The study focused on gas turbine functional parameters, pollutants, electricity prices, and capital cost payback periods. The results show that the absorption chiller is the best cooling system for hot climates, improving gas turbine net power by 18% and energy efficiency by 5.8%. In Bandar Abbas and Yazd, respectively, inlet air cooling reduced power generation costs by 6.5% and 6.0% and reduced NO_x pollution emissions by 60%. In dry areas, the inlet fogging system

functions well. The best cooling system will rely on certain goals, including increasing power, reducing fuel use, or decreasing pollutants. The heat pump technology is appropriate for chilly climates like Ardabil because of its cheap initial investment cost.

Baakeem, et al. [45] compared cooling technologies for a gas turbine under Riyadh weather conditions, analysing power output, fuel consumption, and thermal efficiency. It proposed systematic approaches to determine air-cooled temperature and cooling capacity for TIAC systems. The optimum values were 8°C and 36 kW/m3 s^{-1}. Media evaporative cooling, mechanical vapour compression, and single-effect Water-Ammonia absorption cooling systems were not suggested. Moreover, Sub-cooling based multistage compressor systems and single-effect LiBr-H_2O absorption refrigeration systems show better performance.

Deng, et al. [46] reviewed the performance of combined cycle power plants (CCPP) using various inlet air cooling systems. The researchers aimed to develop technologies for cooling inlet air to capture wasted heat from exhaust gases, with the goal of minimizing environmental impacts. The output power of CCPPs depended on the mass flow rate of air through the air compressor, a factor that decreased during hot weather. The fogging cooling system improved the CCPP's performance by up to 17%, while evaporative cooling only enhanced it by 4%. Mechanical chillers have a higher energy consumption compared to evaporative cooling due to their effectiveness based on inlet airflow humidity. Mechanical cooling systems can provide cooling for 7-hour on-peak periods, increasing performance by 13.6%. The absorption chiller is the best solution, demonstrating a 23% increase in performance. Overall, the study highlights the need for improved inlet air cooling systems in CCPPs.

Zare [47] proposed a methodology for a biomass-fuelled CCPP system using exhaust gas waste heat to run an ammonia-water absorption refrigeration cycle for compressor inlet cooling. Thermoeconomic analysis was conducted to compare the performance of the two systems under optimal operating conditions. The study found that compressor inlet cooling significantly improved system performance in terms of thermodynamics and economics, despite additional costs imposed by adding the absorption refrigeration cycle. Under optimal conditions, incorporating compressor inlet cooling improved net power production by 30.1% while reducing the levelized Cost of Electricity by 22.5%.

Matjanov [48] analysed a gas turbine cycle of 28.1 MW in Tashkent CHP which is affected by ambient conditions, experiencing a decrease in power output and electrical efficiency. To cool the inlet air, an absorption chiller is proposed using gas turbine waste gases, HRSG waste gases, and solar energy. However, using gas turbine waste gases in the chiller is not economically profitable due to reduced CHP efficiency. The technical-economical attractiveness of using HRSG waste gases in the single-stage absorption chiller is found to be more economical when the temperature of HRSG waste gases is below 120°C.

A study by Singh [49] on Brayton-Rankine combined cycle power plants showed that reducing compressor inlet air temperature can improve gas turbine performance. A simulation model of an Indian power plant with a NH_3-H_2O absorption refrigeration system was established because absorption refrigeration systems may make use of low-grade waste energy. According to the model, this configuration boosted power production by 400 kW in the winter and enhanced thermal and exergy efficiency by 1.193% and 1.133% in the summer. The research also looked at how changes in ammonia condenser temperature in North Indian meteorological conditions affected plant performance.

Sahu, et al. [50] conducted an energy based analysis of the gas turbine-based triple-pressure reheat cycle, which incorporates vapour compression inlet air cooling and air-film turbine blade cooling. The study found that integrating these cooling methods significantly reduces CO_2 emissions per unit of plant output. The study also found that plant efficiency increases with increased TIT, and the cost of environmental impact due to CO_2 emissions decreases with increased TIT and decreased CIT.

An article by Pourhedayat, et al. [51] reviewed various pre-cooling strategies for gas turbine power plants, including absorption refrigeration, direct evaporative cooling, fogging systems, indirect evaporative cooling, vapor compression refrigeration, air-earth heat exchanger, iced thermal energy storage, turbo-expander system, liquefied natural gas system, and hybrid systems. It discussed the potential strengths and weaknesses of each strategy, highlighting its potential applications and providing propositions, current research gaps, and future research directions. The absorption

refrigeration pre-cooler was found to be one of the promising pre-cooling technologies, as it uses waste heat at the gas turbine's outlet.

2.2.3 Effect of other operational parameters

Ibrahim and Rahman [52] reported that the performance of gas turbines is heavily influenced by climate conditions. To reduce this, increasing the inlet turbine temperature and reducing the inlet air temperature of the gas turbine compressor can be beneficial. CCPPs are often used for high-efficiency power plants. A performance model developed using MATLAB software shows that overall efficiency increases with the peak compression ratio, with higher efficiency occurring at lower ambient temperatures and higher turbine inlet temperatures.

Almajali and Quran [53] scrutinized the efficiency of CCPP, which consists of steam and gas turbines. The study found that CCPP plants with open-cycle gas turbines and bottoming cycle steam turbines achieve the highest thermal efficiency. The study also found that the overall plant thermal efficiency is significantly greater than either of the two turbines, reducing the greenhouse effect. The regenerative steam cycle reduces the overall efficiency of the combined cycle while using the reheat steam cycle increases both the plant's thermal efficiency and the dryness factor of steam at the turbine exit.

Shireef and Ibrahim [54] analyzed energy and exergy efficiency in a triple-pressure CCPP and its components. It was found that the combustion chamber was the primary source of exergy destruction, accounting for 58% of total exergy destruction. The study also revealed that reducing the heat transfer rate in the gas turbine and increasing the turbine inlet temperature can improve overall efficiency. The study suggested that achieving maximum efficiency can be accomplished by diminishing ambient temperature and rising turbine inlet temperature.

Dev and Attri [55] examined seven commonly used CCPP configurations using an engineering equation solver (EES) software. The study examines influence of pressure ratio, turbine inlet temperature, and relative humidity on the first and second laws. The thermodynamic analysis revealed that overall pressure ratio, turbine inlet temperature, and air filter pressure loss significantly affect exergy destruction in CCPP components. Also, the effect of ambient air humidity is insignificant.

Ahmed, et al. [56] focused on the design of a dual-pressure steam generator cycle for a 60 MW gas turbine unit. The study found that maximum heat transfer occurs in the evaporator section for high-pressure levels and in the economizer section for low-pressure levels. The optimal design pressure for high-pressure was 100 bar, while for low-pressure it was 10 bar. Exergy analysis showed a 35% overall exergy loss, with 16% in flue gasses and 10% in the heat exchanger. The remainder was converted into 35 MW of useful work.

Hoang and Pawluskiewicz [57] analysed three CCPP configurations based on several operational parameters: single-pressure with supplementary firing, dual-pressure, and triple-pressure reheat cycle. It identified ambient temperature, gas part pressure ratio, and inlet gas turbine temperature as key factors affecting system efficiency and power production.

Mahian, et al. [58] reviewed exergy analyses for various combined Heating Power (CHP) systems, including gas turbines, Organic Rankine cycles, fuel cells, and hybrid energy systems. It suggested that high-performance small-scale CHPs for residential areas were insufficient, and more research is needed on hybrid CHPs with renewable sources. Economic studies in association of exergy analyses were also recommended. Future developments should focus on incorporating renewable sources and improving exergy efficiency.

Ali, et al. [59] analysed the energy and exergy of a Guddu combined cycle power plant with a triple pressure heat recovery steam generator (HRSG). It calculated the energy loss and efficiency of each plant component and the exergy destruction of the HRSG. The combustion chamber and condenser had the highest exergy destruction and energy loss, respectively. The total net power output, energy, and exergy efficiency were calculated as 737.8 MW, 59.12%, and 58.24%, respectively.

Babaei Jamnani and Kardgar [60] examined the energy-exergy analysis of a gas-fired combined-cycle power plant in Kuantan and Kapar, Malaysia, to evaluate its components. The analysis focused on the gas turbine unit, condenser, HRSG, and multiple pressure steam turbines. The study also examined the effects of environmental conditions on the plant components, such as compressor pressure ratio, environmental temperature, HPT, condenser pressure, and reheating. The study revealed that the gas

turbine cycle is the main source of exergy destruction, accounting for 83.79% of total exergy destruction. The study also determined exhaust gas fractions from the gas turbine across the combustor, revealing an average molar fraction of nitrogen, oxygen, carbon dioxide, and water vapour. The findings suggest several potential areas for CCPP's performance development, and the study suggests that energy-exergy assessment and optimization guidance could help modify operating conditions and capitalize on the trivial destruction rate.

2.3 Review based on Exergoeconomic Analysis and Optimization

The study of exergoeconomics by Rosen and Dincer [31] examined the relationship between capital costs and thermodynamic losses in modern electrical generating stations. A correlation was identified between capital costs and exergy loss, but no such correlation was found between capital costs and energy loss. This correlation implies that devices in operational stations were arranged in a manner that attained an optimal design by striking a balance between thermodynamic and economic features. The findings provided valuable insights into the interaction of thermodynamics and economics, showcased the advantages of second-law analysis, and had broader implications for the entire electrical utility sector.

The study by Sahin, et al. [61] analysed the exergoeconomic aspects of a combined cycle power plant using thermodynamics, and economic principles. It defined an overall performance index (OPI) to evaluate the optimal operational and design configurations. Four performance indicators were considered: energy efficiency, exergy efficiency, levelized cost of electricity, and total investment cost. Three scenarios were considered: conventional, environmentally conscious, and economical. The optimum size and configuration of the power plant were determined by user priorities and weight factors assigned to the performance indicators. The gas turbine's optimal size, determined by the pressure ratio, is 18 for the conventional scenario, 16 for the environmentally concerned scenario, and 12 for the economical case.

Gu, et al. [62] considered the exergy efficiency of a 200 MW gas-steam combined cycle system, focusing on energy quality. The total cost model was established using exergy economics theory, and three associated models were recognised as objective functions. The NSGA II genetic algorithm was used to attain Pareto frontier results, resulting in

optimized parameters for high efficiency, low cost, and low emissions. Sensitivity analysis was also conducted under different operating conditions to understand the optimal parameters.

Memon, et al. [63] analysed a CCPP using thermo-environmental, exergoeconomic, and statistical methods. Therefore, exergoeconomic analysis examined the impact of operating parameters on fuel, capital, and exergy destruction costs. The optimal operating parameters were determined using the Nelder-Mead simplex method. Parametric analysis showed that operating parameters significantly affect performance and cost rates. Optimization results showed a correlation between increased exergy efficiency and decreased cost rates.

Ganjehkaviri, et al. [64] conducted the thermodynamic modelling of a CCPP to observe the impact of economic strategies and design parameters on plant optimization. Exergoeconomic analysis is used to determine electricity and exergy destruction costs. The study also investigates the effects of economic parameters on sustainability, carbon dioxide emission, and fuel consumption. The results show that changes in economic parameters can alter the balance between cash flows and fixed costs, and limit the reduction of carbon emissions and fuel consumption. The study concludes that optimum values increase exergy efficiency by about 6% and decrease CO_2 emissions by 5.63%.

Bolatturk, et al. [65] studied the exergy and thermoeconomic aspects of Turkey's Çayırhan thermal power plant, focusing on the thermodynamic properties of the inlet and outlet points of each component. The results showed the energy and second law efficiencies of 38% and 53%, respectively. The highest exergy losses were found in the boiler, turbine, condenser, heater, and pump groups. The turbine group had the highest exergoeconomic factor.

Awaludin, et al. [66] conducted an exergoeconomic analysis on a 21.6 MW gas turbine power plant using logbooks from the Pekanbaru Unit, Indonesia. The analysis determined the exergy destruction of each component using the 1^{st} and 2^{nd} laws of thermodynamics. The study combined exergy and economic analysis to evaluate the accrued cost caused by irreversibility, including investment costs. The combustion chamber was the largest destruction site, followed by the compressor and gas turbine. The economic analysis revealed a total cost loss of 2,793.14$/hour due to exergy

destruction. The thermal and exergetic efficiencies of the gas turbine power plant were 24.51% and 22.73%, respectively.

Unal and Ozkan [67] conducted a thermodynamic and exergoeconomic analysis of a thermal power plant in Turkey. It determined the thermodynamic properties of 27 node points, calculated energy, and exergy values, and calculated mean exergy costs. The results showed that the boiler had the highest loss of exergy, followed by the turbine group and the condenser. The exergoeconomic factor values were 33.58% for the boiler, 38.02% for the turbine group, and 8.70% for the condenser.

Kaviri, et al. [68] performed comprehensive thermodynamic modelling of a dual-pressure combined cycle power plant, comparing results with actual data from an Iranian power plant. The model included a duct burner and optimized objective functions were component costs, fuel cost, duct burner cost, and cycle exergy efficiency. The optimization was performed using a computer simulation code using a genetic algorithm approach. The study also investigates the effect of cycle key parameters on these objectives. Results show that gas turbine temperature, compressor pressure ratio, and pinch point temperatures are significant design parameters, indicating that changes in these parameters can significantly alter the objective functions.

Bakhshmand, et al. [69] performed the exergoeconomic analysis and optimization of a triple-pressure combined cycle plant with one reheat stage. The study found that the optimization process increased energetic and exergetic efficiencies by 3% and reduced cost criteria by 9%. The specific cost of the plant was reduced from 21.48 (€/h) to 20.90 (€/h), resulting in a 3% decrease in the product and electricity cost.

Javadi, et al. [70] utilized a mathematical model to optimize a 500 MW combined cycle power plant, considering gas and steam turbine units. The optimization used the Non-Dominated Sorting Genetic Algorithm (NSGA-II). The results showed that the efficiency of the plant was influenced by design parameters like gas turbine input temperature, compressor pressure ratio, and pinch point temperature. Changes in these parameters can increase efficiency by up to 8.12%, reduce heat rate by 7.23%, and decrease exergy destruction by 7.23%.

2.4 Review of Advanced Exergy Analysis

Morosuk and Tsatsaronis [71] explored an advanced exergy-based assessment for energy conversion systems. These assessments considered the interactions between different components and the potential for improvement in each significant component. This provided valuable information for developers and operators to improve system design and functionality. By categorizing exergy destruction, capital investment cost, and environmental impact into endogenous/exogenous and avoidable/unavoidable parts, a better understanding of several thermal processes was developed in order to apply potential improvements. The study examined the characteristics and advancements in advanced exergy-based methodologies and applied the method to basic air refrigeration equipment to validate its accuracy.

Mossi Idrissa and Goni Boulama [72] investigated a combination of 2 Brayton cycles (as both topping and bottoming cycle) using advanced exergy methodology. The combustor was found to be the component with the major exergy destroyer, but most irreversibility generation was endogenous and unavoidable. The turbines and compressors were largely endogenous and avoidable. The total exergy destruction decreased with the topping cycle pressure ratio, while the endogenous avoidable and exogenous unavoidable exergy destruction increased with the bottoming cycle pressure ratio.

Koroglu and Sogut [73] employed both conventional and advanced exergy studies to evaluate a marine steam power plant. The objective was to provide designers with valuable insights that might assist in making informed decisions regarding component renewal matters. The study findings indicated that the boiler experiences the most significant exergy degradation mostly as a result of chemical processes. Furthermore, it exhibited the largest amount of preventable exergy degradation. The pumps in the system contributed to the degradation, albeit to a slight extent. Turbines hold more significance in comparison to heat exchangers. The results on avoidable exergy losses suggested that attempts to enhance performance should primarily target the boiler, turbines, condenser, and pump equipment. Additionally, the efficiency of feed water heaters could be enhanced indirectly by upgrading other components. Furthermore, it was determined that the entire system has a potential for a 10% enhancement in exergy

efficiency. The majority of this increase, almost 75%, can be attributed to two specific components: the boiler with a potential improvement of 6%, and the low-pressure turbine with a possible improvement of 1.3%. The remaining components have limited potential for development.

Barreto, et al. [74] applied advanced exergetic and exergoeconomic analyses to improve energy and economic performance in steam injection gas turbine (STIG) cycle power plants with inlet air cooling through a compression refrigeration machine. Results showed that the Combustion Chamber, Heat Recovery Steam Generator, and Gas Turbine had the greatest potential for improvement, which could be achieved by improving the overall system configuration.

Açıkkalp, et al. [75] presented a novel combined extended-advanced exergy analysis method for assessing thermodynamic systems. The method combined an extended exergy analysis with advanced exergy analysis, aiming to achieve the same criteria as the traditional methods. The method was applied to a gas turbine system, which included a combustion chamber, compressor, and turbine units. The conventional, advanced, and extended exergy analyses were applied separately, but the combined extended-advanced exergy analysis results differed from the advanced and extended exergy analyses. However, the novel analysis tool can apply all these analyses into one simple methodology. The exergy efficiencies of the case study were 28% and 31%, indicating better efficiency in all input parameters. The combined extended-advanced exergy analysis showed a higher exogenous exergy destruction rate, indicating increased relationships between other components.

Uysal and Keçebaş [76] conducted an advanced exergoeconomic analysis of a gas turbine cycle in Inchon, South Korea. It revealed that the endogenous avoidable cost of destruction of a gas turbine was determined to be 584.30 $/h with advanced exergoeconomic analysis. The highest endogenous avoidable cost of destruction was observed for the combustion chamber. The combustion chamber had the endogenous avoidable cost of destruction value of 2831.73 $/h in advanced exergoeconomic analysis.

Caglayan and Caliskan [77] analyzed the exergy of a cogeneration system in a ceramic factory, including a gas turbine unit and spray dryers, under five different environment

conditions. The maximum exergy efficiency was found to be 29.850% at 30°C, while the maximum exergy destruction rate was calculated to be 17810.61 kW. Advanced exergy analysis revealed that the combustor may not be the only component to be intensive for exergy destruction. The overall exergy efficacy of the system exhibited a range of 45% to 47%, with five distinct inactive temperatures contributing to an approximate 15% to 17% increase. The CC and air compressor exhibited increased rates of unavoidable exergy destruction compared to avoidable exergy destruction. Notably, avoidable exergy destruction had a substantial impact on the remaining components.

2.5 Research gaps

In consideration of the literature reviewed formerly, discernible research gaps persist, necessitating diligent analysis and essential modification to augment the efficiency and operational functionality of the CCPP system. These gaps are elaborated below:

1. The utilization of Water-LiBr based VARS for inlet air cooling in previous studies is scant.
2. Most researchers have utilized the single-effect VARS for inlet air cooling, despite the fact that it has a lower COP than a double-effect VARS.
3. The exergy-based sustainability analysis of an inlet air cooler integrated CCPP has not been performed in previous literature.
4. Component-wise exergy analysis of the CCPP is scant in existing literature.
5. Literature on advanced exergy analysis (considering the splitting of exergy destruction) of CCPP is inadequate.
6. The work done on economic analysis based on advanced exergy analysis of CCPP is scant.
7. The optimized combination of design variables has not been acknowledged considering the thermodynamic performance and set-up & operational costs.

2.5 Research Objectives

In light of the identified gaps and insights gleaned from the literature review, the following research objectives are outlined as follows:

1. To decrease the inlet air temperature to the compressor
2. To determine the optimized gas turbine inlet temperature

3. To analyse the combined cycle gas turbine power plant on the basis of various parameters
4. To evaluate the performance of the combined cycle power plant.

Along with the utilisation of the energy, exergy, and optimisation methodologies described in the following chapters, an inlet air cooler has been implemented to achieve these objectives.

CHAPTER 3

SYSTEM DESCRIPTION AND METHODOLOGY

3.1 Introduction

This chapter focuses on the description of CCPP configurations that have undergone multiple analyses, followed by the mathematical modelling of each analysis. This chapter also explores the context of multi-objective optimization, which is effective for identifying an optimal set of solutions (design variables) in order to obtain optimal design and conditions.

3.2 System Description

3.2.1 Combined Cycle power Plant

The CCPP system, equipped with a dual-pressure Heat Recovery Steam Generator (HRSG), is an innovative and efficient power generation arrangement. This integrated system utilizes energy from both the gas and steam cycles, optimizing the total thermal efficiency and power generation. Fig. 3. 1 represents the schematic diagram of CCPP.

3.2.1.1 Gas Turbine Cycle

The basic component of the CCPP system is a highly efficient gas turbine cycle that burns natural gas or other appropriate fuels to generate gases with high pressure and temperature. The gas turbine cycle involves an air compressor that compresses the ambient air based on the designed pressure ratio. Subsequently, the compressed air is directed into the combustion chamber, where fuel is introduced to initiate combustion and generate the high-temperature gas. The gas is subsequently expanded within a gas turbine, generating power that is predominantly utilized by the compressor. The remaining power supplies are used by the generator to create electricity. The actual set up places all three components in a sequence, with the axial type of compressor and turbine being utilized in the assembly.

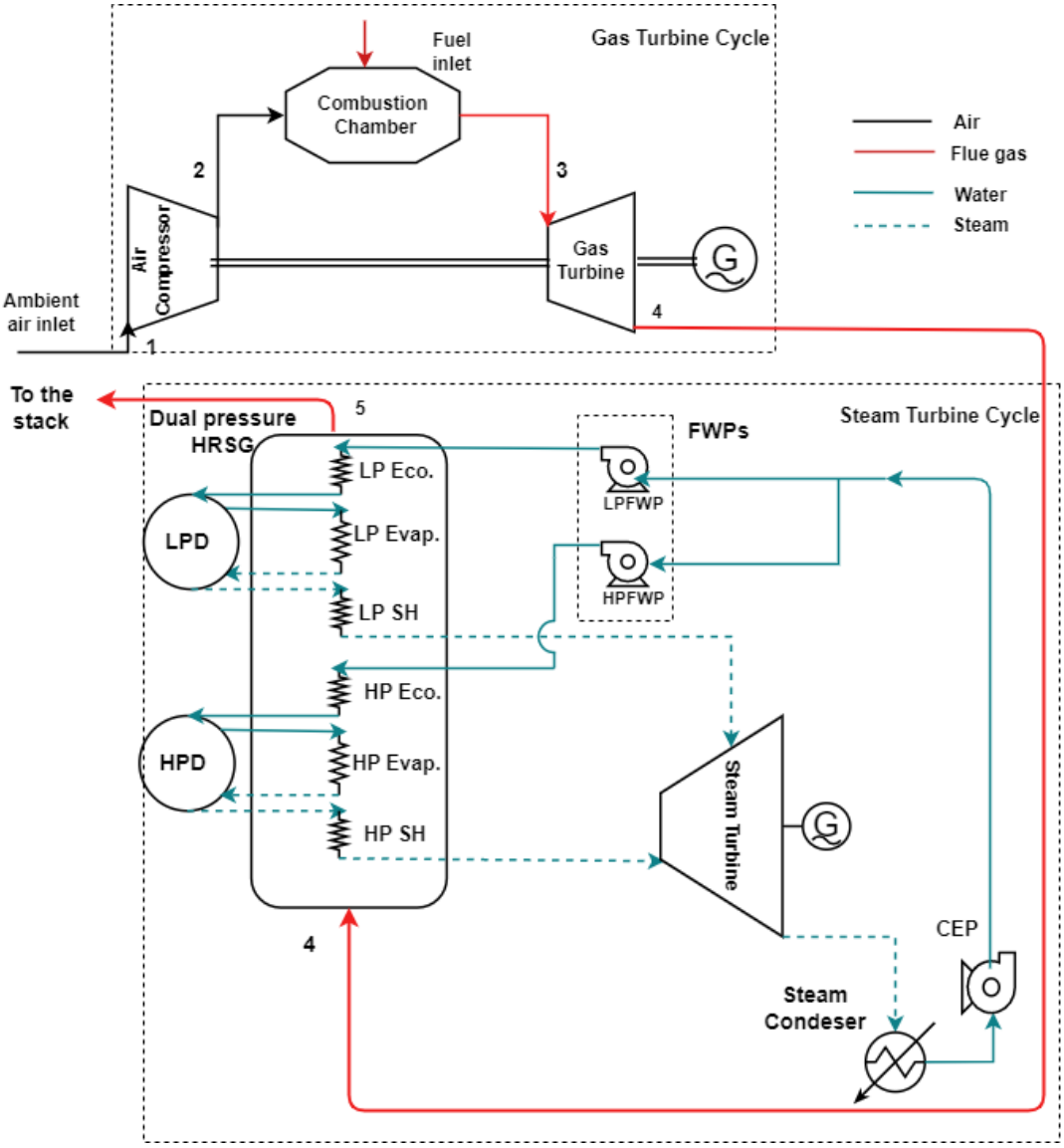

Fig. 3. 1 Schematic diagram of dual pressure HRSG-based CCPP

3.2.1.2 Heat Recovery Steam Generator

The system utilizes a dual-pressure Heat Recovery Steam Generator (HRSG) to effectively absorb waste energy from the exhaust of the gas turbine. The HRSG is engineered with dual pressure levels to maximize steam production and enhance the overall efficiency of the system. The high-pressure part generates steam at elevated temperatures and pressures, while the low-pressure section harnesses extra energy from exhaust gases at lower temperatures.

3.2.1.3 Steam Turbine Cycle

The steam turbine cycle starts with the HRSG, which efficiently recovers and utilizes the heat from the exhaust gases emitted by the gas turbine. The heat that has been regained is utilized to transform water into steam inside the HRSG. The steam turbine receives the high-pressure steam produced in the HRSG. The steam turbine receives the high-pressure steam in its high-pressure section. Moreover, the low-pressure steam is directed to the low-pressure steam turbine, where additional energy is extracted before being condensed. After passing through the LP turbine, the steam is condensed back into water in a condenser. The condensation process releases additional heat, which can be used for district heating or rejected into the environment. The condensate is then fed to a deaerator with the help of a condensate extraction pump (CEP). The water that comes out of the deaerator is pushed back into the HSRG at different pressure levels using a set of Feed water pumps (FWPs).

3.2.2 Inlet air cooling integrated CCPP system

The intake air of the compressor is cooled by the incorporation of an inlet air cooler. A double-effect water-LiBr VARS is used alongside CCPP to cool the air entering the compressor. The double effect Water-LiBr vapour absorption refrigeration system (VARS) is an advanced and highly efficient cooling system specifically engineered for a wide range of uses, such as air conditioning, industrial operations, and refrigeration. This system employs the absorption refrigeration cycle, with water as the refrigerant and lithium bromide (LiBr) as the absorbent.

3.2.3 Double Effect Water-LiBr VARS

Fig. 3. 2 shows the schematic of the Double Effect Water-LiBr VARS. This system comprises an evaporator, absorber, condenser, high-pressure generator (HPG), and low-pressure generator (LPG). Two solution heat exchangers facilitate the transfer of heat from a solution at a higher temperature to a solution at a lower temperature.

The concentrated LiBr solution in the HPG liberates water vapour by the application of heat. This procedure is commonly accomplished by using waste heat sources, such as the exhaust from a gas turbine. The LPG system produces an additional water vapour by using the high temperature of the vapour formed in the HPG system, which is derived

from the leftover solution obtained from the solution heat exchanger (HE 2). Consequently, the process of vapour formation occurs twice in the double effect VARS. The water vapour from both high-pressure gas (HPG) and low-pressure gas (LPG) fed to the condenser is condensed, returning to a liquid state. This process releases the heat that was absorbed by the water vapour to either the surrounding environment or a designated heat sink. Water evaporates in the evaporator, absorbing heat from the surrounding air or the process that has to be cooled. The absorber collects the vapour emitted by the evaporator and facilitates its absorption into the LiBr solution. The outcome is a highly concentrated solution of LiBr together with water vapour. This solution is again pumped to the HPG pressure level which also gains heat first at another solution heat exchanger (HE 1) with the weak solution (weak in refrigerant) returning from the LPG.

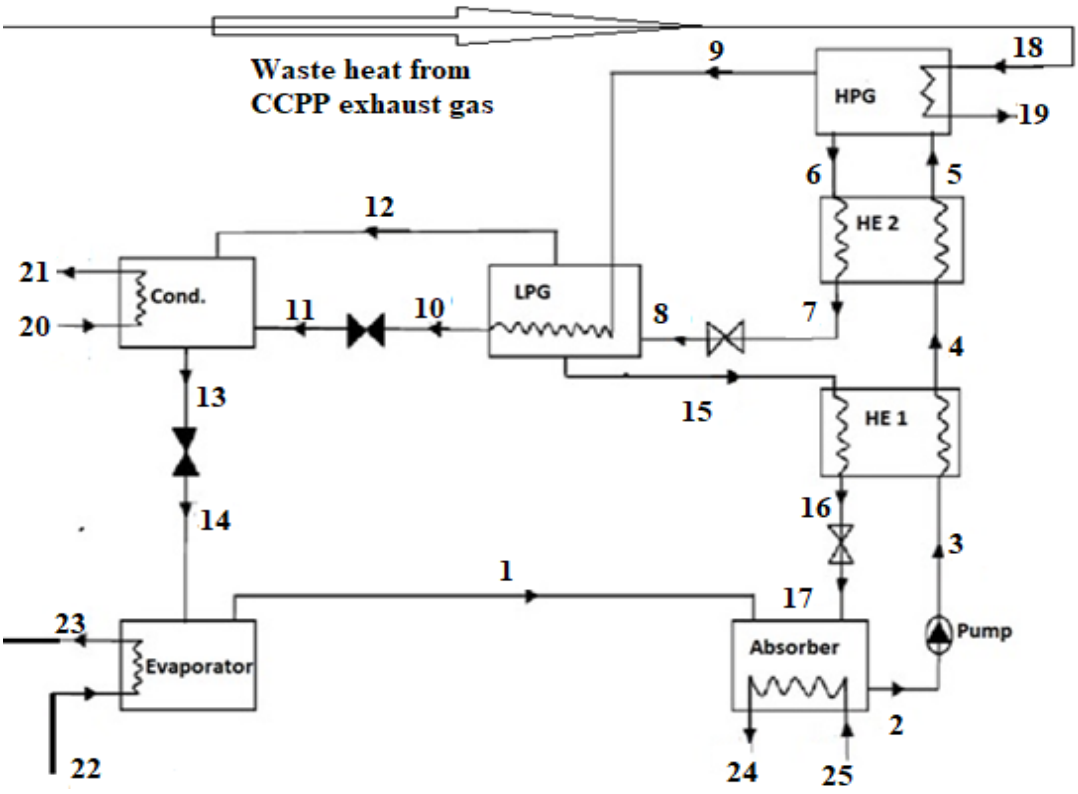

Fig. 3. 2 Schematic diagram of Double-effect Vapour absorption refrigeration system

This double-effect VARS is utilized as an inlet air cooler to cool the ambient air at the inlet of the compressor of the CCPP system.

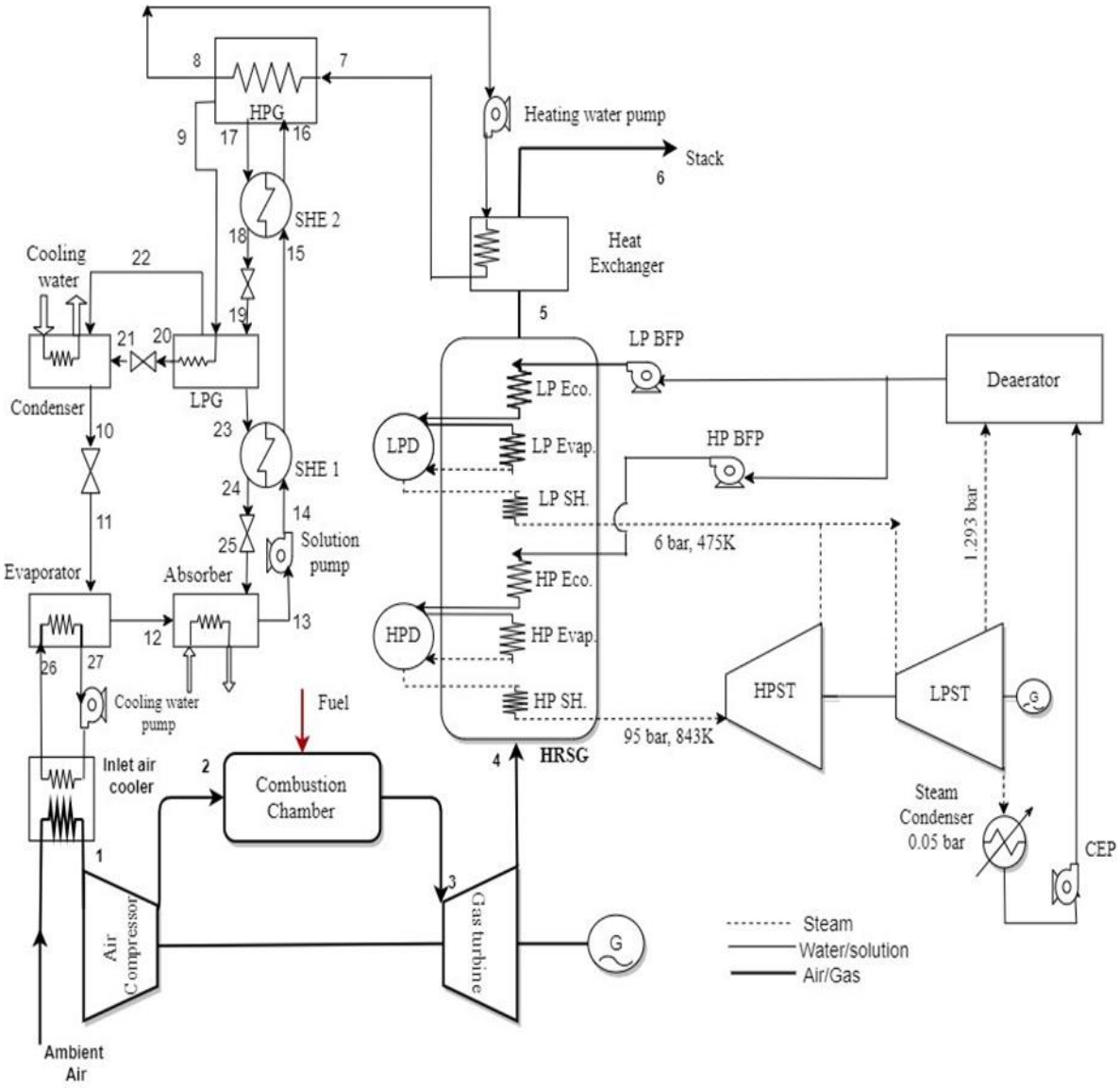

Fig. 3. 3 Dual-pressure HRSG-based CCPP integrated with double effect water-LiBr Absorption refrigeration system

3.3 Mathematical Modelling

This chapter also focuses on the mathematical model development of energy systems utilizing thermodynamic principles including the concept of exergy and economic analysis.

The thermodynamic assessment of an energy system consists of mass balance, energy balance, entropy balance, and exergy balance as detailed below.

3.3.1 Mass balance

The principle of mass conservation is a vital concept in the analysis of all thermodynamic systems. The principle is termed for a control volume, as illustrated in Fig. 3. 4, in the following manner [78]:

$$\sum_k \dot{m}_i - \sum_k \dot{m}_e = \frac{dm_{CV}}{dt} \qquad (3.1)$$

In equation 3.1, m and $\dot{m}$ represent the mass and mass flow rate, correspondingly. The subscripts *e* and *i* indicate the exit and inlet of the control volume, respectively. The term "subscript cv" denotes the control volume.

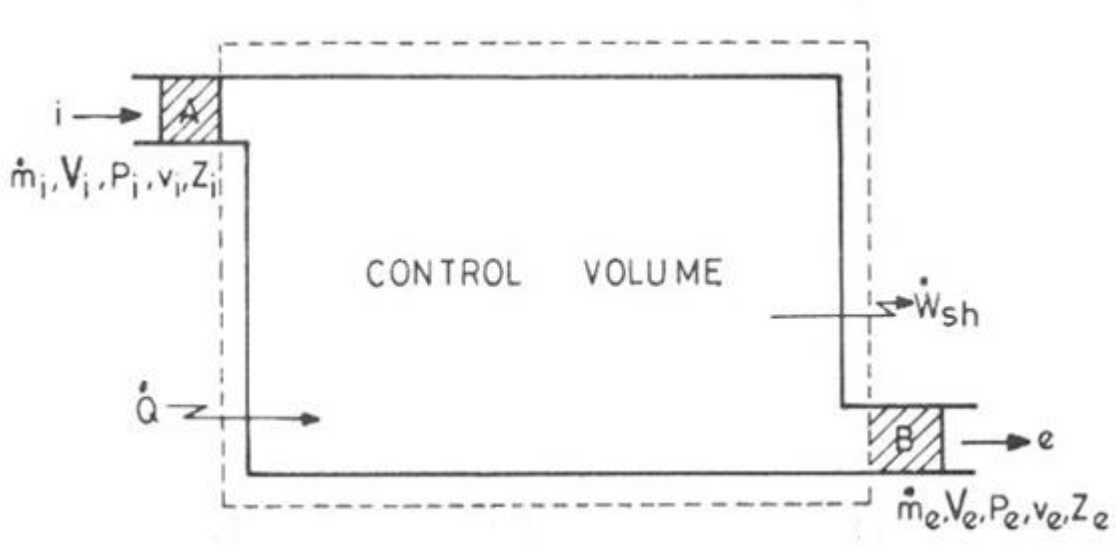

Fig. 3. 4: A control volume for mass and energy balance

3.3.2 Energy Balance

The energy balance of a control volume (as shown in Fig. 3. 4) pertains to the total energy inputs and outputs of a specified control volume. The 1st law of thermodynamics, also referred to as the concept of energy conservation, is described as [79]:

$$\dot{Q} - \dot{W} + \sum_i \dot{m}_i \left(h_i + \frac{V_i^2}{2} + gZ_i\right) - \sum_e \dot{m}_e \left(h_e + \frac{V_e^2}{2} + gZ_e\right) = \frac{dE_{CV}}{dt} \qquad (3.2)$$

where E_{CV} represents the energy of the control volume. $\dot{Q}$ and $\dot{W}$ represent the rates at which heat and work are transferred, respectively, and *t* represents the time. The symbols *V*, *g*, *Z*, and *h* represent the velocity, gravitational acceleration, elevation, and specific enthalpy, respectively.

3.3.3 Entropy Balance

Entropy in a physical system is linked to the quantification of energy that cannot be utilized (i.e., losses). These losses are referred to as entropy generation from a thermodynamic standpoint. The entropy generation rate ($\dot{S}_{gen}$) for a control volume can be expressed as [9]:

$$\dot{S}_{gen} = \sum_e \dot{m}_e s_i - \sum_i \dot{m}_i s_i - \sum_k \frac{\dot{Q}}{T_k} + \frac{dS_{CV}}{dt} \quad (3.3)$$

where *s* is the specific entropy and *T* is the temperature in Kelvin.

3.3.4 Exergy Analysis

Exergy analysis is a method of evaluating a system in a rational manner by applying the principles of the 1st and 2nd laws of thermodynamics [80]. It allows for the assessment and comparison of processes and identifies areas for improvement by reducing irreversibility on a component level [81]. The exergy of a substance is frequently classified into four discrete elements. The two most prevalent forms of exergy are chemical and physical. The two additional forms of exergy, kinetic and potential exergy, are considered insignificant in this context due to the minor changes in elevation and comparatively low speeds [82]. The physical exergy is the highest amount of useful work that can be obtained when a system interacts with an equilibrium state. Moreover, the chemical exergy is linked to the deviation of a system's chemical composition from its chemical equilibrium. It is particularly relevant in processes that include burning and other chemical transformations. Comprehensively, the exergy balance equation in control volume is written as:

$$\frac{dE_{CV}}{dt_j} = \Sigma \left(1 - \frac{T_0}{T_i}\right) \dot{Q}_i - \left(\dot{W} - P_0 \frac{dV_{CV}}{dt}\right) + \sum_i \dot{m}_i e_i - \sum_e \dot{m}_e e_e - \dot{E}x_D \quad (3.4)$$

If there is no energy exchange across the control volume, the above equation can be derived as follows [79]:

$$\dot{E}x_Q + \sum_i \dot{m}_i e_i = \sum_e \dot{m}_e e_e + \dot{E}x_W + \dot{E}x_D \quad (3.5)$$

where e is the exergy and $\dot{E}x_D$ is the rate of exergy destruction in kW.

$$\dot{E}x_D = T_0 \dot{S}_{gen} \quad (3.6)$$

$$\dot{E}x_Q = \left(1 - \frac{T_0}{T_i}\right) \dot{Q}_i \quad (3.7)$$

$$\dot{E}x_W = \dot{W} - P_0 \frac{dV_{CV}}{dt} \quad (3.8)$$

$$e_{ph} = (h - h_0) - T_0(s - s_0) \quad (3.9)$$

where, e_{ph} is the physical exergy function to determine the exergy of any inlet or outlet stream of any component of the CCPP.

3.3.4.1 Plant fuel exergy

The exergy assessment of combustion is determined by taking into account the physical exergies of flowing streams and the chemical exergy of the fuel [81]. The expression for the total exergy of a fluid is given as:

$$\dot{E}x_{total} = \dot{E}x_{ph} + \dot{E}x_{ch} \quad (3.10)$$

The physical component of exergy is calculated using the ideal gas model [83].

$$\dot{E}x_{ph} = \dot{m}_f C_p^h (T - T_0) - \dot{m}_f T_0 \left[C_p^s \ln \frac{T}{T_0} - R \ln \frac{P}{P_0} \right] \quad (3.11)$$

The mean specific heat for enthalpy and entropy can be further calculated by:

$$C_p^h = \frac{1}{T - T_0} \int_{T_0}^{T} C_p dT \quad (3.12)$$

$$C_p^s = \frac{1}{\ln \frac{T}{T_0}} \int_{T_0}^{T} C_p dT \quad (3.13)$$

The chemical exergy fuel $\left(ex_f^{ch}\right)$ is calculated using the following relation [84]:

$$\xi = \frac{ex_f^{ch}}{LHV} \quad (3.14)$$

the value of ξ is close to unity for common gaseous fuels [85]. The value ξ is taken as 1.06 for methane. An experimental correlation is useful to calculate the value of ξ for any gaseous fuel with a composition $C_x H_y$ [86]:

$$\xi = 1.033 + 0.0169 \frac{y}{x} - \frac{0.0698}{x} \quad (3.15)$$

3.3.5 Sustainability Assessment

Exergy analysis is an attractive method to assess the sustainability level of several energy systems. Sustainability is described as a policy of supplying energy resources at a reasonable cost and with little or no environmental impact [87]. Several sustainability indicators have been examined for the CCPP system based on the theoretical foundation for exergy analysis. Moreover, the effect of inlet air cooling on these parameters has been discussed.

The following exergy-based sustainability indicators [88] considered for this study are:

i. Fuel depletion ratio
ii. Environmental effect factor
iii. Environmental sustainability index
iv. Exergetic improvement potential

3.3.5.1 Fuel depletion ratio

The fuel depletion ratio is the ratio of the exergy destruction rate in a component to the fuel exergy. A lower fuel depletion ratio is preferred because it indicates that the system has destroyed less exergy corresponding to fuel exergy. Consequently, more exergy is available at the output [88].

$$Fuel\ depletion\ ratio = \frac{\dot{E}x_{D,componet}}{\dot{E}x_{fuel}} \tag{3.16}$$

3.3.5.2 Environmental effect factor

Environmental effect factor (r_{eef}) is a crucial sustainability factor that is defined as the ratio between waste exergy ratio (WER) and exergetic efficiency. It specifies the severity of environmental damage because of exergy destruction. As a result, r_{eef} is preferred to have low value.

$$WER = \frac{Total\ exergy\ waste}{Total\ exergy\ input} \tag{3.17}$$

$$r_{eef} = \frac{WER}{\eta_{ex}} \tag{3.18}$$

3.3.5.3 Environmental sustainability index

It is another vital parameter to assess the sustainability level of the system. As a definition, it is represented by the reciprocal of r_{eef}. This index has a value between 0 and 1. A higher exergetic efficiency indicates less waste exergy and a lesser environmental impact, resulting in an increased environmental sustainability index (ESI) of the system. Therefore, an ESI close to 1 indicates a more environmentally sustainable system [89].

$$ESI = \frac{1}{r_{eef}} \tag{3.19}$$

3.3.5.4 Exergetic improvement potential rate

The exergetic improvement potential is associated with the combined effect of exergetic efficiency and the exergy destruction rate. A higher improvement potential advocates

that the system requires improvement over time [88]. Hence, a low exergetic improvement potential is preferred.

$$Exergetic\ improvement\ potenial\ rate = (1 - \eta_{ex}) \times \dot{E}x_D \quad (3.20)$$

3.3.6 Exergoeconomic Analysis

Exergoeconomic analysis is an approach that effectively integrates economic principles and thermodynamic evaluations of system components, utilizing exergy analysis as a foundation, to offer insights that are valuable for the design and operation of cost-effective systems. These insights are beyond the scope of traditional energy, exergy, and economic analyses [31]. At the component level of a system, an exergoeconomic analysis reveals (a) the relative cost significant to each component and (b) potential enhancements to the overall cost effectiveness [90]. The cost balance equation for a component 'k' of an energy system can be written as:

$$\dot{C}_{q,k} + \sum_i \dot{C}_{i,k} + \dot{Z}_k = \sum_e \dot{C}_{e,k} + \dot{C}_{w,k} \quad (3.21)$$

The above equation can be rearranged in a more elaborated way.

$$\sum\left(c_e \dot{E}x_e\right)_k + c_{w,k}\dot{W}_k = c_{q,k}\dot{E}x_{q,k} + \sum\left(c_i \dot{E}x_i\right)_k + \dot{Z}_k \quad (3.22)$$

$$\dot{C}_m = c_m \dot{E}x_m \quad (3.23)$$

In the cost balance expression (Equation 3.22), there is no term associated with the cost of the exergy destruction rate of the component. Hence, it may be considered as a hidden cost. The same can be evaluated as follows [28]:

$$\dot{C}_{D,k} = c_{F,k}\dot{E}x_{D,k} \quad (3.24)$$

where $c_{F,k}$ is the cost rate associated with fuel for the component 'k'. The cost factors can be computed by applying the cost balance equations to the several components of the CCPP system.

In Equation 3.22, $\dot{Z}_k$ is the investment cost per unit time of the component 'k'. It can be written as [81]:

$$\dot{Z}_k = \frac{Z_k \times CRF \times \alpha}{N \times 3600} \quad (3.25)$$

$$CRF = \frac{i \times (1+i)^n}{(1+i)^n - 1} \quad (3.26)$$

where N is the number of operating hours in a year, Z_k is the purchase equipment cost (PEC) of a component 'k', α is the maintenance factor, which is commonly taken to be

1.06, and CRF is the capital recovery factor, which is again a function of the interest rate (i) and the span of the plant's operating period (n) in years.

3.3.6 Advanced Exergy Analysis

Thermodynamically, comprehensive exergy analysis is the method that reveals the total irreversibilities produced within a single component or the entire energy system. However, an elementary exergy analysis doesn't reveal what part of exergy destruction is avoidable and what is not. Ultimately the avoidable part of exergy destruction also correlates with the avoidable cost. Tsatsaronis et al. [91] were the first researchers to split the exergy destruction of a system or component into avoidable and unavoidable parts. After the addition of one more splitting (i.e., endogenous and exogenous part of exergy destruction), this method was resurrected as advanced exergy analysis. The avoidable portion of exergy destruction refers to the amount that can be prevented through the enhancement of component design. The rest is an unavoidable component. The total exergy destruction of a component based on this splitting is written as follows:

$$\dot{E}x_{D,k} = \dot{E}x_{D,k}^{AV} + \dot{E}x_{D,k}^{UN} \quad (3.27)$$

In Equation 3.27, the superscripts AV and UN represent the avoidable and unavoidable portions of the exergy degradation of component 'k', respectively.

Based on another splitting associated with endogenous and exogenous parts of exergy destruction, the total exergy destruction of a component is written as follows:

$$\dot{E}x_{D,k} = \dot{E}x_{D,k}^{EX} + \dot{E}x_{D,k}^{EN} \quad (3.28)$$

This second decomposition makes it pertinent to consider that the total exergy destruction in a component is caused not only by the irreversibilities within that component but also by the irreversibilities in the remaining system components resulting from the interaction among them.

3.3.7 Advanced Exergoeconomics

It is prudent to determine the avoidable and unavoidable factors of cost when the same components of exergy destruction and investment cost are known. When combined with advanced exergy analysis (taking into account the avoidable and unavoidable components of exergy degradation), the exergy costing method is referred to as an approach of advanced exergoeconomics. The various combinations of cost of exergy destruction can also be classified as avoidable-endogenous, avoidable-exogenous,

unavoidable-endogenous, and unavoidable-exogenous [76]. However, this study delves deeper into the cost analysis and it is important to determine whether the cost factor associated with exergy destruction is avoidable or unavoidable as well as to examine the impact of various operational parameters on these cost factors.

3.3.8 Optimization

Optimization aims to identify the optimal values for variables that maximize or minimize a multivariate objective function while adhering to a certain set of constraints. Constraints provide the boundaries of a search space, sometimes referred to as the feasible region, in which the solution must be contained [92]. Defining the system boundaries is the initial step in every optimization problem. It is necessary to incorporate all subsystems that have an impact on the performance of the system. When the system becomes excessively intricate, it is frequently preferable to breakdown it into smaller subsystems. The objective function, constraints, and decision variables are all vital components of an optimization problem [93].

3.3.8.1 Objective Function

In mathematical optimization problems, the objective function is a real-valued function that must be maximized or minimized with respect to the set of feasible alternatives. The objective function is determined by the decision maker's desire or goal. Considering the energy systems, the objective function can be based on the performance (energy or exergy efficiency, power generation rate, and COP), cost (cost of exergy destruction, investment cost, and total cost), and environmental standpoint (emissions, fuel utilization), etc. [94].

When there are more than objective functions that are to be maximized or minimized utilizing the same constraints, this type of problem is known as multi-objective optimization [95].

3.3.8.2 Decision variables and constraints

Another crucial aspect in defining an optimization problem is the choice of independent decision variables that accurately represent the potential design possibilities. In order to choose these decision variables, it is crucial to incorporate all significant parameters that might impact the system's performance and cost factor, and exclude variables that have less relevance.

The constraints in a specific design challenge are imposed by limitations on the ranges of the operating parameters, the need to satisfy basic conservation principles, and other limitations. The optimization problems are also addressed by utilizing the restrictions in the form of the search space of operational parameters [96].

3.3.8.3 Optimization Techniques

There are several techniques to solve the optimization problems as described below:

Classical Techniques

The classical optimization method is a basic problem-solving technique for continuous and differentiable functions. It is convenient in the determination of the maximum and minimum of unconstrained differentiable functions. However, these methods have limited use in practical applications as in real life the continuous functions are not so frequent [97].

Numerical Methods

There are several numerical methods based on optimization techniques described below:

Linear programming: Optimization problems where the objective function is linear and the solution space is defined by linear equalities and inequalities.

Integer programming: Optimization problems where the solution set has at least one integer in it.

Nonlinear programming: Optimization problems in which the objective function or constraints or both encompass nonlinear terms of decision variables.

Stochastic programming: Optimization problems in which some of the constraints depend on random variables.

3.3.8.4 Evolutionary algorithms

An evolutionary algorithm employs methodologies that draw inspiration from biological processes such as selection, mutation, recombination, and reproduction [98]. Candidate solutions to the optimization problem are represented as members of a population, and their "living environment" is determined by the fitness function. Fuzzy logic, genetic algorithms (GAs), and artificial neural networks (ANNs) are all examples of evolutionary algorithm methodologies [99]. These methods are elaborated upon in greater detail below.

3.3.8.5 Genetic algorithms (GA)

A genetic algorithm is a search methodology that utilizes evolutionary principles, such as inheritance, learning, selection, and mutation, to find an ideal answer. The process starts by establishing a group of potential solutions referred to as people. It then advances through successive generations, with the evaluation of each individual's fitness. Fitness is determined by the goal function. Subsequently, many individuals are chosen from the present generation according to their fitness and altered to create a fresh population. The subsequent iteration utilizes this updated population, enabling the algorithm to advance toward the intended optimum point [100].

3.3.9 Multi-objective optimization

Optimal conditions rely heavily on the objective function. However, most real applications generally prioritize numerous performance characteristics. When designing thermal and energy systems, efficiency, production rate, output, quality, and heat transfer rate should be maximized, while cost, input, and environmental effects should be minimized. The objective function for a problem can be any of these, however, it is typically more relevant and valuable to consider several objectives. A single-objective optimization issue involves finding the optimal value for a single objective function. Multi-objective optimization refers to the process of optimizing several objective functions. A popular method for minimizing or maximizing numerous goal functions is to merge them into a single function. For illustration, maximizing heat transfer rate is important when designing heat exchangers and cooling systems for electronic equipment [101]. Nevertheless, this leads to increased fluid flow rates and pressure losses due to friction. In recent years, there has been significant attention directed toward multi-objective optimization as an additional approach. This method involves the consideration of two or more relevant objective functions for a given problem, followed by developing a strategy to balance or trade-off each objective function in relation to the others [102].

3.4 Analyses of the CCPP system

The CCPP system has undergone thermodynamic (energy and exergy analyses) as well as exergoeconomic analysis. Further, the advanced exergoeconomic assessment has

also been performed to evaluate avoidable and unavoidable cost factors of the system. The component-wise mathematical modelling is described as follows:

3.4.1 Energy Analysis

3.4.1.1 Air compressor

Air is fed to the compressor at a pressure, P_1 and temperature, T_1. The exit temperature, T_2 is a function of the polytropic efficiency of the compressor (η_{AC}) , pressure ratio (r_p) and specific heat ratio of air (γ_{comp}) as follows:

$$T_2 = T_1 \times \left(1 + \frac{1}{\eta_{AC}}\left(r_p^{\frac{\gamma_{comp}-1}{\gamma_{comp}}} - 1\right)\right) \quad (3.29)$$

Where, η_{AC} is isentropic efficiency of air compressors as given below [103]:

$$\eta_{AC} = 0.91 - \frac{r_p - 1}{300} \quad (3.30)$$

The required work rate for the compressor is defined as the function of the air mass flow rate $(\dot{m}_a)$, the specific heat $(C_{p,comp})$, temperature difference, and mechanical efficiency of the compressor (η_m).

$$\dot{W}_C = \frac{\dot{m}_a C_{p,comp}(T_2 - T_1)}{\eta_m} \quad (3.31)$$

Here, $C_{p,comp}$ [104] and γ_{comp} are determined as follows. Hence,

$$C_{pa} = 1.04841 - \left(\frac{3.3871T}{10^4}\right) + \left(\frac{9.4537T^2}{10^7}\right) - \left(\frac{5.49031T^3}{10^{10}}\right) + \left(\frac{7.9298T^4}{10^{14}}\right) \quad (3.32)$$

$$C_{va} = C_{pa} - 0.287 \quad (3.33)$$

$$C_{p,vap} = 1.8778 - \left(\frac{5.112T}{10^4}\right) + \left(\frac{1.9157T^2}{10^6}\right) - \left(\frac{1.367T^3}{10^9}\right) + \left(\frac{3.723T^4}{10^{14}}\right) \quad (3.34)$$

$$C_{v,vap} = C_{p,vap} - 0.4614 \quad (3.35)$$

$$C_{p,comp} = C_{pa} + \omega_{a,i} C_{p,vap} \quad (3.36)$$

$$C_{v,comp} = C_{va} + \omega_{a,i} C_{v,vap} \quad (3.37)$$

$$\gamma_{comp} = \frac{C_{p,comp}}{C_{v,comp}} \quad (3.38)$$

Where $C_{p,vap}$ and $C_{v,vap}$ represent the specific heat of water vapour at constant pressure and constant volume, respectively. $\omega_{a,i}$ represents the specific humidity of air at the compressor's inlet.

3.4.1.2 Combustion Chamber

The flue gas properties from the exit of the combustion chamber are a function of the lower heating value (LHV) of fuel, airflow rate, and efficiency of the combustor(η_{CC}). The following equation exhibits the energy balance in the combustion chamber:

$$\dot{m}_a C_{pa} T_2 + \dot{m}_f \eta_{CC} . LHV = (\dot{m}_a + \dot{m}_f) C_{pg} T_3 \quad (3.39)$$

The exit pressure is estimated by taking the pressure drop (ΔP_{CC}) into account across the combustion chamber, represented as:

$$P_3 = P_2(1 - \Delta P_{CC}) \quad (3.40)$$

Moreover, the properties of combustion products are evaluated via chemical and thermodynamic equilibrium. The chemical reaction of hydrocarbon fuel is considered, according to Ahmadi, et al. [81], followed by its chemical equilibrium. Specific heat of combustion products is obtained from the standard theory of mixture by taking the specific heat of all constituents individually for different temperatures [105] as follows:

$$C_{pg} = f_h * [y_1 . C_{p,1} + y_2 . C_{p,2} + y_3 . C_{p,3} \dots \dots y_n . C_{p,n}] \quad (3.41)$$

where i = 1,2,3…represents the constituents and $y_i = \frac{m_i}{m}$

f_h is known as the humidity correction factor [39] and represented as

$$f_h = 1 + 0.05\varphi \quad (3.45)$$

where φ is relative humidity at the exit of the inlet air cooler.

3.4.1.3 Gas Turbine

Similar to the compressor, the outlet temperature from the gas turbine is a function of the polytropic efficiency of the gas turbine(η_{GT}), pressure ratio $\left(\frac{P_3}{P_4}\right)$ across the gas turbine, and the specific heat ratio of the gas (γ_g).

$$T_4 = T_3 \times \left(1 - \eta_{GT}\left(1 - \left(\frac{P_3}{P_4}\right)^{\frac{1-\gamma_g}{\gamma_g}}\right)\right) \quad (3.46)$$

A correlation for isentropic efficiency of the gas turbine as a function of $\left(\frac{P_3}{P_4}\right)$ can be given as [103]:

$$\eta_{GT} = 0.90 - \frac{\left(\frac{P_3}{P_4}\right) - 1}{250} \quad (3.47)$$

The expansion work rate from the gas turbine is estimated by considering the flue gas flow rate$(\dot{m}_g)$, gas-specific heat(C_{pg}), the temperature difference between entry & exit, and mechanical efficiency(η_m).

$$\dot{W}_{GT} = \dot{m}_g C_{pg}(T_3 - T_4).\eta_m \quad (3.48)$$

3.4.1.4 Dual Pressure HRSG

A dual-pressure HRSG consists of two sections responsible for heat recovery from hot exhaust gas. Each section has two distinct pressure levels, high pressure, and low pressure sections. Each component in these sections works under the designed pressure levels [106]. For each level of pressure, there is a pinch point (PP) and approach point (AP). The pinch point is the minimum temperature difference between the gas and the water stream at the entry of the evaporator [107]. Pinch points and approach points are considered constant in this study. With each section and component, the temperature of the exhaust gases keeps on decreasing as the heat transfer occurs in each component as shown in **Error! Reference source not found.**.

Each component of the dual pressure HRSG maintains energy balance for the gas and water streams. The equations listed in Table 3. 1.**Error! Reference source not found.**

Table 3. 1 Energy balance equations in HRSG components

HRSG component	**Equations**
HP Superheater	$\dot{m}_g C_{pg}(T_4 - T_{4a}) = \dot{m}_{s,hp}(h_{hp,sh,ex} - h_{hp,sh,in})$
HP Evaporator	$\dot{m}_g C_{pg}(T_{4a} - T_{4b}) = \dot{m}_{s,hp}(h_{hp,evap,ex} - h_{hp,evap,in})$
HP Economizer	$\dot{m}_g C_{pg}(T_{4c} - T_{4d}) = \dot{m}_{s,hp}(h_{hp,eco,ex} - h_{hp,eco,in})$
LP Superheater	$\dot{m}_g C_{pg}(T_{4b} - T_{4c}) = \dot{m}_{s,lp}(h_{lp,sh,ex} - h_{lp,sh,in})$
LP Evaporator	$\dot{m}_g C_{pg}(T_{4d} - T_{4e}) = \dot{m}_{s,lp}(h_{lp,evap,ex} - h_{lp,evap,in})$
LP Economizer	$\dot{m}_g C_{pg}(T_{4e} - T_5) = \dot{m}_{s,lp}(h_{lp,eco,ex} - h_{lp,eco,in})$

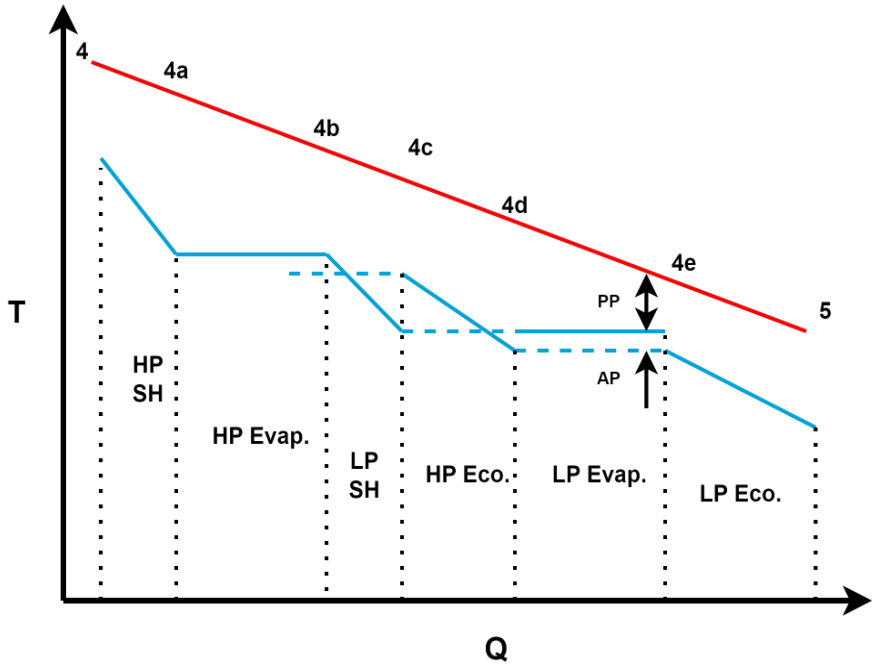

Fig. 3. 5 Temperature and heat transfer in several components of HRSG

3.4.1.5 Steam Turbines

The work generation rate from HPST is obtained by the expansion of steam coming from the high-pressure section of HRSG up to lower pressure. This steam is adiabatically mixed with low-pressure steam coming from the low-pressure section of HRSG. Likewise, the mixed steam is expanded in LPST to produce further work. The energy equations of both steam turbines are as follows:

$$\dot{W}_{HPST} = \eta_m . \eta_{isen,hpst} . \dot{m}_{s,hp} \left(h_{hp,sh,ex} - h_{lp,sh,ex} \right) \quad (3.49)$$

$$\dot{m}_{s,lp} + \dot{m}_{s,hp} = \dot{m}_s \quad (3.50)$$

Here, $\dot{m}_s$ is the total mass flow rate of steam that is to be expanded in LPST.

$$\dot{W}_{LPST} = \eta_m . \eta_{isen,lpst} . \left(\dot{m}_s \left(h_{lp,sh,ex} - h_{lpst,dea,pres} \right) + \left(\dot{m}_s - \dot{m}_{s,dea} \right) \left(h_{lpst,dea,pres} - h_{lpst,ex} \right) \right) \quad (3.51)$$

3.4.1.6 Steam condenser

The exiting steam from LPST is condensed in the steam condenser. The energy balance between the steam and cooling water is depicted as follows:

$$\left(\dot{m}_s - \dot{m}_{s,dea} \right) \left(h_{lpst,ex} - h_{cond,ex} \right) = \dot{m}_{cw} C_{p,cw} \left(t_{cw,in} - t_{cw,out} \right) \quad (3.52)$$

3.4.1.7 Deaerator

The deaerator removes dissolved gases such as O_2 and CO_2 from the condensate by using steam bled from the LPST; as a result, feed water is obtained at deaerator pressure. Deaerator pressure is calculated using the deaerator temperature ratio for the optimum heat recovery from the exhaust [108]:

$$\theta_{dea} = \frac{T_{fw,dea,ex} - T_{cond}}{T_{fw,sat,hp} - T_{cond}} \tag{3.53}$$

The mass flow rate of steam bled for deaeration is calculated with the help of energy balance as follows:

$$\dot{m}_{s,dea}\left(h_{s,dea,in} - h_{cep,ex}\right) = \dot{m}_s\left(h_{fw} - h_{cep,ex}\right) \tag{3.54}$$

3.4.1.8 Condensate extraction pump

The work input rate in CEP is given as:

$$\dot{W}_{cep} = \frac{\left(\dot{m}_s - \dot{m}_{s,dea}\right)\left(h_{cep,ex} - h_{cond,ex}\right)}{\eta_{m,cep}} \tag{3.55}$$

3.4.1.9 Boiler feed pumps

The required work input rate for low and high-pressure boiler feed pumps (BFP), respectively is written as:

$$\dot{W}_{BFP,lp} = \frac{\dot{m}_{s,lp}\left(h_{hrsg,lp} - h_{fw}\right)}{\eta_{m,BFP,lp}} \tag{3.56}$$

$$\dot{W}_{BFP,hp} = \frac{\dot{m}_{s,hp}\left(h_{hrsg,hp} - h_{fw}\right)}{\eta_{m,BFP,hp}} \tag{3.57}$$

The total work output of standalone CCPP is given as:

$$\dot{W}_{CCPP} = \dot{W}_{GT} - \dot{W}_C + \dot{W}_{HPST} + \dot{W}_{LPST} - \dot{W}_{BFP,lp} - \dot{W}_{BFP,hp} - \dot{W}_{cep} \tag{3.58}$$

The efficiency of standalone CCPP is established as

$$\eta_{CCPP} = \frac{\dot{W}_{CCPP}}{\eta_{CC}.\dot{m}_f LHV} \tag{3.59}$$

3.4.2 Analysis of Double effect water-LiBr VARS

The working fluid for a series flow double-effect vapour absorption refrigeration system (DE-VARS) comprises a refrigerant (Water) and an absorbent (LiBr) [109]. It is modeled using the approach and assumptions of Gomri and Hakimi [110]. The thermodynamic properties (enthalpy and entropy) of water-LiBr solution at different points are calculated using the correlations suggested by Pátek and Klomfar [111].

The concentrations of strong solution (function of the absorber and evaporator temperature) and weak solution (function of VARS condenser and LPG temperature) are calculated as follows [112]:

$$X_{ss} = \frac{49.04+1.125t_a-t_e}{134.65+0.47t_a} \quad (3.60)$$

$$X_{ws} = \frac{49.04+1.125t_{LPG}-t_c}{134.65+0.47t_{LPG}} \quad (3.61)$$

The concentration of the medium solution(X_{ms}) lies between X_{ws} and X_{ss}. X_{ms} is calculated using an iterative method unless the energy balance in LPG reaches up to 0.0001 kW [110]. Hence, the mass flow rate of weak, strong, and medium solutions is calculated using the concentration values. The energy balance in LPG is given as follows:

$$Q_{LPG} = m_9h_9+m_{19}h_{19} = m_{20}h_{20} + m_{22}h_{22} + m_{23}h_{23} \quad (3.62)$$

The concentration value should be less than the critical concentration to eliminate crystallization at any point in the system. The critical concentration as a function of temperature (in °C) was developed by a dynamic simulation model for double effect VARS [113]. It can be expressed as:

$$X_C = 0.0809 \times t + 61.341 \quad (3.63)$$

The heat load in HPG and evaporator is given by:

$$Q_{HPG} = m_{g,HPG}C_{pg}(T_5 - T_6) = m_9h_9 + m_{17}h_{17} - m_{16}h_{16} \quad (3.64)$$

$$Q_{evap} = m_{a,evap}C_{pa}(T_0 - T_1) = m_{12}h_{12} - m_{11}h_{11} \quad (3.65)$$

The energy balance in the condenser and absorber is written as follows:

$$Q_{cond} = m_{w,cond}C_{pw}(\Delta T_{w,cond}) = m_{21}h_{21} + m_{22}h_{22} - m_{10}h_{10} \quad (3.66)$$

$$Q_{abs} = m_{w,abs}C_{pw}(\Delta T_{w,abs}) = m_{12}h_{12} + m_{25}h_{25} - m_{13}h_{13} \quad (3.67)$$

The overall performance of VARS is estimated by evaluating its COP, represented as:

$$COP = \frac{Q_{evap}}{Q_{HPG}+\dot{W}_{SP}} \quad (3.68)$$

where $\dot{W}_{SP}$ is work input rate to the solution pump and expressed as:

$$\dot{W}_{SP} = m_{13}\frac{(P_{HPG}-P_{abs.})}{n_{sp}\rho_{13}} \quad (3.69)$$

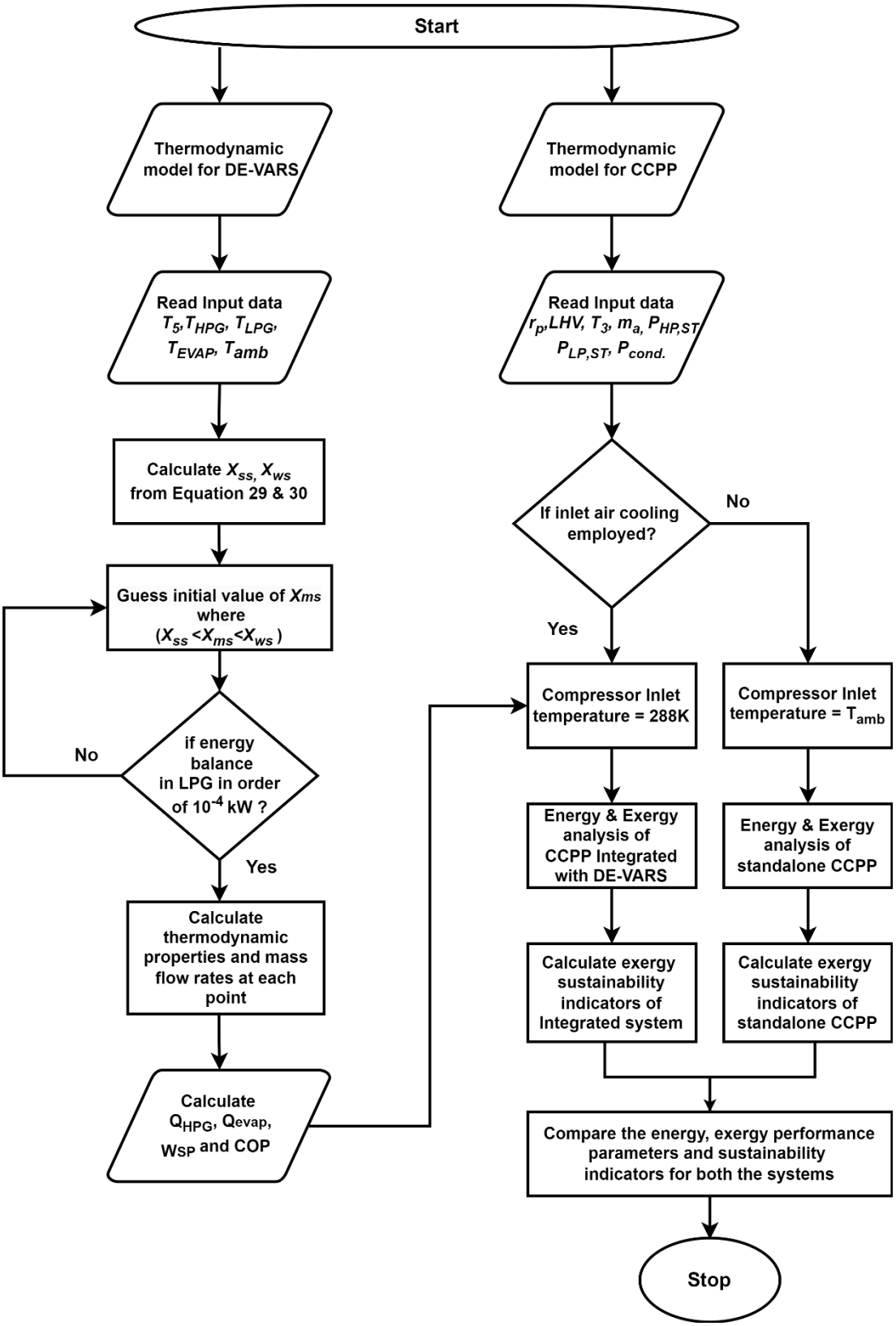

Fig. 3. 6 A mathematical framework and flow-chart of the thermodynamic simulation process

3.4.3 Integrated system (CCPPV)

Now, the total work output of an inlet air cooling integrated system (i.e., CCPPV) is calculated as

$$\dot{W}_{CCPPV} = \dot{W}_{CCPP} - \dot{W}_{SP} \tag{3.70}$$

$$\eta_{CCPPV} = \frac{\dot{W}_{CCPPV}}{\eta_{CC}.\dot{m}_f LHV} \tag{3.71}$$

3.4.4 Exergetic Assessment of CCPP system

The equations for exergy destruction rate and exergetic efficiency are presented in Table 3. 2.

Table 3. 2 Equations for exergy destruction rate and exergetic efficiency for various components

Component	**Exergy destruction rate**	**Exergetic efficiency**
Air compressor	$\dot{E}x_{D,AC} = \dot{E}x_1 - \dot{E}x_2 + \dot{W}_{AC}$	$\eta_{ex,AC} = \frac{\dot{E}x_2 - \dot{E}x_1}{\dot{W}_{AC}}$
Combustion chamber	$\dot{E}x_{D,CC} = \dot{E}x_2 - \dot{E}x_3 + \dot{E}x_f$	$\eta_{ex,CC} = \frac{\dot{E}x_3}{\dot{E}x_2 + \dot{E}x_f}$
Gas turbine	$\dot{E}x_{D,GT} = \dot{E}x_3 - \dot{E}x_4 - \dot{W}_{GT}$	$\eta_{ex,GT} = \frac{\dot{W}_{GT}}{\dot{E}x_3 - \dot{E}x_4}$
HRSG	$\dot{E}x_{D,HRSG} = \sum_{i,HRSG} \dot{E}x - \sum_{o,HRSG} \dot{E}x$	$\eta_{ex,HRSG} = \frac{\sum_{i,water} \dot{E}x - \sum_{i,steam} \dot{E}x}{\dot{E}x_4 - \dot{E}x_5}$
HPST	$\dot{E}x_{D,HPST} = \dot{E}x_{i,HPST} - \dot{E}x_{o,HPST} - \dot{W}_{HPST}$	$\eta_{ex,HPST} = \frac{\dot{W}_{HPST}}{\dot{E}x_{i,HPST} - \dot{E}x_{o,HPST}}$
LPST	$\dot{E}x_{D,LPST} = \dot{E}x_{i,LPST} - \dot{E}x_{o,LPST} - \dot{W}_{LPST}$	$\eta_{ex,LPST} = \frac{\dot{W}_{LPST}}{\dot{E}x_{i,LPST} - \dot{E}x_{o.LPST}}$

Condenser	$\dot{E}x_{D,Cond} = \sum_{i,Cond} \dot{E}x - \sum_{o,Cond} \dot{E}x$	$\eta_{ex,Cond} = 1 - \frac{\dot{E}x_{D,Cond}}{\sum_{i,Cond} \dot{E}x}$
Boiler feed pump	$\dot{E}x_{D,BFP} = \dot{E}x_{i,BFP} - \dot{E}x_{o,BFP} + \dot{W}_{BFP}$	$\eta_{ex,BFP} = \frac{\dot{E}x_{o,p} - \dot{E}x_{i,p}}{\dot{W}_{BFP}}$

The mathematical framework of the simulation process used for the thorough study and comparison to achieve improvement post inlet air cooling using DE-VARS is shown in Fig. 3. *6*.

3.4.5 Cost Balance

It is necessary to compute the cost balance equations for each component in order to ascertain the cost factors applicable to each stream. Given that each component of the CCPP system has multiple inlets and outlets, the number of unknown cost factors exceeds the number of components. As a result, additional equations are necessary. The supplementary equations, referred to as auxiliary exergoeconomic equations, are devised to facilitate the computation of individual cost factors [114]. Thus, the formation of a following system of linear equations can be accomplished by implementing the general cost balance equation (Equation 14) and subsequently solving it.

$$[\dot{E}x_k] \times [c_k] = [\dot{Z}_k] \tag{3.72}$$

where $\dot{E}x_k$, c_k, and $\dot{Z}_k$ represent the matrices of exergy rate, cost vector, and capital cost rate. Moreover, the purchase equipment cost (PEC, in $) function of each component is given below:

- **Air Compressor**

  The PEC of an air compressor depends on the air flow rate, its pressure ratio, and isentropic efficiency as formulated as follows [115]:

  $$Z_{AC} = C_{A1}\dot{m}_{air}\frac{1}{C_{A2}-\eta_{AC}}\frac{P_2}{P_1}\ln\frac{P_2}{P_1} \tag{3.73}$$

  where $C_{A1} = 44.71\ \$/(kg/s)$ and $C_{A2} = 0.95$

- **Combustion Chamber**

The PEC of the combustion chamber is a function of air flow rate and TIT as described below:

$$Z_{CC} = C_{CC1}\dot{m}_{air}\{1 + \exp[C_{CC2}(T_3 - C_{CC3})]\}\frac{1}{0.995-\frac{P_3}{P_2}} \quad (3.74)$$

where $C_{CC1} = 28.98\ \$/(kg/s)$, $C_{CC2} = 0.015\frac{1}{K}$ and $C_{CC3} = 1540$

- **Gas Turbine**

The PEC of the gas turbine depends on the gas flow rate, TIT, gas turbine expansion ratio, and isentropic efficiency as formulated below:

$$Z_{GT} = C_{G1}\dot{m}_{gas}\frac{1}{C_{G2}-\eta_{GT}}\ln\frac{P_3}{P_4}\{1 + \exp[C_{G3}(T_3 - 1570)]\} \quad (3.75)$$

where $C_{G1} = 301.45\ \$/(kg/s)$, $C_{G3} = 0.025\frac{1}{K}$ and $C_{G2} = 0.95$

- **HRSG**

The cost function of dual pressure HRSG is the function of low and high pressures, steam flow rates at different levels, temperatures of steam and gas, and the gas flow rate.

$$Z_{HRSG} = C_{H1}\sum f_{p,i}\, f_{T,steam,i} f_{T,gas,i}\left(\frac{\dot{Q}}{\Delta T_{ln,i}}\right)^{0.8} + C_{H2}\sum(f_{p,j}\dot{m}_{steam,j}) + C_{H2}\dot{m}_g^{1.2} \quad (3.76)$$

where

$$f_{p,i} = 0.0971\frac{P_i}{30\ bar} + 0.9029 \quad (3.77)$$

$$f_{T,steam,i} = 1 + \exp\left(\frac{T_{out,steam,i}-830}{500\ K}\right) \quad (3.78)$$

$$f_{T,g,i} = 1 + \exp\left(\frac{T_{out,g,i}-990}{500\ K}\right) \quad (3.79)$$

- **Steam Turbine**

The PEC of the steam turbine depends on the steam turbine inlet temperature, the isentropic efficiency of the steam turbine, and the work produced by the steam turbine.

$$Z_{ST} = C_{S1}\left(\dot{W}_{ST}\right)^{0.7}\left(1 + \left(\frac{0.05}{1-\eta_{ST}}\right)^3\right)\left\{1 + \exp\left(\frac{T_{in,steam}-866\ K}{10.42\ K}\right)\right\} \quad (3.80)$$

Where $C_{S1} = 3880.5\ \frac{\$}{kW^{0.7}}$

- **Condenser**

The PEC of the steam condenser is the function of heat rejected by the condenser and the cooling water flow rate ($\dot{m}_{CW}$).

$$Z_{Cond.} = C_{C1}\frac{\dot{Q}_{cond}}{k.\Delta T_{ln}} + C_{C2}\dot{m}_{CW} \quad (3.81)$$

where $C_{C1} = 280.74\frac{\$}{m^2}$, $C_{C2} = 746\ \$/(kg/s)$, $k = 2200\frac{\mathrm{W}}{m^2K}$

- **Pump**

  The PEC of the boiler feed pump is the function of pump work and the isentropic efficiency of the pump.

$$Z_{pump} = C_{P1}\left(\dot{W}_P\right)^{0.71}\left(1 + \frac{0.2}{1-\eta_P}\right) \quad (3.82)$$

where $C_{P1} = 705.48\ \$/kW$

3.4.6 Splitting of Exergy destruction rate

Due to both fundamental and economic factors, there will always be a certain level of exergy destruction in any component that is unavoidable. This part is commonly referred to as an unavoidable component of exergy destruction. And here's how it's calculated:

$$\dot{E}x_{D,k}^{UN} = \dot{E}x_{P,k}\left(\frac{\dot{E}x_{D,k}}{\dot{E}x_{P,k}}\right)^{UN} \quad (3.83)$$

The term $\dot{E}x_{P,k}$ represents the exergy rate of the product for a component. The ratio $\left(\frac{\dot{E}x_{D,k}}{\dot{E}x_{P,k}}\right)^{UN}$ is calculated by using the cycle with unavoidable conditions. Subsequently, this ratio is multiplied $\dot{E}x_{P,k}$ by which is determined based on the cycle with real conditions. These conditions of real cycle and unavoidable cycles are given in Table 3. 3 [116, 117]. Furthermore, the remaining portion of exergy destruction (i.e., avoidable exergy destruction, $\dot{E}x_{D,k}^{AV}$) can be written as:

$$\dot{E}x_{D,k}^{AV} = \dot{E}x_{D,k} - \dot{E}x_{D,k}^{UN} \quad (3.84)$$

Table 3. 3 Values considered for real cycle and unavoidable cycle

Parameter	Real Cycle	Cycle with unavoidable Conditions
$\eta_{is,comp}$	86%	94%
$\eta_{is,gt}$	88%	94%
$\eta_{is,st}$	87%	95%
η_{cc}	95%	99%
ε_{sh}	90%	95%
ΔP_{CC}	7%	1%
ε_{cond}	90%	95%
ε_{hrsg}	85%	95%
$\eta_{is,pump}$	85%	95%

The exergy destruction ratios and exergetic efficiency can be adjusted using advanced exergy analysis as described below:

$$y_{mod.,k} = \frac{\dot{E}x_{D,k}^{AV}}{\dot{E}x_{Fuel}} \quad (3.85)$$

$$y_{mod.,k}^{*} = \frac{\dot{E}x_{D,k}^{AV}}{\dot{E}x_{D,total}} \quad (3.86)$$

$$\eta_{ex,k,mod} = \frac{\dot{E}x_{P,k}}{\dot{E}x_{F,k} - \dot{E}x_{D,k}^{UN}} \quad (3.87)$$

3.4.6.1 Avoidable and Unavoidable cost rates

When combined with advanced exergy analysis (taking into account the avoidable and unavoidable components of exergy degradation), the exergy costing method is referred to as an approach of advanced exergoeconomics. The corresponding cost factors of exergy destruction splits can be calculated as follows:

$$\dot{C}_{D,k}^{UN} = c_{F,k}\dot{E}x_{D,k}^{UN} \quad (3.88)$$

$$\dot{C}_{D,k}^{AV} = c_{F,k}\dot{E}x_{D,k}^{AV} \quad (3.89)$$

Similarly, costs associated with investment can be split as avoidable or unavoidable as shown below:

$$\dot{Z}_k^{UN} = \dot{E}x_{P,k}\left(\frac{\dot{Z}_k}{\dot{E}x_{P,k}}\right)^{UN} \quad (3.90)$$

$$\dot{Z}_k^{AV} = \dot{Z}_k - \dot{Z}_k^{UN} \quad (3.91)$$

The modified exergoeconomic factor can be determined as follows:

$$f_{k,modified} = \frac{\dot{Z}_k^{AV}}{\dot{Z}_k^{AV} + c_{F,k}\dot{E}x_{D,k}^{AV}} \quad (3.92)$$

The aforementioned equations and correlations are employed in various analyses to derive outcomes and facilitate additional optimisation of CCPP.

CHAPTER 4

MODEL VALIDATION

4.1 Introduction

Validating the numerical model for this system is essential to avoid discrepancies and attain trust in the precision of the results. The study results have been validated by prior experimental experiments that have been published. The CCPP model and the double-effect VARS intake air cooling system model have been validated by experimental findings from several studies.

4.2 Validation of combined cycle power plant

Fig 4. 1 illustrates the block layout of an actual combined power plant station located in Delhi, India. The plant comprises two intercooled gas turbine cycles, each with a capacity of 104 MW, and a steam turbine with a capacity of 122 MW, resulting in a total capacity of 330 MW. The facility operates under the Pragati Power Corporation Ltd, located in New Delhi, where the experimental data was collected [118]. The plant data (shown in Table 4. *1*) were incorporated into the MATLAB code, which was adjusted to reflect the component arrangement of the aforementioned plant. The outcomes are acquired to illustrate the comparison between data from mathematical modelling and data from experiments.

Table 4. 1 Data collected for model validation

Description	Value
Compressor inlet temperature	30℃
Compressor discharge temperature	390℃
Gas turbine inlet temperature	1085℃
Gas turbine exhaust temperature	560℃
Compressor pressure ratio	11.5
Compressor & turbine efficiencies	85%

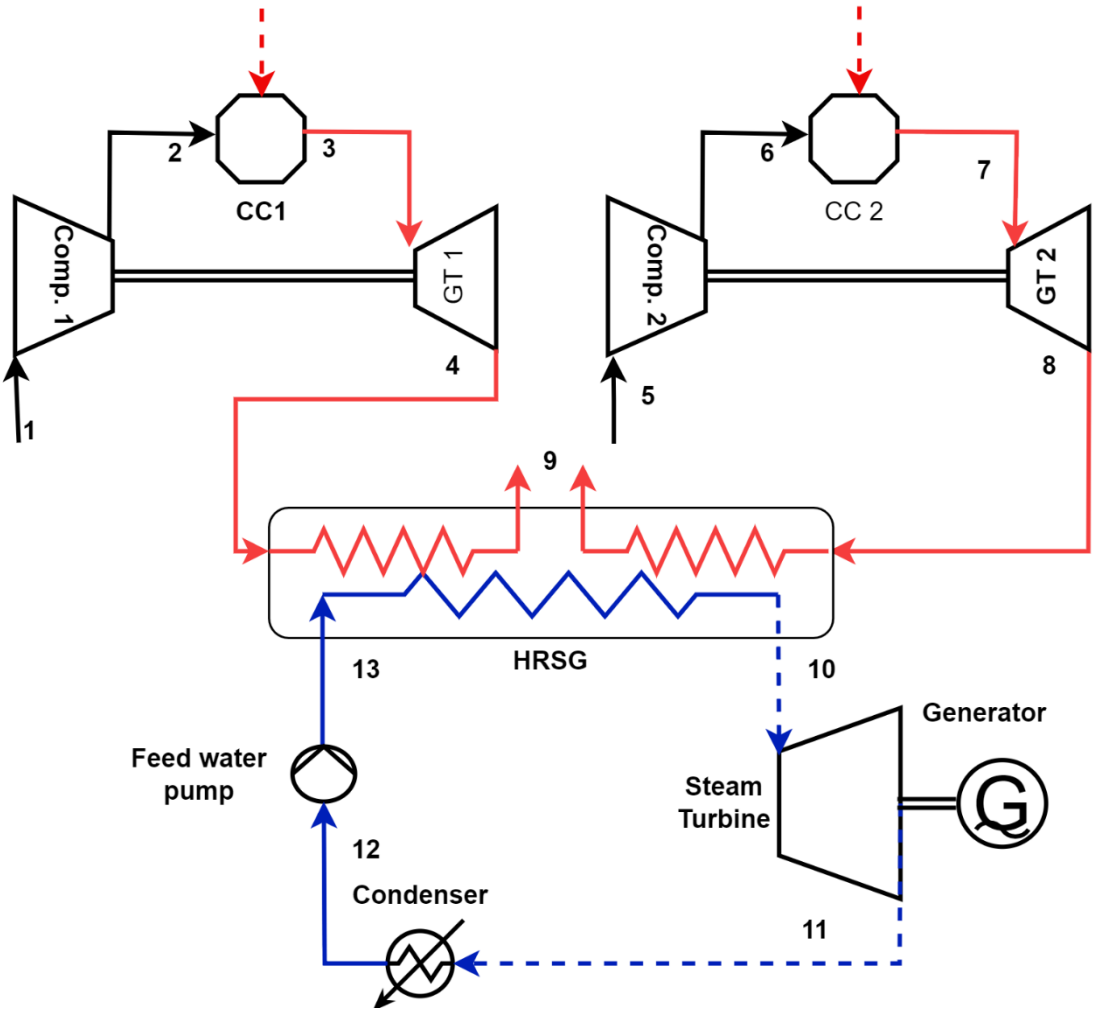

Fig 4. 1 Schematic of an actual combined cycle power plant (2 Gas Turbines - 104 MW x 2 and 1 Steam Turbine – 122 MW x 1)

Fig 4. 2 displays the temperature variations of gas/air at multiple locations in both operation and simulation. The temperature data is obtained by supplying plant data into a mathematical model that includes parameters such as compressor pressure ratio, atmospheric conditions, and fuel intake. The simulated model has been evaluated using the fixed gas turbine intake temperature as of the operational data. A maximum deviation under 5.37% in the corresponding temperatures was observed, indicating a satisfactory level of concurrence between the operational and simulated models.

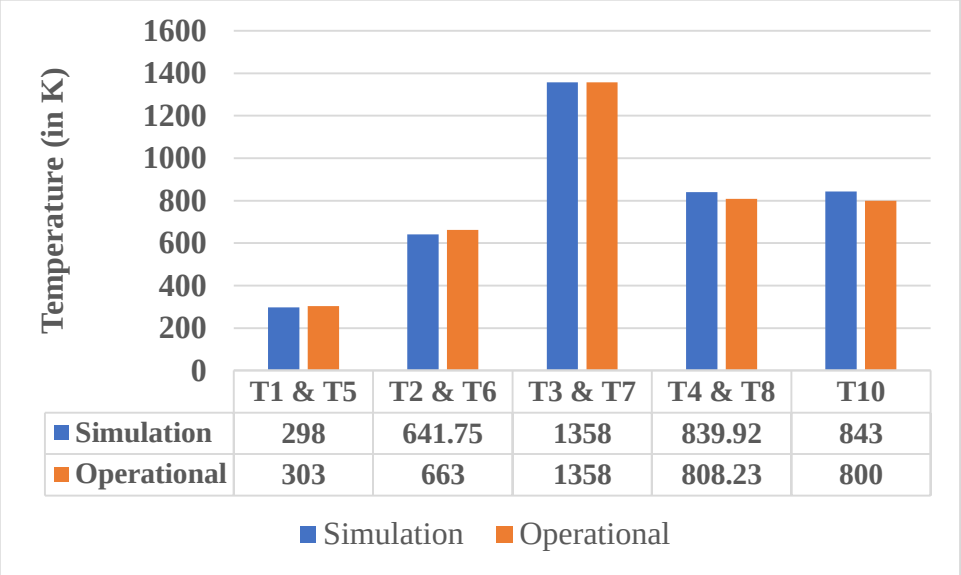

Fig 4. 2 Comparison of air/gas temperature in simulation and operational data at different locations of CCPP

Fig 4. *3* shows the comparison of gas turbine cycle efficiency as an effect of maximum temperature ratio (T_3/T_1) for both actual plant data and mathematical simulation studies. The primary determinant of the maximum temperature ratio is the gas turbine inlet temperature (T_3) which varies between approximately 1170 K and 1750 K. The compressor inlet temperature (T_1) remains constant at 293K, representing the ambient air temperature. It has been observed that the rise in temperature ratio results in a corresponding rise in the efficiency of gas turbines. The efficiency in both scenarios shows similar variation and demonstrates strong agreement. The generated model deviates by a maximum of 3.08% from the actual plant data throughout the whole range of variation. This difference is initially observed at a temperature ratio of 4, after which it gradually decreases. Additionally, at a temperature ratio of 5.39 (T_3= 1579K), it was observed that the efficiency of gas cycles in both cases is nearly equivalent, before the difference begins to rise again. The disparity between the simulation findings and the plant data may be attributed to dissimilar variations in isentropic efficiency (of the compressor and gas turbine) with temperature. Also, the differences in the combustion mechanism and the heat losses in both cases may contribute to the aforesaid deviation.

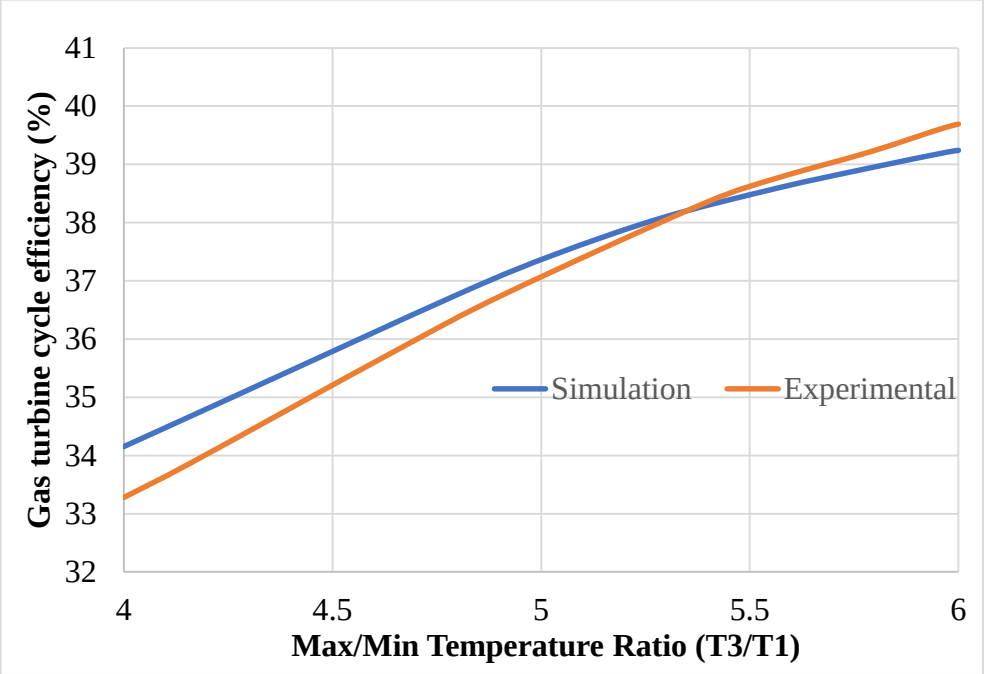

Fig 4. 3 Comparison of experimental and simulation studies for gas turbine efficiency vs. Temperature ratio

4.3 Validation of double-effect VARS

The model of water-LiBr double-effect VARS has been validated by an experimental study of the micro-scale absorption chiller by Yin, et al. [119]. The input parameters of this study are used for generating results from the program made in MATLAB. Table 4. 2 shows the comparison of results obtained from the present model and experimental results of Yin, et al. [119] for validation. The simulated results exhibit a maximum deviation of 5.34% from the experimental data.

Table 4. 2 Model validation of Water-LiBr double-effect VARS

Input Parameters	**Value**		
Chilled water inlet temperature	13.9 °C		
Cooling water temperature	30.78 °C		
Cooling water flow rate	1.546 kg/s		
Chilled water flow rate	0.5616 kg/s		
Output Value	**Simulation results**	**Experimental results [119]**	**Difference between**

			simulation and experimental results
Chilled water outlet temperature	7.05 °C	7 °C	0.71%
Cooling effect	17.19 kW	16.63 kW	3.36%
COP	1.0851	1.03	5.34%

CHAPTER 5

RESULTS AND DISCUSSION

5.1 Introduction

To enhance understanding of the system's performance, it is essential to conduct numerous investigations to evaluate how the performance of CCPP varies under different operating conditions. This chapter provides an explanation of the results pertaining to energy, exergy, sustainability, exergoeconomic analysis, advanced exergoeconomic analysis, and multi-objective optimization. Exergy analysis is employed to investigate different thermal processes, particularly power production in the CCPP system, and can provide valuable insights for devising strategies and guidelines to enhance energy efficiency and effectiveness. The exergy analysis involves calculating the rate at which exergy is being destroyed and the exergy efficiency of each section in the CCPP. It also estimates the total exergy efficiency of the CCPP system. Exergy analysis is convenient for determining and measuring the origin of inefficiencies in the systems, specifically related to each component. Additionally, the enhanced system (inlet air-cooled integrated CCPP system) is being evaluated for its sustainability. The exergy-based sustainability assessment of the system evaluates and analyses various sustainability indicators of a standalone CCPP and an integrated CCPP to determine fuel utilization. In addition, the exergoeconomic analysis demonstrates the use of the exergy costing approach to evaluate the rate at which exergy is destroyed, as well as the cost of investment for each component and how it changes with different operational parameters.

By utilizing optimization, the most advantageous compromises between the CCPP system's numerous operating parameters can be determined. The presence of total cost rate and efficiency in the systems renders a single objective optimization strategy incapable of generating an exact optimal solution. An outcome of this is the implementation of a multi-objective optimization strategy on the system.

This chapter explores several output key parameters. The performance parameters include total work generation, overall exergy efficiency, and total exergy destruction rate, and cost parameters include cost rate of exergy destruction cost, investment cost, and total operational cost. In addition, a thorough parametric analysis is undertaken to improve the comprehension of the system's performance. This study examines the effects of varying various key design parameters on the system's performance. The use of a multi-objective genetic algorithm optimisation technique allows for the determination of the most optimal design parameters by establishing specific objective functions. The input data used for simulation is presented in Table 5. 1.

Table 5. 1 Input data used for analysis

Component	**Parameter**	**Unit**
Compressor	Compression ratio (P_r) = 12-21	-
	Mechanical efficiency $(\eta_{m,comp})$ = 98.5%	-
Combustion chamber	Combustion efficiency (η_{cc}) = 99%	-
	LHV of fuel = 47200	kJ/kg
	Fuel composition CH_4 = 90%	-
	Air composition (by volume) = 21% O_2, 79% N_2	-
	Pressure drop = 7% of entry pressure	-
Gas turbine	Turbine inlet temperature (T_3) = 1400-1750	K
	Flue gas exhaust pressure = 1.093	bar
	Mechanical efficiency $(\eta_{m,GT})$ = 98.5%	-
HRSG	HP steam pressure = 95	bar
	LP steam pressure = 5	bar
	HP steam temperature = 843	K
	LP steam temperature = 475	K
Stack	Stack exhaust temperature ≥ 393	K
Steam turbine	Mechanical efficiency $(\eta_{m,ST})$ = 98.5%	-

	Isentropic efficiency $(\eta_{isen,LPST})$ = 92%	-
	Isentropic efficiency $(\eta_{isen,HPST})$ = 88%	-
	Steam quality at LPST exit = 0.88	-
Steam Condenser	Condenser pressure = 0.05	bar
Deaerator	Deaerator pressure = 1.293	bar
	Deaerator temperature ratio = 0.27	-
VARS	Effectiveness of HPG = 0.96	-
	Evaporator temperature (T_{evap}) = 278	K
	HRSG exhaust temperature ≤ 423	K
	SHE Effectiveness = 70%	-
	Mechanical Efficiency of the solution pump $(\eta_{m,SP})$= 95%	-

5.2 Effect of ambient temperature and inlet air cooling on energy parameters

Based on the thermodynamic equations mentioned in the methodology section, energy analysis is the primary criterion for the assessment of the CCPP and CCPPV (i.e., inlet air cooler inetgrated CCPP). Moreover, the ambient temperature, which is a crucial factor, affects the energy performance of CCPP. Energy performance encapsulates the specific work output and thermal efficiency as the key performance parameters for the comparison of both cases. The CCPP configuration used for energy analysis includes a gas turbine cycle, a dual-pressure HRSG, and a steam cycle with high and low-pressure turbines. The CCPP has been assessed using the base input parameters. In addition to the data provided in Table 5.1, the ambient temperature is assumed to be 15 ℃ (288K), which is the designated ISO ambient temperature for gas turbines. At this ambient temperature, there is no input air cooling being used. Therefore, the compressor inlet temperature (CIT) is equal to the ambient air temperature (i.e., 15 ℃). The CCPP exhibits the performance as 620.91 kJ/kg of specific work output and 61.96% of the thermal efficiency.

If the ambient temperature rises, the existing CCPP is equipped with a DE-VARS based intake air cooler (CCPPV) to ensure that the CIT remains at 288K. The ambient temperature is considered to rise in intervals of 2K, and the enhancement in performance is determined. Both performance parameters show the improvement. Nevertheless, there is a consistent rise in the specific work from 2.07% to 5.04% over the range, while the thermal efficiency improves up to an ambient temperature of 296K (8K degree of cooling) and then begins to decline. The improvement in thermal efficiency increases from 1.58% (at 290K) to 1.64% (at 296K), and then declines to 1.25% (at 360K). The decline can be attributed to a reduction in steam specific work, which occurs at higher ambient temperatures due to the DE-VARS requiring a greater HRSG exhaust energy to produce a cooling effect. The subsequent set of results displays the impact of ambient temperature on the absolute scale for both the CCPP and CCPPV systems.

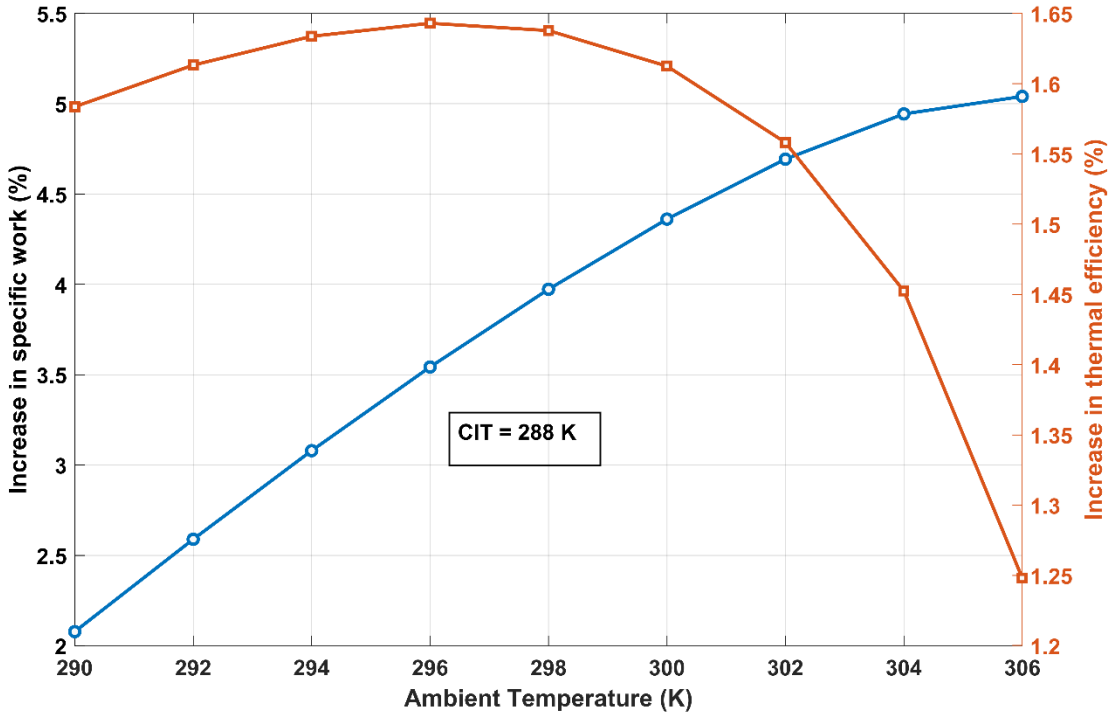

Fig. 5. 1 Performance enhancement as an implementation of inlet air cooler with increasing ambient temperature

The plant-specific work output as a function of ambient temperature is depicted in Fig. 5. 2. The compressor's inlet temperature rises as the ambient temperature rises, resulting in more compression work. As a result, the specific work output rate in CCPP decreases. When the compressor inlet temperature (CIT) is fixed at 288K via inlet air cooling, the

CCPPV-specific work increases by 2.07% to 5.04% when the ambient temperature rises from 290 K to 306 K. On the contrary, CCPPV-specific work decreases across the range because, in order to keep CIT at 288K, VARS must fetch more heat from the HRSG as the ambient temperature rises.

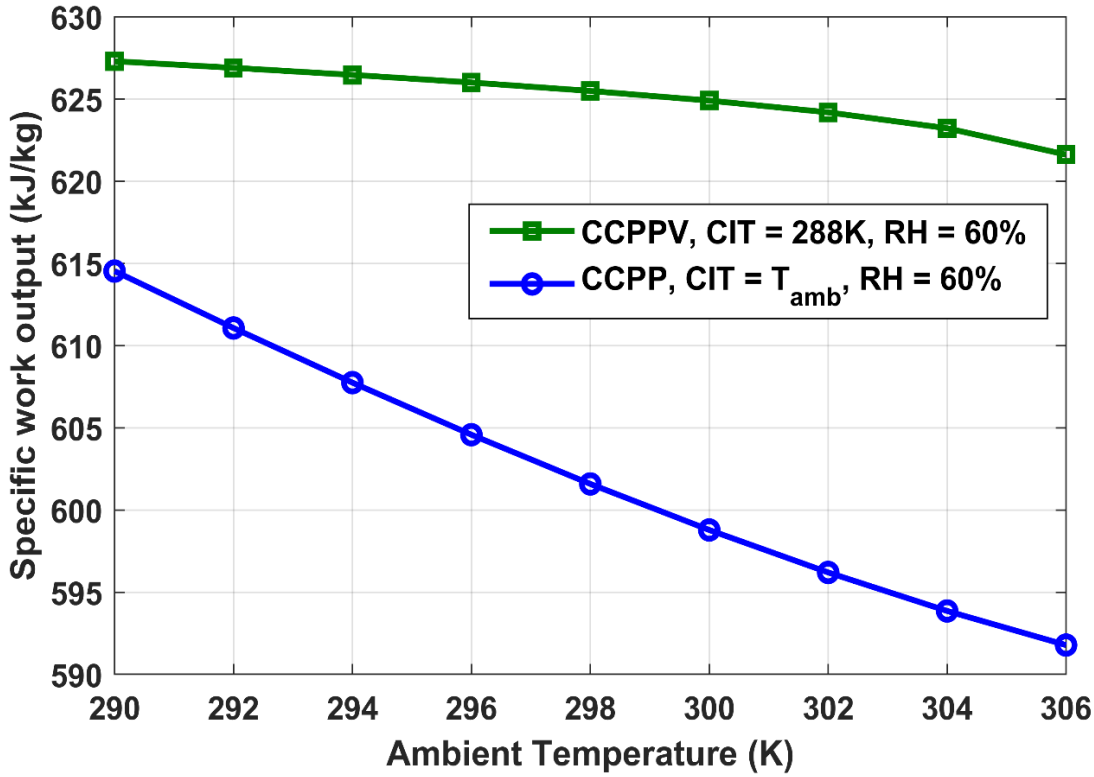

Fig. 5. 2 Effect of ambient temperature on specific work output

As shown in Fig. 5. 3, increased temperature exhaust is required at the HRSG exit. It eventually leads to less STC-specific work. The COP of VARS as a function of ambient temperature is also shown in Fig. 5. 3. When the ambient temperature rises from 290 K to 306 K, the COP falls to 0.83 from 1.44. The reason for this is that as the ambient temperature rises, the evaporator must absorb more heat from the surrounding air in order to maintain CIT at 288K. To increase the heat intake from the evaporator, the VARS must generate more refrigerant, which ultimately increases the heat supplied by the HRSG exhaust at the HPG. However, as the ambient temperature rises, the heat input in HPG rises faster than the heat intake in the evaporator, resulting in a decrease in the COP of VARS.

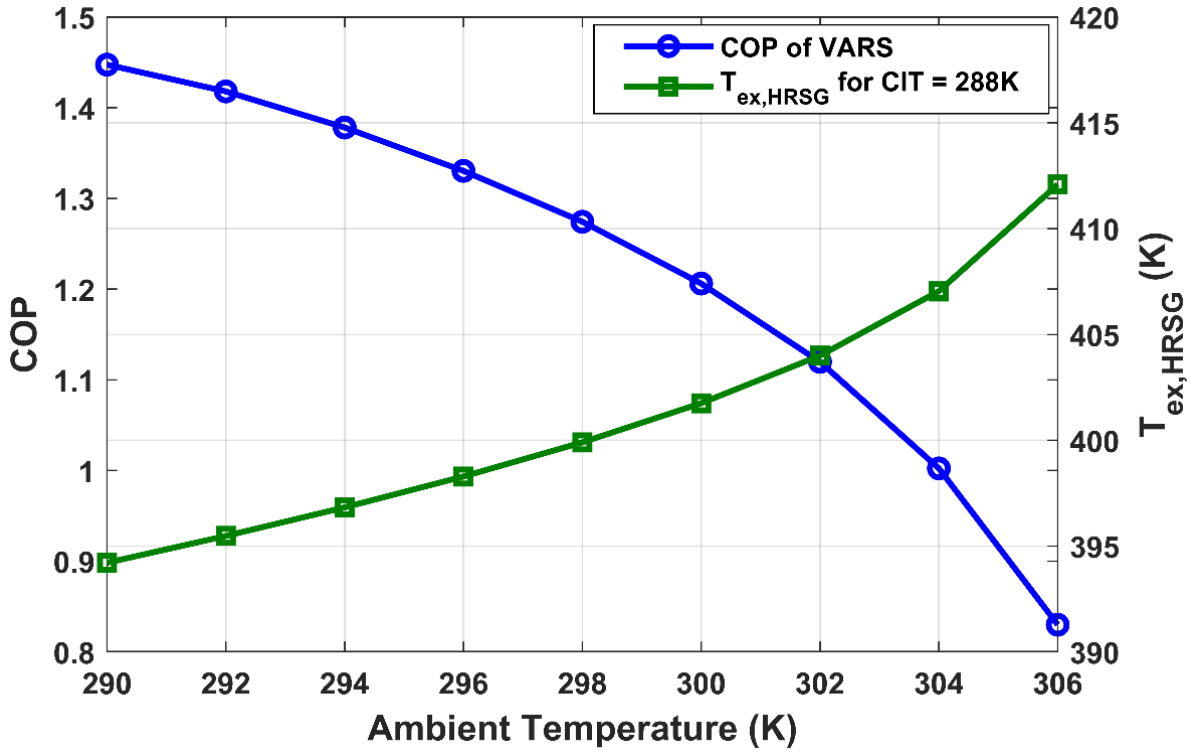

Fig. 5. 3 Effect of ambient temperature on the COP of VARS and HRSG exhaust temperature

Similarly, in Fig. 5. 4, the thermal efficiency is shown as a function of ambient temperature. The thermal efficiency of CCPPV is found to be higher than CCPP, which also indicates lesser fuel consumption per unit of work output. At 290 K, an improvement of 1.58% is observed, which increases to 1.64% at 296 K and then decreases to 1.23% at 306 K. Thus, when the temperature difference between cooled air and ambient air (i.e., the degree of cooling) is 8 K, the greatest increase in thermal efficiency is observed.

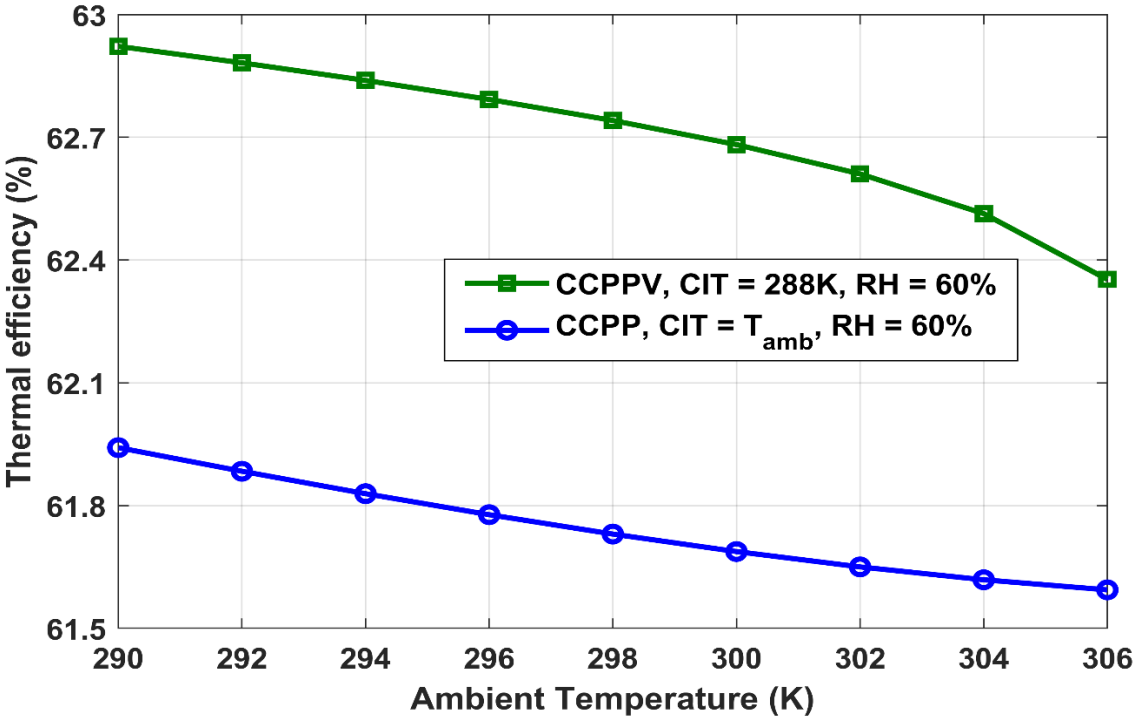

Fig. 5. 4 Effect of ambient temperature on the overall thermal efficiency

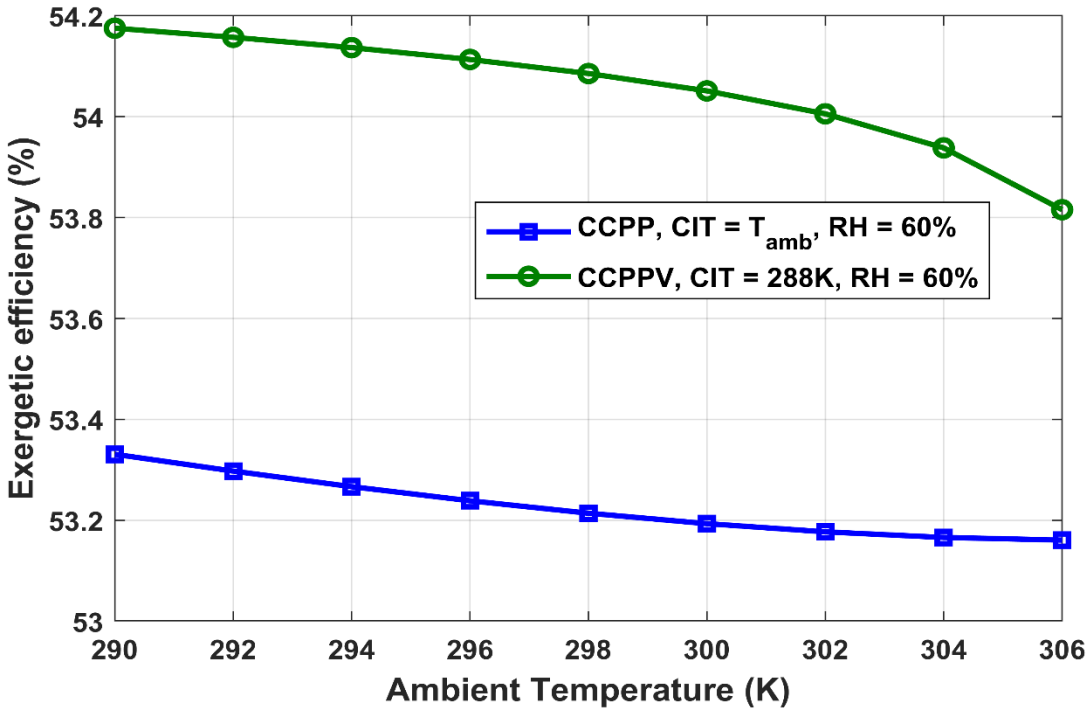

Fig. 5. 5 Effect of ambient temperature on exergetic efficiency

5.3 Effect of ambient temperature and inlet air cooling on exergetic performance

The exergetic performance summarises the exergy destruction rate and exergetic efficiency of each component and the complete CCPP system (as considered in energy analysis).

Fig. 5. 5 depicts the exergetic efficiency of the system as a function of ambient temperature. As the ambient temperature rises, the exergetic efficiency decreases. Since the high CIT decreases the useful exergy (net work output) in CCPP, the resulting exergetic efficiency decreases. After maintaining the CIT at 288 K with the help of inlet air cooling, exergetic efficiency is found to be improved. CCPPV is 1.23% to 1.64% more exergetically efficient than CCPP over the specified ambient temperature range. However, the specific exergy destruction in CCPPV is 0.91% lower than in CCPP at 290K, and the same becomes 1.46% higher at 306 K. This increase is due to an increased fuel supply in the combustion chamber and the addition of the VARS to the existing CCPP. Table 5. 2 shows the component-wise specific exergy destruction in each component. Among all components, the combustion chamber is shown to be the largest exergy destroyer. In both cases, the contribution of the exergy destruction in the combustion chamber is greater than 60.32% of the total specific exergy destruction. These outcomes are owing to the enormous irreversibilities associated with chemical reactions and heat transfer across substantial temperature differences between compressed air and fuel.

Table 5. 2 Specific exergy destruction in various components

Component	**Specific exergy destruction (kJ/kg)**	
	CCPP	**CCPPV**
Compressor	36.45-44.70	44.94-45.93
Combustion chamber	476.55-502.38	478.31-507.94
Gas turbine	58.52-61.40	58.46-60.89
HRSG	106.17-111.58	102.51-110.57
HPST	20.28-20.70	21.13-21.27
LPST	34.81-36.01	36.51-36.76
Steam Condenser	20.35-47.27	21.08-50.32
VARS	-	2.14-2.45

Stack	17.33-23.77	13.13-14.41

Fig. 5. 6 depicts the percentage change in those parameters over the degree of cooling ranges from 2 to 18 K. The rate of fuel intake into the combustion chamber increases as the air cools before the compressor. With it, the rate of increment of total work also increases. Since total work consists of GTC and STC-specific works, as the degree of cooling increases, the increase in gas turbine work increases while the increase in steam turbine work decreases. The increase in gas turbine efficiency is correlated with the constant reduction of compressor work caused by cooled air. The increase in STC-specific work is a result of the increased flue gas rate in the GTC, followed by the HRSG as a result of cooling. However, as the degree of cooling increases, STC-specific work decreases because VARS requires more energy from HRSG exhaust, thereby reducing the steam production rate. And, as the cooling approaches a higher degree, the effect of decreasing increment in STC-specific work becomes predominant. As a result, the rate of increase in total work has been observed to decrease as the degree of cooling increases. After 18K of inlet air cooling, the total work curve could begin to flatten or decrease. In contrast, the increase in the exergetic efficiency of the entire system continues up until 8K of air inlet cooling. After that, it decreases until the degree of cooling reaches 18K.

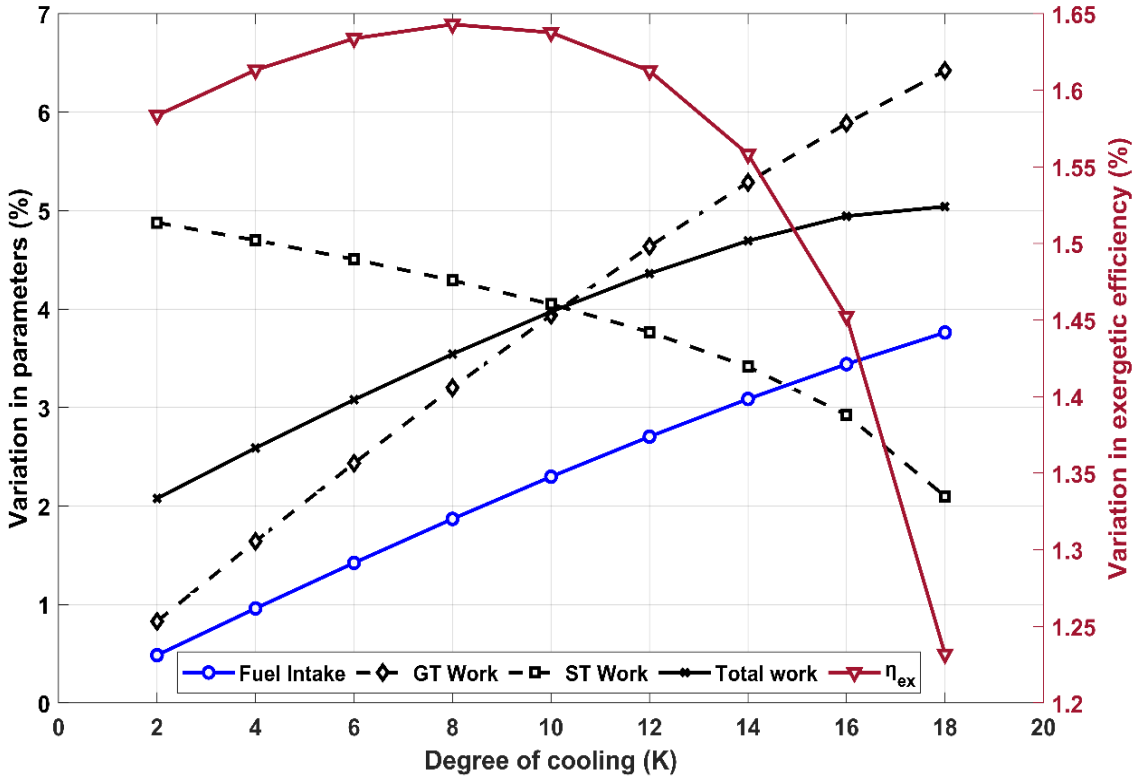

Fig. 5. 6 Effect of degree of cooling on variation in several parameters of CCPPV

This result suggests that the optimal degree of cooling for CCPPV, in terms of total work output and exergetic efficiency, is between 8 and 18 K. CCPPV can operate with a cooling degree of 18K to generate maximum work and with a cooling degree of 8 K to maximize yield in exergetic efficiency. If the price per unit of electricity is high, it may be economically advantageous to operate the CCPPV with 18 K of cooling; if the price per unit of fuel increases, the degree of cooling could approach 8 K in order to balance overall operational costs.

5.4 Effect of inlet air cooling on sustainability indicators

The range of fuel depletion ratios for all major components with and without inlet air cooling is shown in Table 5. 3. The total fuel depletion ratio is shown to be 1.38% to 1.26% lower after using inlet air cooling. It suggests that CCPP with inlet air cooling (i.e., CCPPV) ends up destroying less exergy per unit of fuel than standalone CCPP. Therefore, CCPPV turns out to be more exergetically superior to standalone CCPP. The fuel depletion ratio in both the major exergy destroyers, i.e., the combustion chamber and HRSG, is found to be decreased in CCPPV.

Table 5. 3 Comparison of Fuel depletion ratios

Component	**Fuel depletion ratio*100 (%)**	
	CCPP	**CCPPV**
Compressor	3.27-3.87	3.88 – 4.06
Combustion Chamber	41.35-45.12	41.30 – 43.92
Gas turbine	5.07-5.51	5.04 – 5.27
HRSG	9.21-10.02	8.85-9.57
HPST	1.76-1.85	1.82-1.83
LPST	3.02-3.23	3.15-3.18
Steam condenser	1.82-4.11	1.82-4.29
Total	68.85-70.74	67.60-69.22

Fig. 5. 7 shows the exergetic improvement potential as a function of ambient temperature. CCPPV has shown lower overall exergetic improvement potential than CCPP. However, the increase in improvement potential in CCPPV is rapid with the increase in ambient temperature. At 290 K, the difference in exergetic improvement potential is 3.07%, which decreases to 0.37% at 306 K. The combustion chamber in CCPPV is found to have marginally increased improvement potential by 0.60% to 1.70%, while HRSG has shown a decline of 2.89% to 8.97% in the same.

Fig. 5. 8 demonstrates the effect of increased ambient temperature on the environmental effect factor (r_{eef}) and environmental sustainability index (ESI). The r_{eef} varies between 1.285 and 1.331 for CCPP while for CCPPV, it varies between 1.247 and 1.285, showing a reduction of 2.92% to 3.40% over the specified range. On the other hand, ESI varies from 0.777 to 0.751 for CCPP, and 0.803 to 0.778 for CCPPV, showing an improvement of 3.01-3.52%. Thus, a reduction in r_{eef} shows less damage to the environment after cooling the inlet air. Also, the increase in ESI implies that there is a reduction in waste exergy, as decreasing the CIT is an effective way.

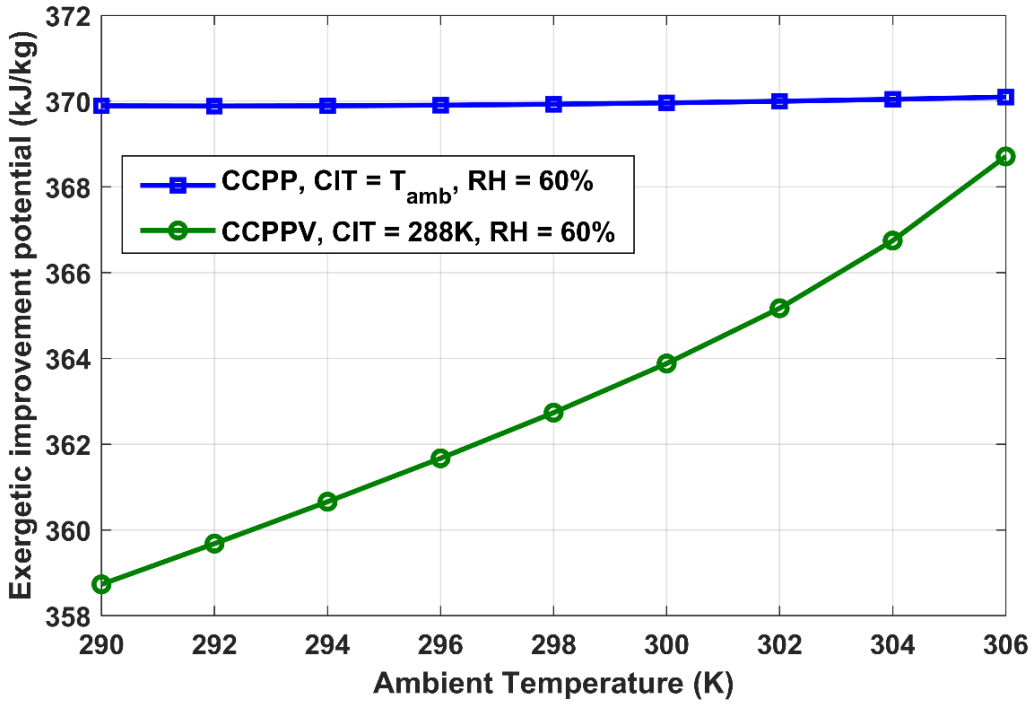

Fig. 5. 7 Effect of ambient temperature on exergetic improvement potential

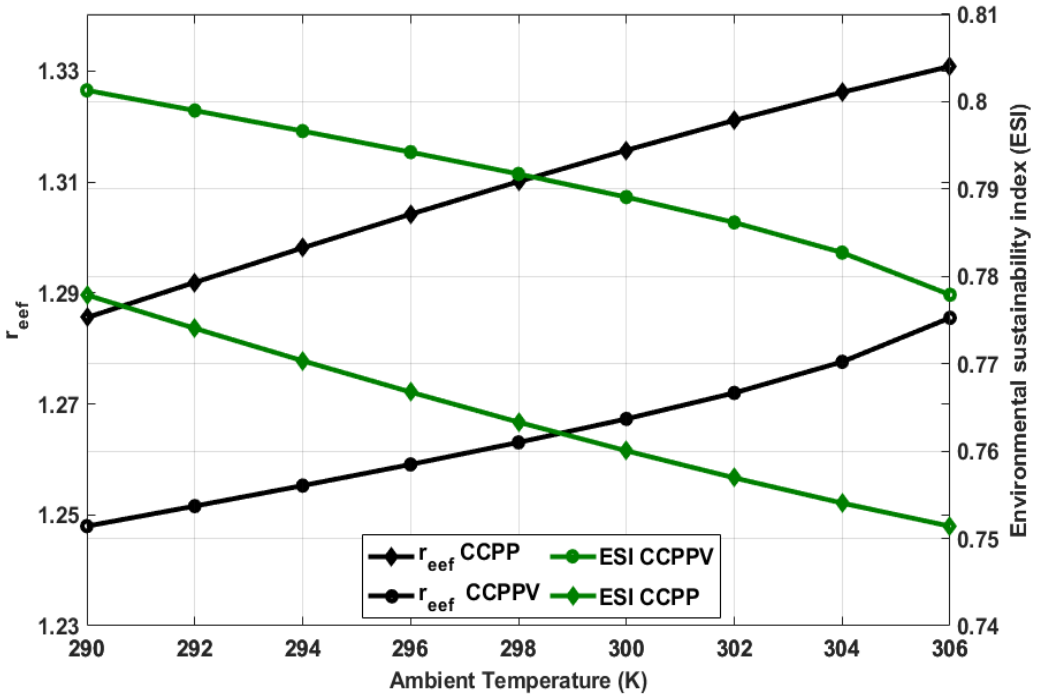

Fig. 5. 8 Effect of ambient temperature on Environmental effect factor and ESI

Fig. 5. 9 shows the variation of r_{eef} with exergetic efficiency. As exergetic efficiency increases, the r_{eef} decreases. Also, the range of r_{eef} shifted even lower after the

integration of inlet air cooling. It implies that the CCPPV is more exergetically efficient because it releases fewer emissions into the atmosphere. Since ESI is reciprocal to r_{eef}, ESI increases with an increase in exergetic efficiency. Therefore, CCPPV has witnessed greater sustainability due to reduced irreversible losses and, hence, efficient utilization of fuel.

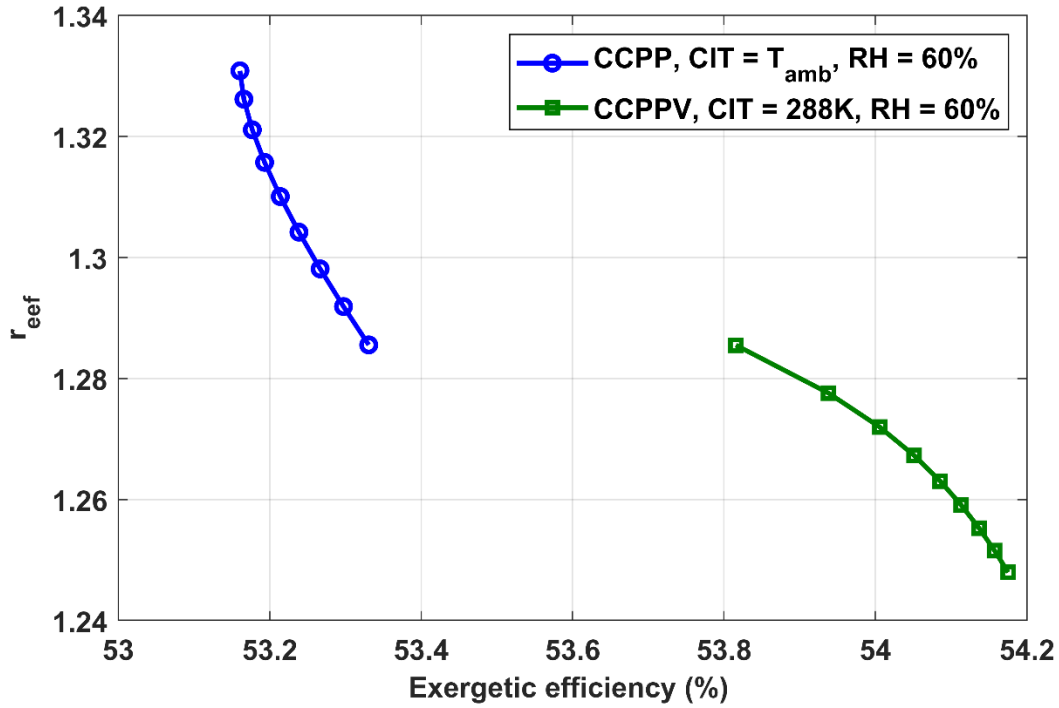

Fig. 5. 9 Variation of exergetic efficiency with Environmental effect factor

5.5 Effect of operating parameters on the components of CCPP

It is imperative to consider the influence of other operational factors such as compressor pressure ratio (PR) and turbine inlet temperature (TIT) along with ambient temperature. A component-by-component assessment is recommended for attaining better insight. This assessment takes into account a typical CCPP configuration that includes a gas turbine cycle, a single-pressure HRSG, and a steam cycle.

Fig. 5. 10 depicts the compressor work versus the specific exergy destruction and exergetic efficiency of the compressor. These exergy parameters are calculated when the ambient temperature falls to 288 K from 306 K. At the leftmost points of each curve, the pressure ratio is 12, increasing to 21 at the rightmost point. The compressor work,

exergy destruction rate, and exergetic efficiency all increase with the pressure ratio for a given ambient temperature. It is observed that decreasing the ambient temperature to 288 K from 306 K results in lesser exergy destruction for any pressure ratio. It is noteworthy to see that exergetic efficiency at ambient temperature 288 K is observed to be lesser than that at 306 K. When the ambient temperature drops, the difference in exergy between the compressor's outlet and inlet decreases faster as the compressor work decreases.

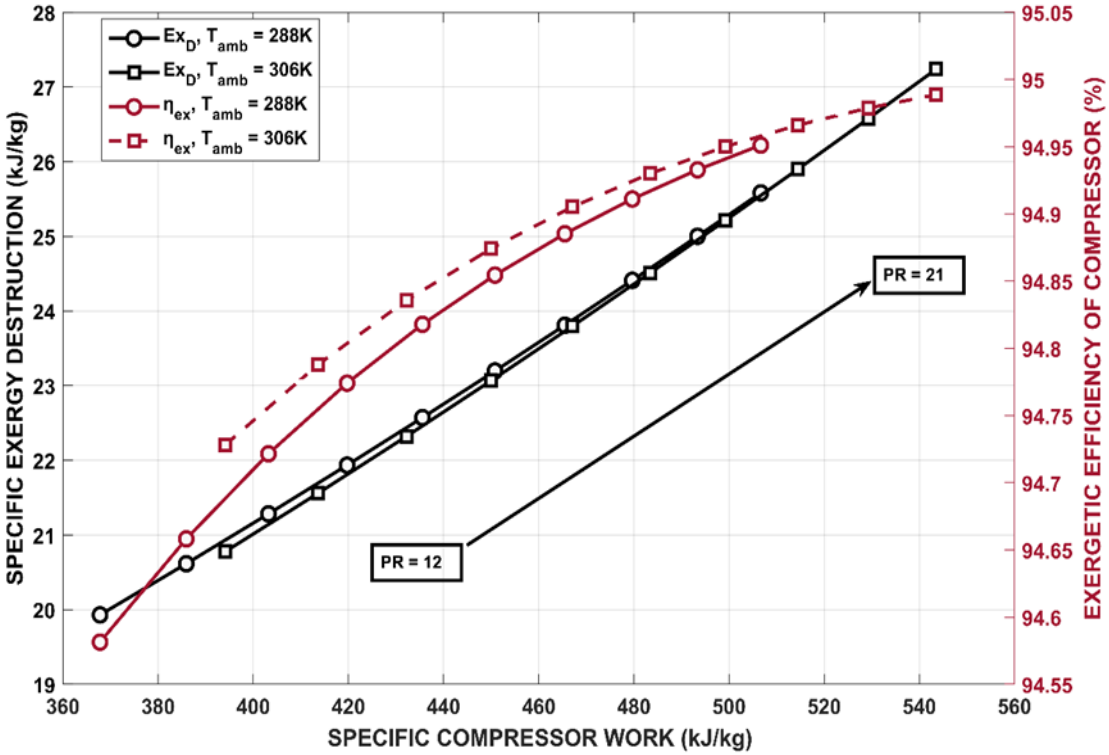

Fig. 5. 10 Effect of pressure ratio and ambient temperature on specific work and exergetic performance of the compressor

Fig. 5. 11 exhibits the pressure ratio versus specific exergy destruction and exergetic efficiency of the combustion chamber for pressure ratios from 12 to 21 and TIT of 1400 K and 1600 K, and ambient temperatures of 288 K and 306 K. For a given TIT, the specific exergy destruction decreases as the pressure ratio increases. On the contrary, for any pressure ratio, the specific exergy destruction increases as TIT increases. Considering the fuel flow rate makes it possible to explain both of these tendencies. When the pressure ratio keeps increasing, the fuel flow rate goes down, which makes it

possible for the exergy destruction in the combustion chamber to continue to fall. When the TIT increases, however, the fuel flow rate increases, resulting in increased exergy destruction. Although exergy destruction increases as ambient temperature drops from 306 K to 288 K, this ultimately reduces the exergy of air at the compressor outlet, increasing the fuel required to achieve a specific TIT. In terms of exergetic efficiency, when the pressure ratio increases for a particular TIT, the fuel flow rate decreases (and thus the exergy of fuel), lowering the net input exergy to the combustion chamber, even though the exergy of air coming from the compressor increases. And the output exergy remains constant (for a constant TIT), resulting in increased exergetic efficiency for increasing pressure ratio. However, when the TIT increases or decreases, the corresponding results are observed. A fall in ambient temperature reduces exergetic efficiency, which can be explained by exergy input and output into the combustion chamber. The difference is more noticeable at higher pressure ratios.

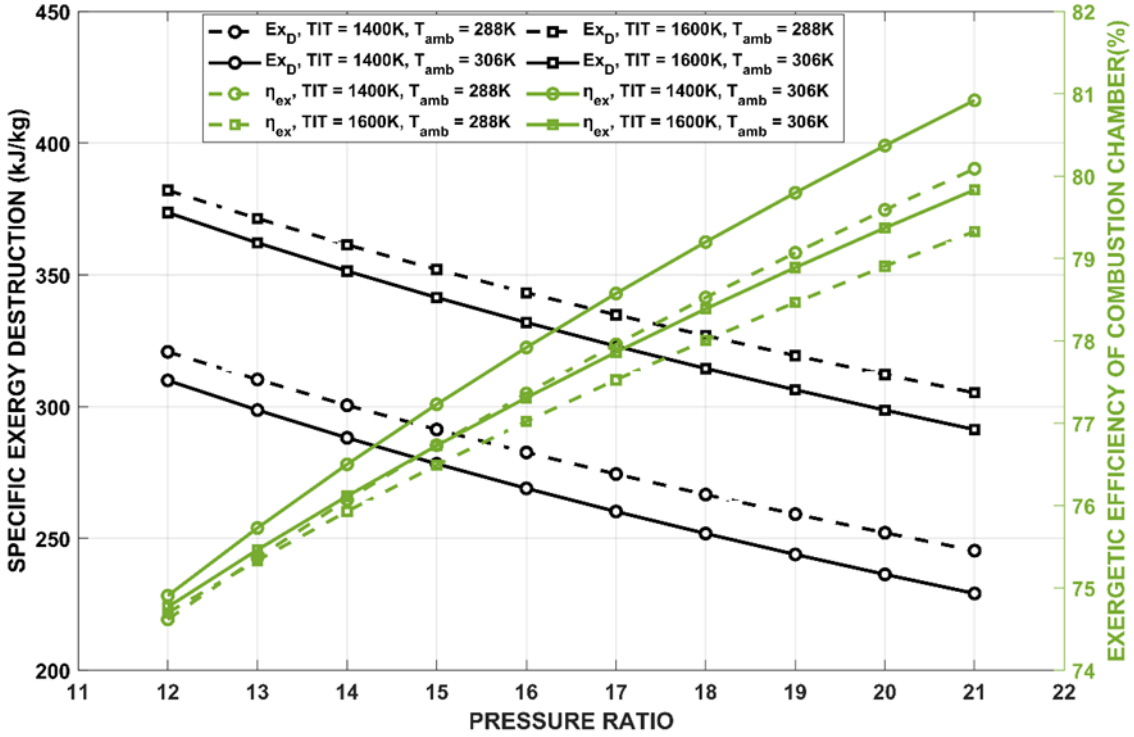

Fig. 5. 11 Effect of pressure ratio, TIT, and ambient temperature on the exergetic performance of combustion chamber

Fig. 5. 12 shows the change in specific exergy destruction and exergetic efficiency of the combustion chamber as an effect of inlet air cooling. It is evident from the plot that

cooling compressor inlet air to 288 K from ambient temperatures of 294 K and 306 K increases the specific exergy destruction for any TIT. For the same DOC, the marginal increase in specific exergy destruction is more pronounced at 1400 K than at 1600 K. As the DOC for given TIT increases, so does the marginal increase in exergy destruction. Change in exergetic efficiency of the combustion chamber exhibits the opposite behaviour as the change in exergy destruction. The decrease in exergetic efficiency has been observed as contrary to the increase in exergy destruction as the pressure ratio increases.

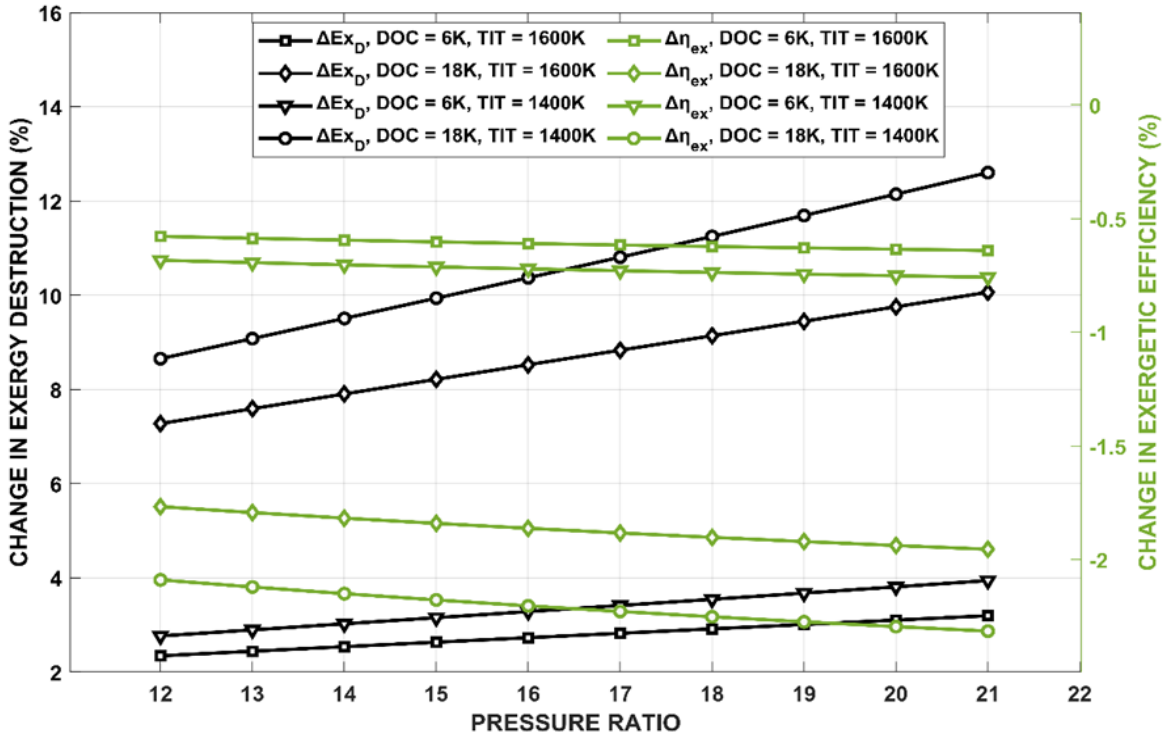

Fig. 5. 12 Variation in exergetic performance of the combustion chamber as the function of pressure ratio, TIT, and DOC

Fig. 5. 13 depicts the relationship between the gas turbine's exergetic performance and the pressure ratio, TIT, and ambient temperature. For a given value of TIT, with an increase in the pressure ratio of the gas turbine, the exhaust temperature decreases (and thus the exergy of the exhaust gas), resulting in increased exergy destruction despite the gas turbine's increased work output. For a given pressure ratio and ambient temperature, as the increased TIT links to increased exergy at the inlet of the gas turbine, the exergy destruction increases. Also, the same decreases as the ambient temperature decreases.

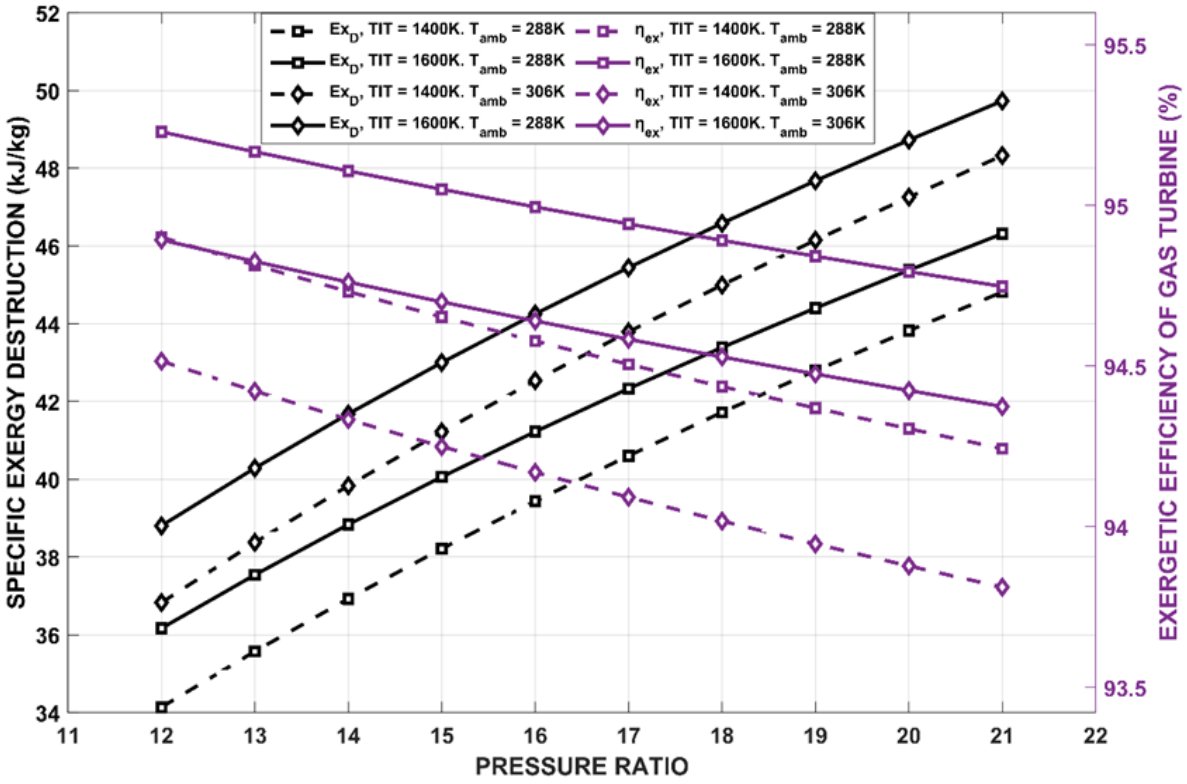

Fig. 5. 13 Effect of pressure ratio, TIT, and ambient temperature on exergetic performance of gas turbine

Fig. 5. 14 shows the change in exergy parameters of the gas cycle when inlet air cooling is applied. It is evident from the graph that the rate of increase in the specific exergy destruction of the gas cycle is more significant at lower TIT (i.e., 1400 K) at the same amount of cooling. Using the same TIT, a lesser DOC (6 K) results in a greater rate of increase in exergy destruction. Similarly, the graphs of exergetic efficiency exhibit a correlating trend.

Fig. 5. 15 represents the exergetic performance of HRSG as the function of HRSG pressure, TIT, and ambient temperatures. The results for TIT 1400 K to 1600 K are calculated in increments of 50. The leftmost points on each curve represent a TIT of 1400 K, which increases to 1600 K at the rightmost point. At a particular pressure ratio, increasing the TIT also causes a rise in gas turbine exhaust temperature, increasing exhaust gas exergy entering the HRSG. Hence, the curves show that the exergy destruction rate in HRSG increases as TIT increases. When the HRSG pressure rises for a given TIT and ambient temperature, the exergy destruction rate decreases, and

exergetic efficiency increases. At an HRSG pressure of 110 bar, it is intriguing to observe that the exergetic efficiency begins to rise with an increase in TIT, despite an increase in exergy destruction.

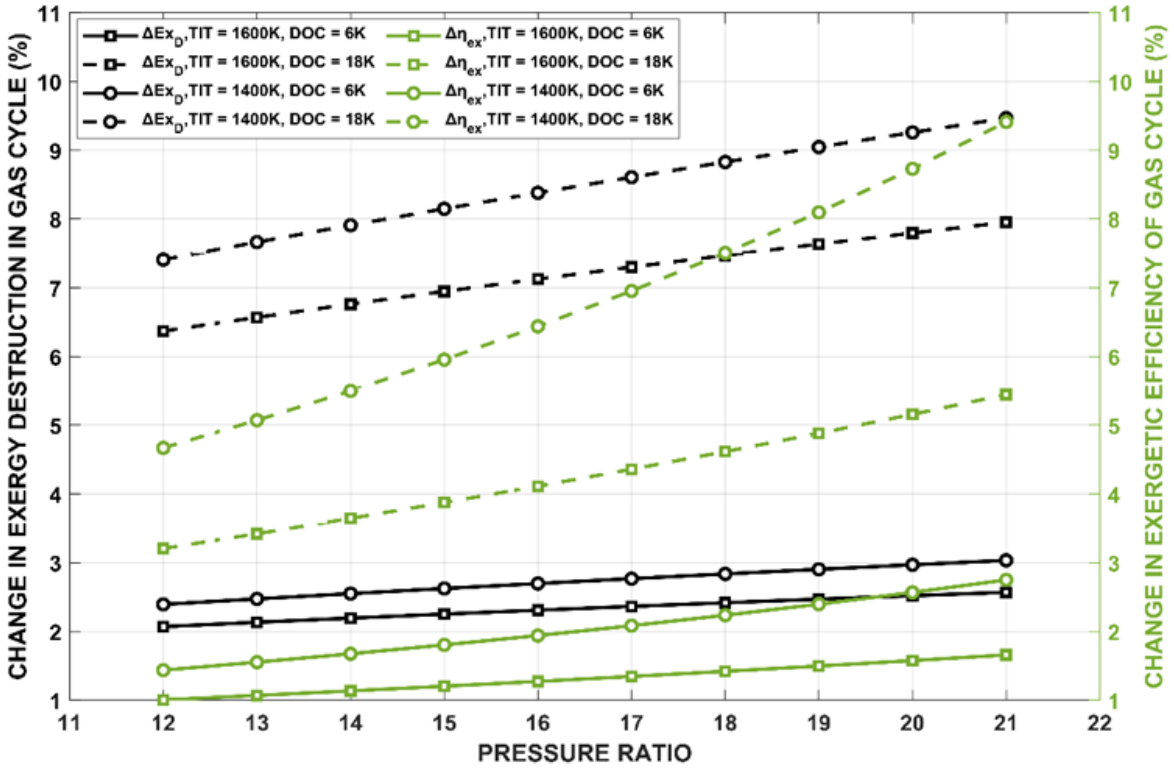

Fig. 5. 14 Variation in exergetic performance of the gas cycle as the function of pressure ratio, TIT and DOC

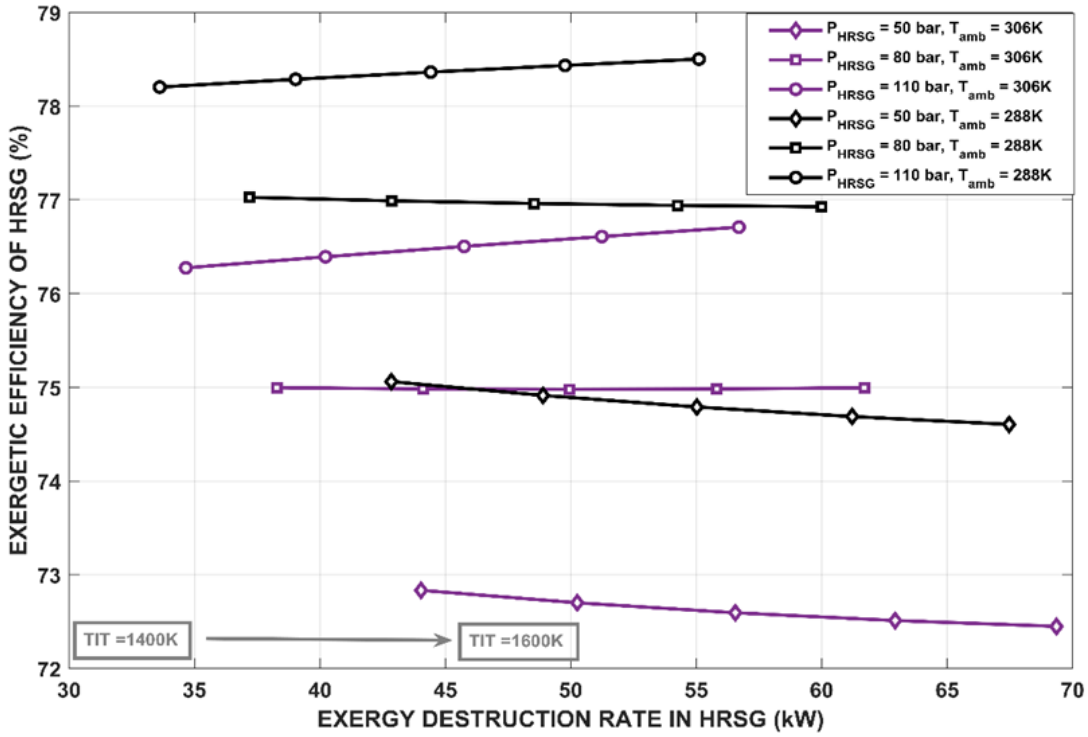

Fig. 5. 15 Effect of HRSG pressure, TIT, and ambient temperature on the exergetic performance of HRSG

Fig. 5. 16 depicts the steam turbine's work and its exergy destruction rate as the function of HRSG pressure, TIT, ambient temperature, and condenser pressure. At any TIT, the steam-specific work increases with the increase in the HRSG pressure from 30 to 70 bar and then gradually decreases. Because before the HRSG pressure reaches 70 bar, the steadily rising temperature at the inlet of the steam turbine takes over, and after that, the steadily falling rate of steam production dominates. At TIT 1400K, the work rate continues to decrease as the effect of the steam generation rate also decreases. Also, at a given HRSG pressure, higher TIT results in increased steam turbine work output due to the high exhaust temperature of the gas turbine, considering both the high steam generation rate and the high superheated steam inlet temperature. As shown in the graph, increasing condenser pressure reduces the work rate. However, the ambient temperature does not affect the steam turbine work output. Furthermore, a similar pattern of work rate has been observed for the exergy destruction rate in steam turbines at TIT 1500K (i.e., an increase until HRSG pressure reaches 70 bar, followed by a

decrease) at an ambient temperature of 306K. Nonetheless, when the ambient temperature falls to 288K, the exergy destruction diminishes similarly. While decreasing the TIT to 1400K, the exergy destruction steadily decreases, which can be explained by the steady decline in the steam production rate.

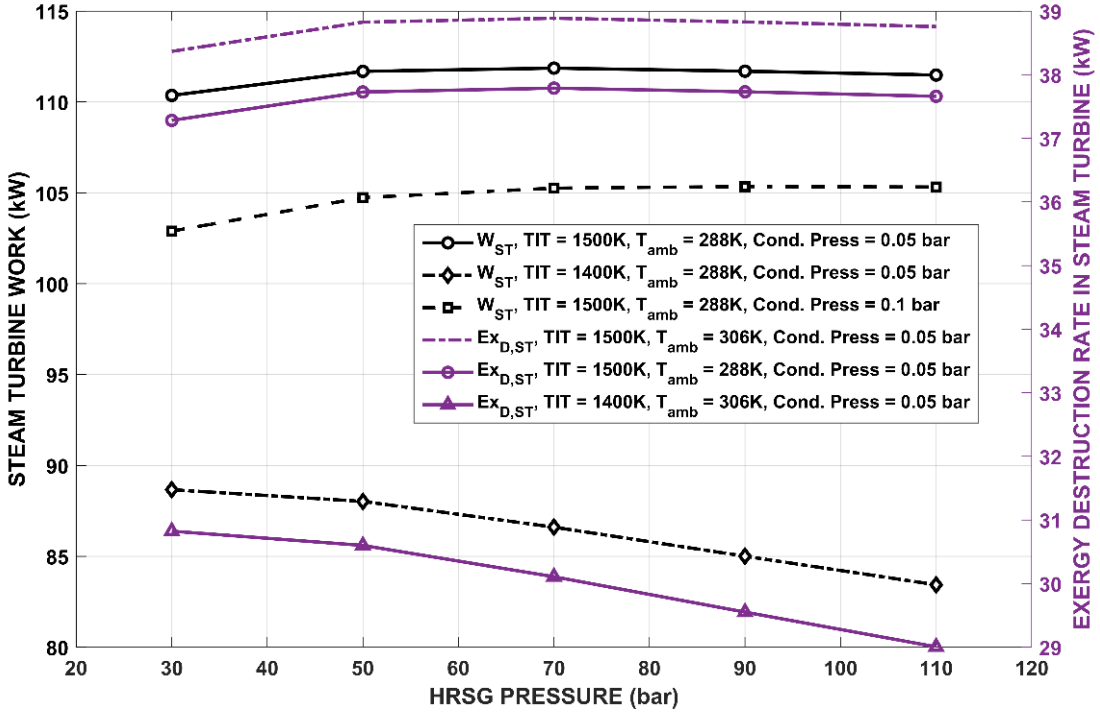

Fig. 5. 16 Effect of HRSG Pressure, TIT, ambient temperature, and condenser pressure on the performance of the steam turbine

It is necessary to investigate the impact of inlet air cooling on the 1st law performance parameters of CCPP. Considering the ambient temperatures of 306 K and 294 K, the air is cooled by 18 K and 6 K, respectively. The difference in performance parameters between cooling and no cooling has been determined. Fig. 5. 17 shows the change in the performance of CCPP due to inlet air cooling. The work output and efficiency of CCPP are enhanced when air is cooled before the compressor. This is supported by the fact that when air is cooled, the compressor work decreases, thereby increasing the gas turbine's net specific work output. Even with minimal increases in fuel consumption, efficiency gains are observed. The improvement in both performance factors is greater with higher pressure ratios for a given TIT and DOC. Additionally, cooling the compressor's inlet air by 18 K while maintaining the same pressure ratio and TIT yields

greater work and efficiency than cooling it by 6 K. At a pressure ratio of 21 and a TIT of 1400 K, it has been observed that cooling the air by 18 K increases the work rate and efficiency by 14.16% and 3.93 %, respectively.

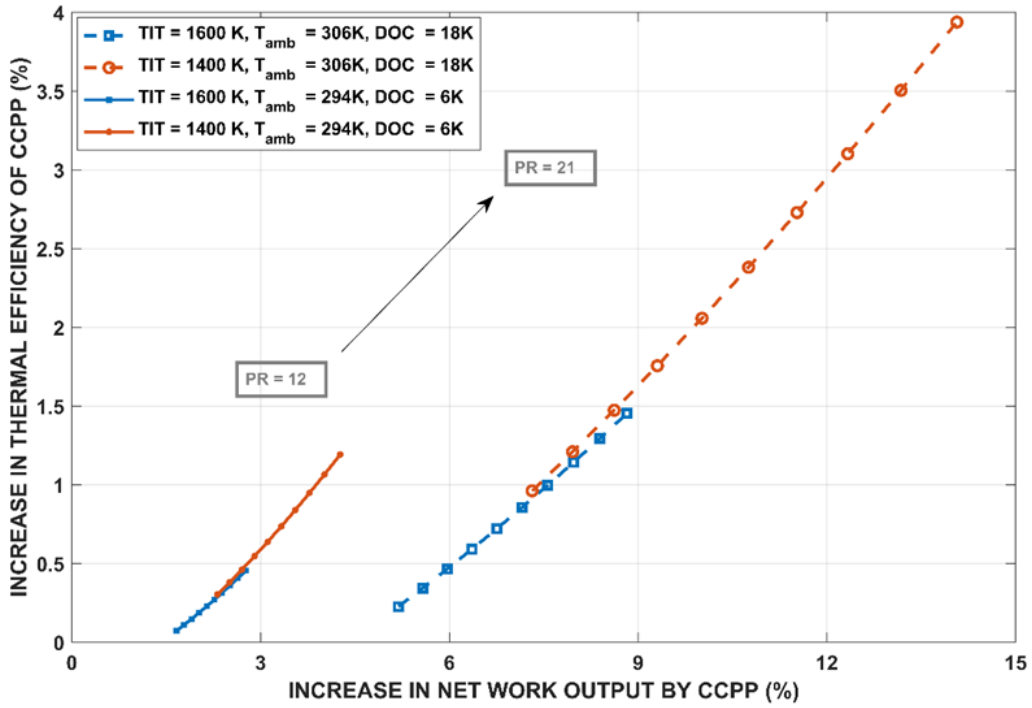

Fig. 5. 17 Performance enhancement of CCPP due to inlet air cooling

The rate of change in CCPP exergetic performance due to inlet air cooling is depicted graphically in Fig. 5. 18 as a function of pressure ratio and TIT. The highest increment in exergy destruction is observed when the TIT is 1400 K, and the compressor inlet air is cooled by 18 K. If TIT is increased to 1700 K while maintaining the same DOC, the net increase in exergy destruction decreases. The same increment diminishes significantly when the DOC is reduced to 6 K.

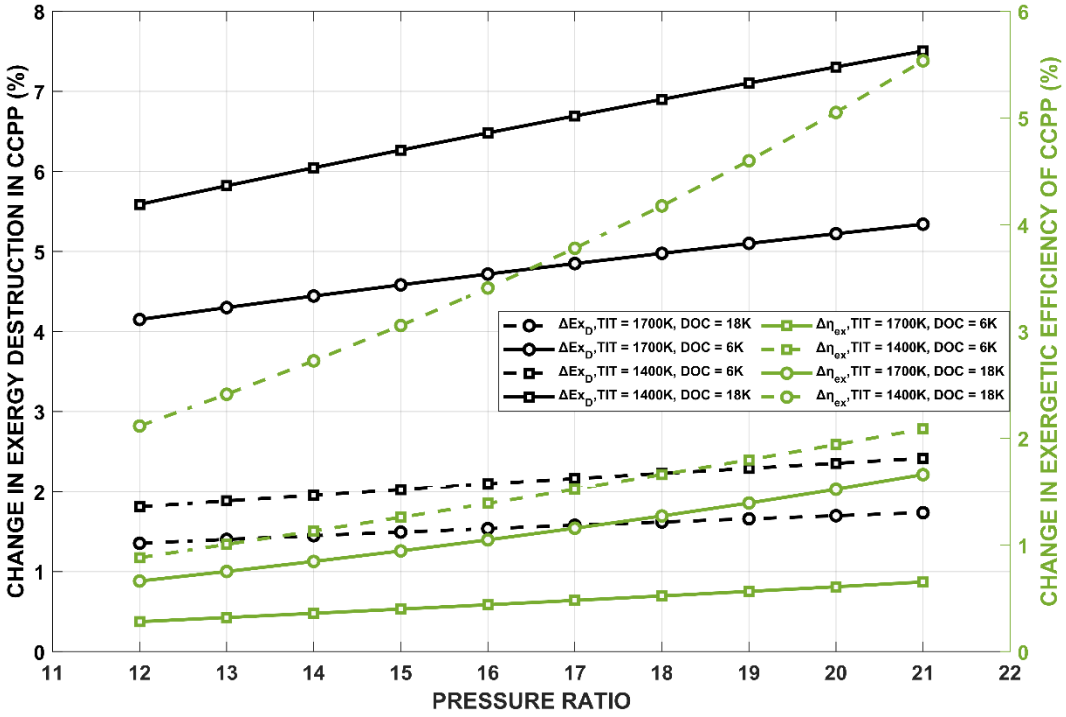

Fig. 5. 18 Variation in exergetic performance of CCPP as the function of DOC, TIT, and pressure ratio

5.6 Sensitivity Analysis

In this study, the sensitivity is investigated for different components of CCPP exergetically based on various operating parameters. Sensitivity is assessed by varying a parameter within a specified range while keeping all other operating parameters fixed, then observing the performance factor for different components and the entire plant. The parameters are TIT, pressure ratio, HRSG pressure, and DOC. The sensitivity analysis results are presented in a non-dimensional format, i.e., exergy destruction ratio, y_D. This ratio is also referred to as the efficiency defect. The lower value of this term is favorable, as it indicates superior exergy performance.

Fig. 5. 19 highlights the variation in the exergy destruction ratio, y_D of several components of CCPP with the variation of aforementioned parameters. In Fig. 5. 18(a), with the increase in TIT, the y_D for the gas cycle decreases owing to the decrease in y_D for the combustion chamber and gas turbine. The gas cycle contributes significantly to the overall exergy performance of CCPP. Consequently, the y_D for the CCPP decreases

from 0.5238 at TIT 1400K to 0.4851 at TIT 1700K, despite an increase in y_D for the steam turbine and HRSG. In Fig. 5. 18(b), the sensitivity of various components is observed over the change in pressure ratio. Observations indicate that the y_D for the gas cycle has increased from 0.4072 to 0.4181. This variation is attributable to the decreasing y_D for combustion chamber against the increasing y_D for both gas turbine and compressor throughout the range of pressure ratio. However, an increasing pressure ratio results in a slight reduction (from 0.5195 to 0.5117) in y_D for the CCPP system, which makes the system superior from an exergy standpoint. The reason for this is that increasing the pressure ratio reduces both the fuel requirement (and thus the fuel's exergy) and the exergy destruction of CCPP. However, the latter decreases at a faster rate than the former. Fig. 5. 18(c) illustrates the effect of a change in HRSG pressure on the HRSG and steam turbine, as these are the only two components affected by the variation. y_D for HRSG is observed to decrease marginally (from 0.0658 to 0.0532) over the HRSG pressure range of 50-110 bar. Nevertheless, y_D for the steam turbine is almost constant over the specified range. The combined effect of both ultimately results in a marginal decrease (from 0.5241 to 0.5115) in y_D for the CCPP system. Although increasing the HRSG pressure does not necessarily increase the steam-specific work, it does reduce the system's overall exergy destruction. When external cooling is employed in a standalone CCPP system, it is anticipated that the various components will exhibit distinct patterns over the range of 0K to 18K. Fig. 5. 18(d) depicts the variations in y_D for the CCPP and its components over the specified DOC range. y_D for CCPP is observed to be slightly decreased (from 0.5115 to 0.5075) throughout the range. This is because both the exergy of fuel and the exergy destruction of CCPP increase due to the increased requirement for fuel (due to cooling) to achieve the specified TIT. However, the former increases more rapidly than the latter. However, y_D for the gas turbine cycle has increased slightly, in contrast to the more rapid decrease in the same for the steam cycle, resulting in a reduction of y_D for CCPP. Thus, inlet air cooling makes the CCPP exergetically superior.

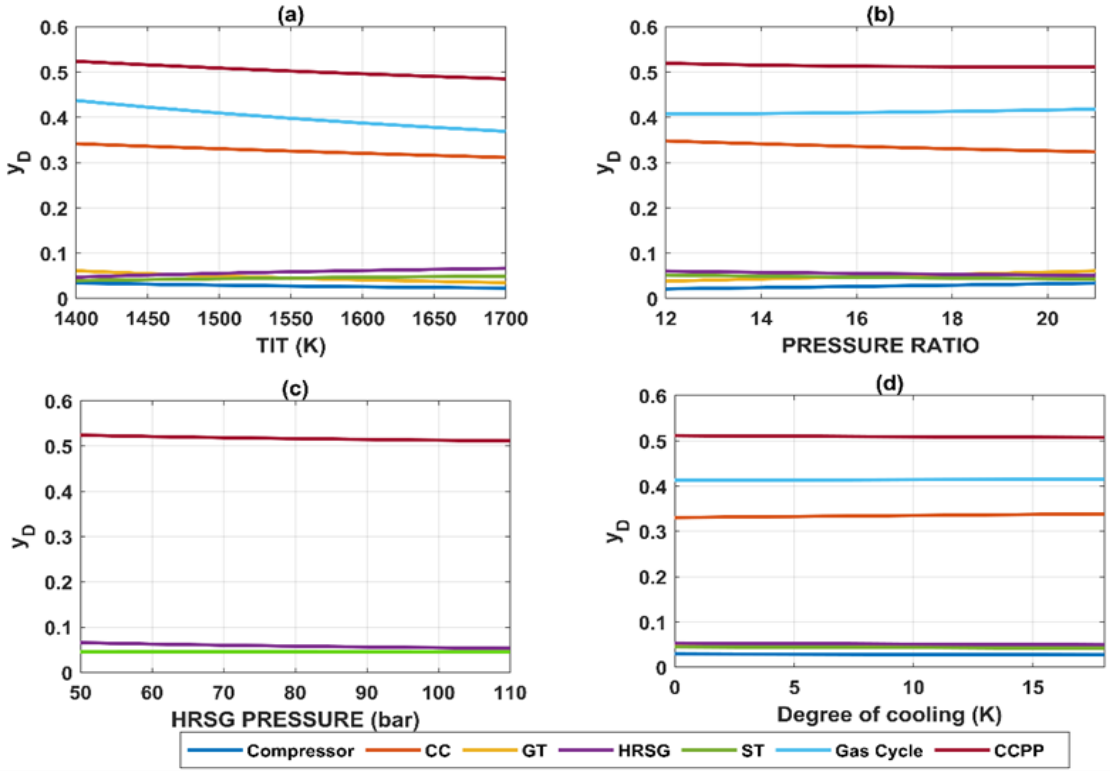

Fig. 5. 19 Sensitivity of various components of CCPP with variation in TIT, pressure ratio, HSRG pressure, and DOC

5.7 Exergy-based multi-objective optimization

To optimize the CCPP integrated with inlet air cooling for a given range of design variables, i.e., operating parameters, an appropriate set of correlations depicting the pattern of the above system is required. The parametric investigation and sensitivity analysis results indicate that the most dominant design variables influencing the performance of CCPP are the DOC, pressure ratio (PR), and TIT. The range of selected design variables is presented in Table 5. 4. Based on different combinations of distinct values of these variables, the main performance factors, i.e., net specific work (W_{net}), total exergy destruction (TED), and exergetic efficiency ($\eta_{ex,ccpp}$) are selected. Another reason for choosing these performance parameters is that when inlet air cooling is implemented, the CCPP work and exergetic efficiency increase, as does total exergy destruction. However, an increase in exergy destruction is undesirable. As a result, the variables (input parameters) should be optimized to minimize exergy destruction. Subsequently, three distinct types of regression models have been developed with the help of Design Expert software. These are linear, two-factor interaction (2FI), and

quadratic regression models. The comparison of all regression models is displayed in Table 5. 5. For each model, the coefficient of determination, R^2, has been calculated. The smaller the difference between predicted R^2 and adjusted R^2, the greater will be the adequate precision. The quadratic model has the highest adequate precision (AP) values for all three performance factors.

Table 5. 4 Range of design variables

Design variable (Unit)	Range
DOC (K)	0-18
PR (-)	12 - 21
TIT (K)	1400 – 1700

Table 5. 5 Accuracy estimation of linear, two-factor interaction, and quadratic models

Performance factor	**Linear**			**2FI**			**Quadratic**		
	Pre-R^2	**Adj-R^2**	**AP**	**Pre-R^2**	**Adj-R^2**	**AP**	**Pre-R^2**	**Adj-R^2**	**AP**
W_{net}	0.998	0.9993	276.7	0.99	0.9995	451.5	0.9999	1.0000	771.2
TED	0.992	0.9954	98.2	0.98	0.9948	83.1	0.9999	1.0000	816.9
$\eta_{ex,ccpp}$	0.903	0.9367	23.9	0.90	0.9564	24.7	0.9855	0.9979	95.83

Based on the selected regression model, a set of equations for each factor is derived with the help of statistical analysis in Design Expert software, shown in Table 5. 6 Correlations derived for each objective function. These equations, in terms of actual factors, can be used to predict each response variable (selected factor) within a given range of design variables. Therefore, these equations are implemented for two dual multi-objective optimizations. In this case, the two sets of objective functions are formulated. The 1st set of objective functions consists of W_{net} (to be maximized) and TED (to be minimized). The 2nd set consists of an increment in exergetic efficiency (to be maximized) & increment in TED (to be minimized).

Table 5. 6 Correlations derived for each objective function

Objective function	**Correlations**
W_{net}	$-513.61155 + 0.657968 \times DOC - 17.05966 \times PR + 0.755263 \times TIT + 0.067151 \times DOC \times PR + 0.000056 \times DOC \times TIT + 0.004318 \times PR \times TIT - 0.000990 \times DOC^2 + 0.028463 \times PR^2 - 0.0000431 \times TIT^2$
TED	$-273.70044 + 1.19080 \times DOC - 16.93857 \times PR + 0.750096 \times TIT + 0.010232 \times DOC \times PR + 0.000128 \times DOC \times TIT - 0.004171 \times PR \times TIT + 0.001534 \times DOC^2 + 0.368648 \times PR^2 - 0.000048 \times TIT^2$
Increase in exergetic efficiency (%)	$9.10931 + 0.427817 \times DOC + 0.51112 \times PR - 0.017239 \times TIT + 0.009280 \times DOC \times PR - 0.000313 \times DOC \times TIT + 0.000375 \times PR \times TIT - 0.000636 \times DOC^2 - 0.002561 \times PR^2 + 7.477 \times 10^{-6} \times TIT^2$
Increase in exergy destruction (%)	$-3.50385 + 0.700386 \times DOC + 0.210045 \times PR + 0.002232 \times TIT + 0.009417 \times DOC \times PR - 0.000339 \times DOC \times TIT - 0.000134 \times PR \times TIT + 0.000334 \times DOC^2$

The abovementioned problem is then solved using multi-objective optimization using a genetic algorithm (MOGA). As a result, each set has obtained Pareto optimality. While carrying out the genetic algorithm, the following values were chosen as its parameters: population size of 200, Pareto front population of 0.35, and crossover fraction of 0.8. Additionally, "tournament" is considered a selection function with a size of 2, and "intermediate" is considered a crossover function.

MOGA is a metaheuristic approach that provides a broad population of solutions that attempts to give all possible trade-offs between two or more objective functions. As a

result, Pareto optimality has been obtained between the two objectives. Fig. 5. 20 depicts the Pareto optimal trade-off points for W_{net} and TED as a result of inlet air cooling. Points A, B, and C on the Pareto curve are chosen arbitrarily to illustrate the design variables. As one moves from A to C, the DOC and TIT decrease while the PR increases. However, increasing the DOC increases in W_{net} but at the expense of the exergy destruction. The increase in DOC decreases the compressor work and improves net specific work output while simultaneously increasing the fuel intake (and, thus, total exergy destruction), as substantiated by previous results. In order to produce the maximum work, the parameters on point A are 16.5 K DOC, pressure ratio, and TIT of 1695.4 K, but the exergy destruction rate is also higher. Furthermore, the exergetic efficiency of CCPP is highest at point A, i.e. 47.36%. If the cost of electricity per unit is high, operating the CCPP on point 'A' may be advantageous. However, if fuel prices are high, the destruction of exergy should not be considered acceptable.

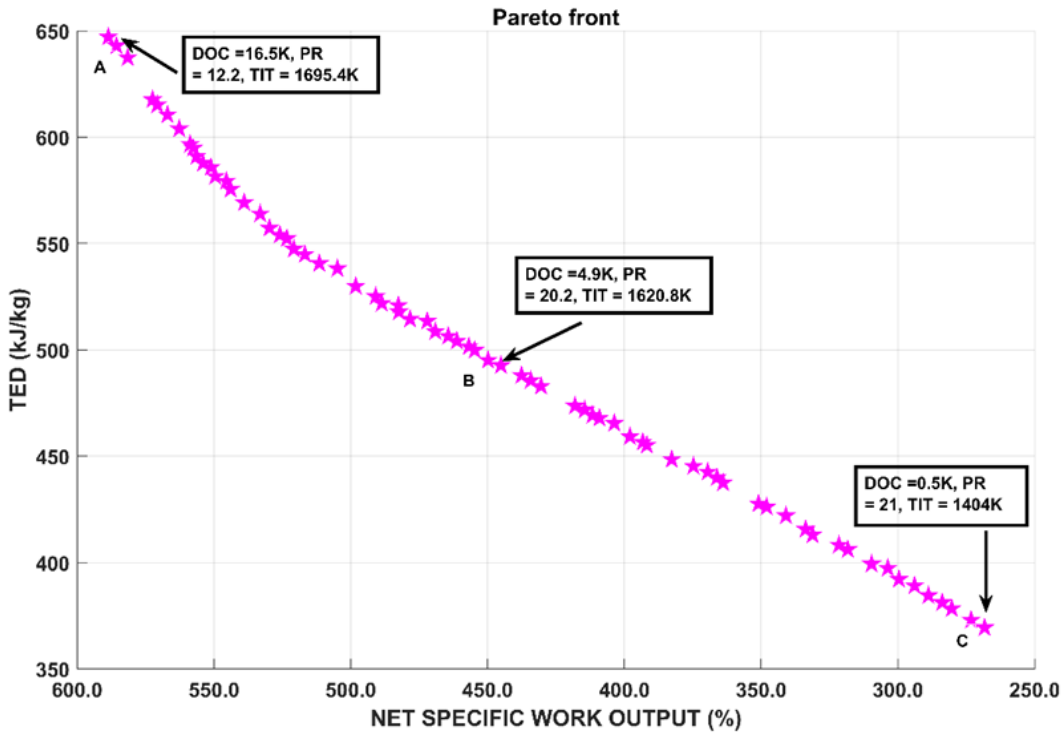

Fig. 5. 20 Pareto optimality between net specific work output of CCPP and total exergy destruction

Fig. 5. 21 illustrates the Pareto front, which depicts the solutions that are the best suited between increments in both exergetic efficiency and TED as a result of inlet air cooling

and variation in other parameters. The curve illustrates the optimal solutions that can be achieved when an increment in exergetic efficiency is maximized, and the corresponding increase in TED is minimized across the entire range of design variables that have been specified. The values of the design variables are displayed by placing points A, B, and C in random order. Point A is located in the vicinity where the highest increment in both factors is witnessed. The DOC at point A is 17.6 K, which is the highest recommended considering the increase in both exergetic efficiency and TED to be maximum, while the PR is 20.9 (close to the upper limit of PR), and the TIT is 1405.9 K (close to the lower limit of TIT). The DOC decreases continuously from point A to point C, reaching 0 K (no cooling condition) at point C. Notably, the optimal solutions demonstrate a negligible variation in pressure ratio and that its value is set close to the upper limit specified. The DOC is a major decisive factor in setting the optimized solution. Also, TIT is observed to be close to the lower limit in all solutions because lower TIT generates lower exergy. As a result, any intermediate point can be considered to find the optimal compromise between increased exergy destruction and increased exergetic efficiency.

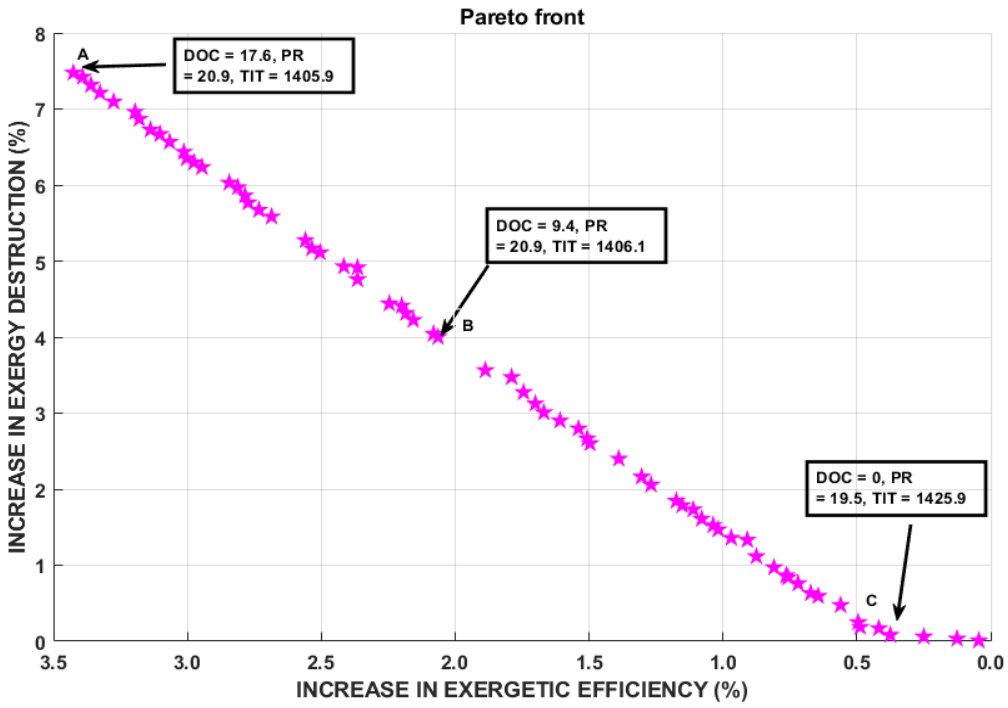

Fig. 5. 21 Pareto optimality between increment in exergetic efficiency and exergy destruction of CCPP

5.8 Conventional Exergoeconomic analysis

Table 5. 7 Conventional exergoeconomic parameters of the CCPP presents the exergoeconomic parameters derived from a conventional exergy costing analysis, utilizing the specific settings for the pressure ratio of 15, a TIT of 1600K, and an ambient temperature of 288K. The correlation between the cost rate of destruction and the exergy destruction rate is conveniently apparent. The highest cost rate of exergy destruction has been computed for the combustion chamber with 260.38 $/h which is evident as the exergy destruction for the combustion chamber is also the highest. Whereas, the combustion chamber has the lowest capital cost rate compared to all other components, resulting in its little contribution to the total cost (specifically, 0.899%). The steam turbine has the second greatest cost rate of destruction, despite having the highest capital cost rate of 70.07 $/h among all the components in the combined cycle power plant (CCPP) system. The combined sum of capital cost and destruction rate amounts to 698.90 $/h, with the capital cost accounting for 36.48 % of this total. The fuel cost rate is calculated to be 764.28 $/h, resulting in an overall cost of 1463.18 $/h for the CCPP system.

Table 5. 7 Conventional exergoeconomic parameters of the CCPP

Component	$\dot{C}_D$ ($/h)	$\dot{Z}_K$ ($/h)	$\dot{Z}_K + \dot{C}_D$ ($/h)	f_k (%)
Comp.	24.3059	30.9160	55.2219	55.98
CC	260.3844	2.3631	262.7475	0.899
GT	44.1623	55.5675	99.7298	55.72
HRSG	21.9545	59.7490	81.7035	73.61
ST	87.9506	70.076	158.03	44.33
Cond.	4.7758	35.4236	40.1994	88.11
FWP	0.4075	0.8625	1.2701	67.90
Overall CCPP	443.94	254.96	698.90	36.48

Fig. 5. 22 illustrates the effect of degree of cooling on the variation in cost rates associated to work output, investment, and exergy destruction on the different turbine inlet temperatures and pressure ratios. After cooling the compressor inlet air, both the work production and cost rate of work production by the CCPP system increase. In addition to this cost, the investment and cost associated with exergy destruction also increase. Here, the investment cost comprises capital cost and fuel cost. The results are shown for TIT values between 1400 K and 1600 K, pressure ratios of 10 & 13, and degrees of cooling of 12 K & 18 K. Also, the results demonstrate an increase in the cost of work in comparison to the increment in costs of total investment and exergy destruction. However, it should be noted that the cost of work exhibits a higher rate of increase compared to both costs of investment and exergy destruction, regardless of the pressure ratio and degree of cooling. In the case of a pressure ratio of 13, the 18K of inlet air cooling reveals better gain in work cost, as well as the other two cost increments, compared to the lower cooling of 12 K. However, the gap between an increase in work cost and the cost associated with exergy destruction becomes more pronounced when operating at a lower degree of cooling. Conversely, when the pressure ratio is reduced, there is an observed increase in all types of cost rates as shown. This relationship can be explained from a thermodynamic standpoint, as lowering the pressure ratio results in a decrease in compressor work (leading to an increase in net work) and an increase in fuel supply, thereby causing an increase in investment cost.

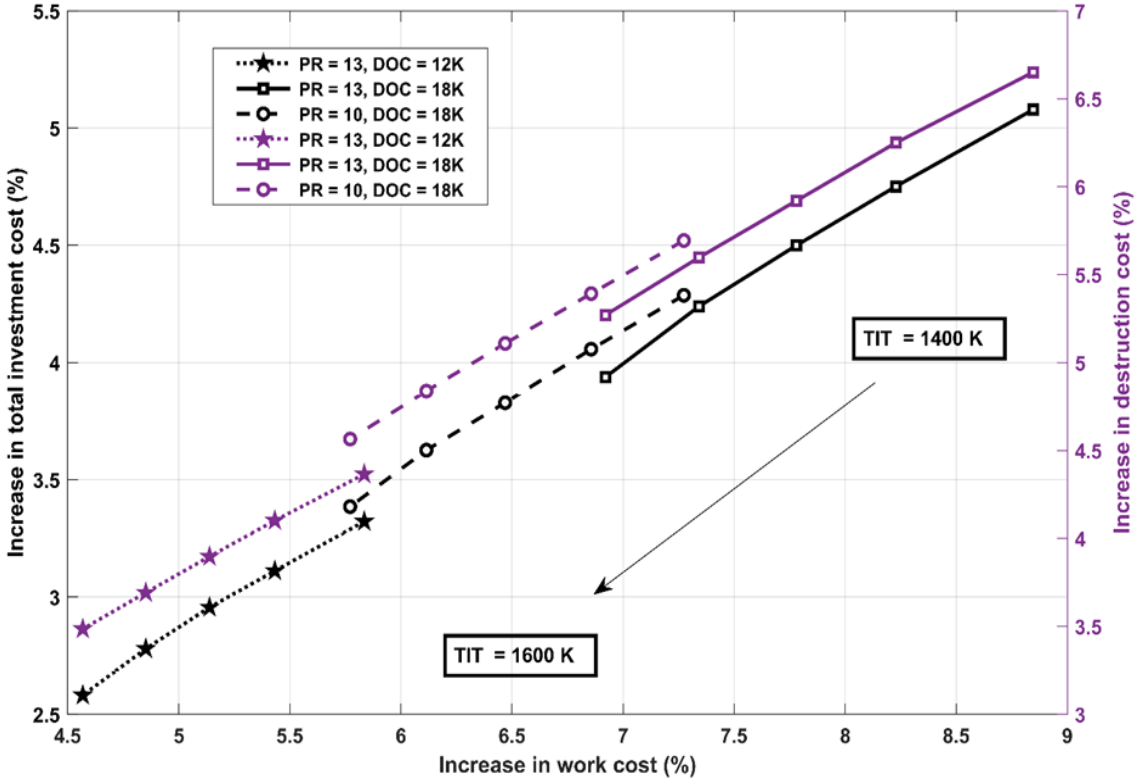

Fig. 5. 22 Effect of turbine inlet temperature, pressure ratio and degree of cooling on the increase in work cost, investment cost and destruction cost

5.9 Advanced exergy analysis

Following the identical operational conditions as previously established, the exergy destruction rate of each component and the overall CCPP system have now been segmented into avoidable and unavoidable components. Fig. 5. 23 illustrates a bar graph that displays the proportion of avoidable and unavoidable exergy destruction rates for each component of the CCPP system. The combustion chamber has the highest level of unavoidable exergy destruction, amounting to 93.06%, whereas the avoidable portion accounts for just 6.94%. The primary cause of exergy destruction stems from the irreversibility resulting from the mixing (highly irreversible) of air and fuel, as well as the heat transfer caused by significant temperature differentials, which appears to be an inevitable phenomenon. The avoidable component is obtained by preventing pressure drop within the combustion chamber and the improvement of combustion efficiency, resulting in a reduction in fuel supply to achieve a specific turbine inlet temperature. The components exhibiting the highest rates of avoidable exergy destruction are the

HRSG, the air compressor, and the steam turbine, with respective fractions of 91.53%, 83.52%, and 80.78%. The avoidable exergy destruction rates are attributed to the utilization of unavoidable settings linked to these components. The comprehensive analysis of the CCPP system reveals that the avoidable and unavoidable components of exergy destruction account for 25.02% and 74.98% of the total, respectively. The avoidable component of the exergy destruction in the CCPP system is greatly impacted by the same of steam turbine, which accounts for 31.68% of the overall avoidable exergy destruction rate.

Fig. 5. 24 displays the effect of variation in vital operating parameters such as TIT, pressure ratio, and degree of cooling on every component of exergy destruction rate (unavoidable and avoidable) and total exergy destruction rate. The results were obtained implementing TIT ranging from 1500 K to 1700 K, pressure ratios of 10 and 14, and degrees of cooling of 0K (no cooling) and 18 K. Also, the CCPP power output for these variations is displayed in the result. As the TIT increases, both the formats of destruction rate exhibit an increase, thereby leading to an overall increase in the total destruction rate. The rationale behind this result is that increasing TIT will necessitate more fuel being supplied inside the combustion chamber, and the exergy destruction in the combustion chamber and CCPP system will ultimately increase. An additional noticeable effect of increasing the TIT is that the rate of increase of unavoidable exergy destruction is greater than that of avoidable exergy destruction.

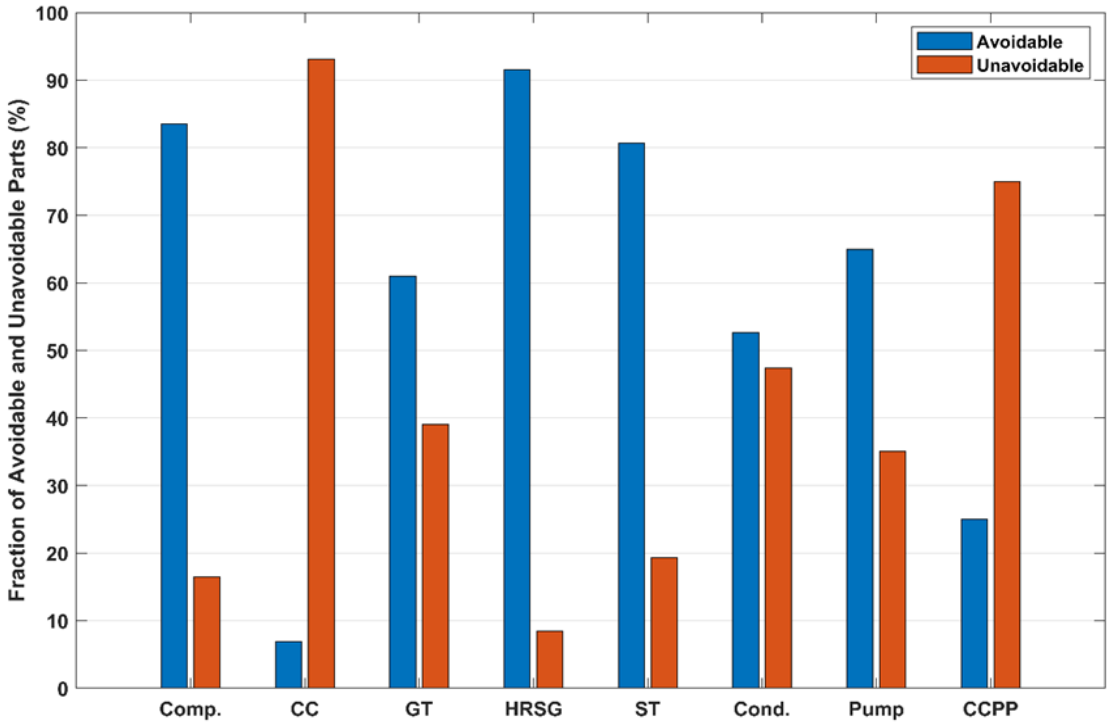

Fig. 5. 23 Avoidable and Unavoidable part of exergy destruction in several components of CCPP

Further, the effect on the avoidable portion of each component has been seen by changing the value of the pressure ratio, while maintaining a constant TIT of 1600K and ambient temperature of 288K. The pressure ratio has been elevated from 10 to 14. The contribution attributed to the gas turbine cycle exhibits an increase, but the overall avoidable exergy destruction diminishes with an increase in pressure ratio. Furthermore, the influence of an increase in the degree of cooling has also been emphasized. However, it should be noted that while cooling the compressor inlet may lead to an increase in the total avoidable exergy destruction of the CCPP system, its impact on specific power cycles, such as the gas turbine cycle and steam turbine cycle, is minimal. Nevertheless, it is seen that the power output of the CCPP system exhibits a rise in response to an increase in the degree of cooling.

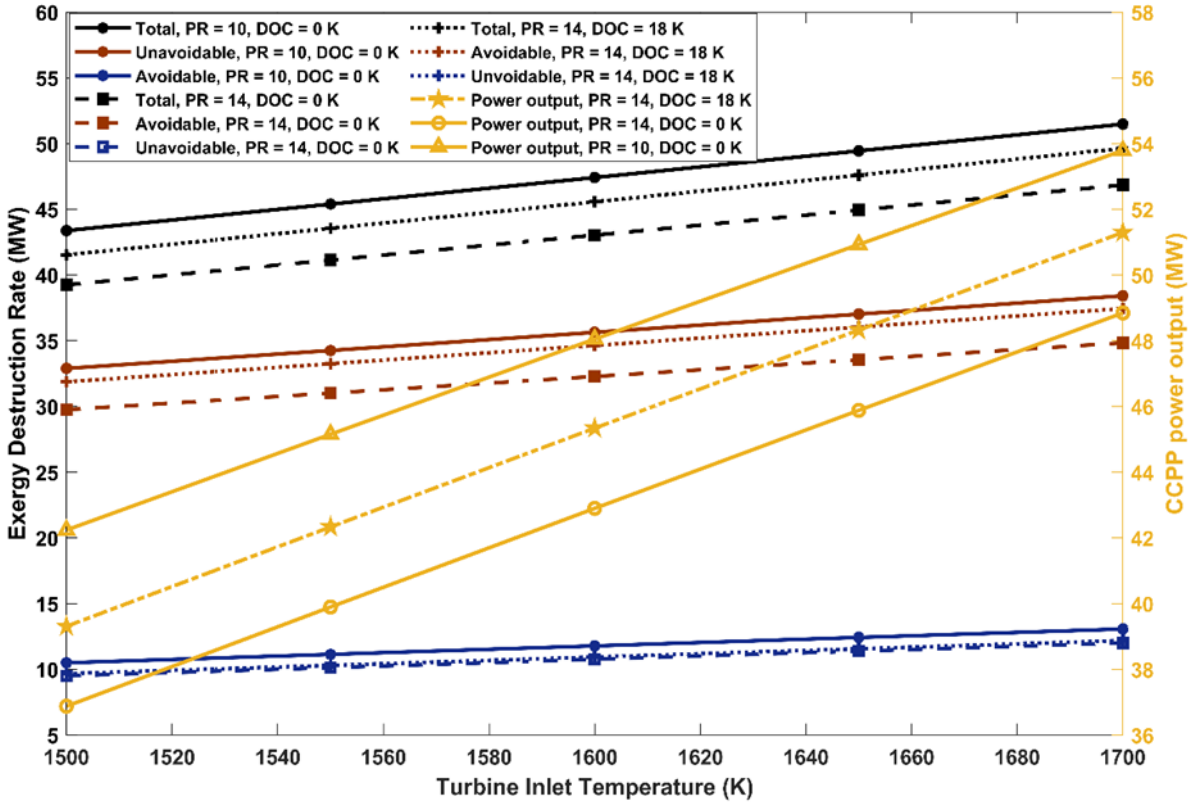

Fig. 5. 24 Effect of TIT, Pressure ratio, and degree of inlet air cooling on the Total, Unavoidable, avoidable exergy destruction rate, and power output of CCPP

5.10 Advanced exergoeconomic analysis

The exergy costing approach is linked to advanced exergy analysis, which aims to determine the cost of exergy destruction by dividing it into two components: avoidable and unavoidable. The cost rate is linked to the destruction of exergy and the capital cost i.e., purchase equipment cost (PEC). Table 5. 8 provides a comprehensive breakdown of the cost factors including the total avoidable cost ($\dot{C}_{D,k}^{AV} + \dot{Z}_k^{AV}$), total unavoidable cost ($\dot{C}_{D,k}^{UN} + \dot{Z}_k^{UN}$), and the modified exergoeconomic factor ($f_{k,modified}$). Based on the findings, it has been determined that the combustion chamber incurs the highest proportion of $\dot{C}_D^{UN}$, accounting for 93.06% of the total destruction related cost rate. Similarly, the HRSG exhibits the highest proportion of $\dot{C}_D^{AV}$, representing 91.53% of the avoidable cost rate of destruction. However, the overall cost of destruction has been divided into 35.84% and 64.16% for avoidable and unavoidable conditions, respectively. The combustion chamber incurs the highest overall cost, encompassing both exergy destruction related cost and capital cost, in the case of unavoidable

conditions. Conversely, in an avoidable counterpart, the steam turbine exhibits the highest total cost. In contrast, it is observed that the combustion chamber alone accounts for 49.3% of the total unavoidable cost ($\dot{C}_D^{UN} + \dot{Z}_k^{UN}$). As a result, the modified exergoeconomic factor is found to be highest for the condenser, with the HRSG following closely behind. Reducing the avoidable capital cost for these two components can contribute to a decrease in the overall avoidable cost. However, $\dot{Z}_{CC}^{AV}$ and $\dot{Z}_{ST}^{AV}$ have least impact on the overall cost-effectiveness of a CCPP system as $f_{CC,modified}$ and $f_{ST,modified}$ calculated as 1.29% and 8.98%, respectively.

Table 5. 8 Advanced exergoeconomic parameters of each component of CCPP

Component	$\dot{C}_{D,k}^{AV}$(\$/h)	$\dot{C}_{D,k}^{UN}$ (\$/h)	$\dot{Z}_k^{AV}$(\$/h)	$\dot{Z}_k^{UN}$ (\$/h)	$\dot{C}_{D,k}^{AV} + \dot{Z}_k^{AV}$ (\$/h)	$\dot{C}_{D,k}^{UN} + \dot{Z}_k^{UN}$ (\$/h)	$f_{k,modified}$ (%)
Comp.	20.301	4.004	3.0916	27.8244	23.3931	31.8288	13.21
CC	18.047	242.33	0.2363	2.1268	18.2834	244.4641	1.29
GT	26.921	17.240	11.1135	44.4540	38.035	61.6948	29.21
HRSG	20.095	1.8590	18.522	41.2268	38.6175	43.0858	47.96
ST	70.983	16.967	7.0076	63.0687	77.99	80.036	8.98
Cond.	2.5145	2.2613	3.8966	31.5270	6.4111	33.7883	60.77
FWP	0.2647	0.1429	0.1294	0.7332	0.3941	0.8761	32.83
Overall CCPP	159.13	284.13	43.9972	210.96	203.1241	495.78	21.66

Fig. 5. 25 illustrates the changes in the cost parameters indicated above in response to variations in the TIT and compressor pressure ratio. The overall cost of the system ($\dot{Z}_K + \dot{C}_D$) rises for both pressure ratios of 10 and 14 with the increase in TIT from 1450K to 1600K. It is important to highlight that the variation in the overall cost is mostly driven by the cost of exergy destruction, $\dot{C}_D$ rather than the capital cost, $\dot{Z}_K$. Furthermore, the impact of pressure ratio on the cost associated with exergy destruction is more apparent. Also, the results demonstrate that a lower pressure ratio results in a higher cost of destruction when compared to a higher pressure ratio. This is due to the fact that the overall exergy destruction of CCPP increases as the compressor pressure

ratio decreases, as demonstrated in the previous findings presented in Fig. 5. 24. When considering avoidable destruction costs, the marginal increase in cost rates for the unavoidable portion becomes more significant as the TIT increases. Additionally, the impact of the pressure ratio is more evident in the unavoidable portion of destruction costs.

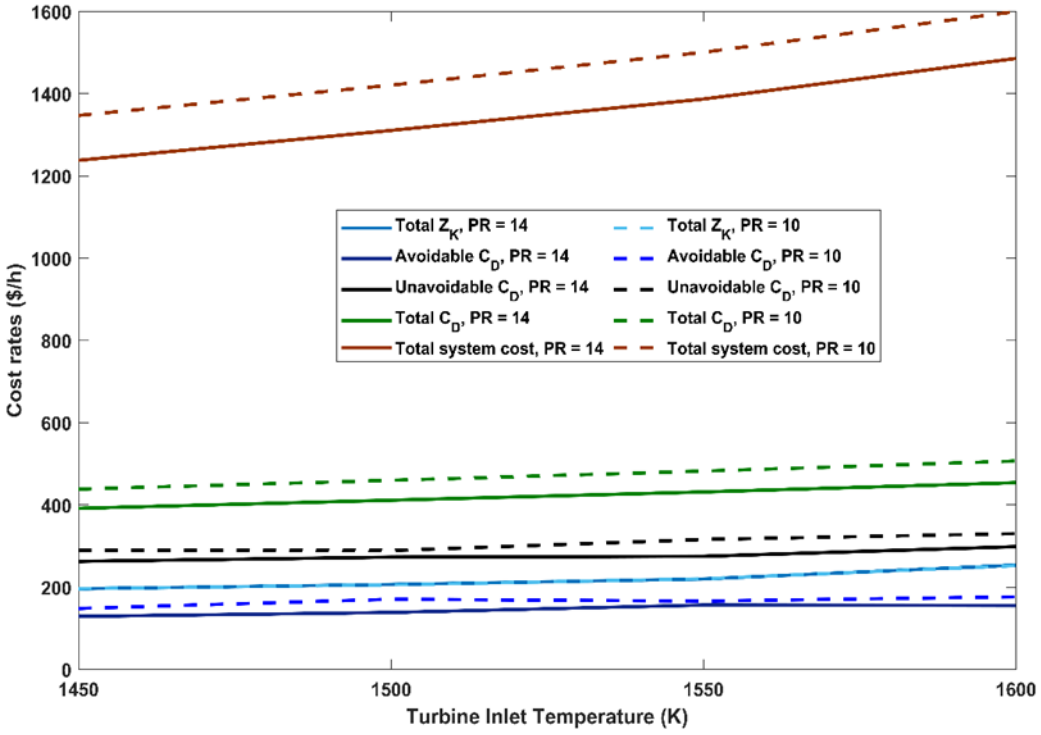

Fig. 5. 25 Effect of TIT and pressure ratio on the several components of cost rates

5.11 Exergoeconomics-based multi-objective optimization

To accomplish exergoeconomic optimization of the CCPP system, several cost and performance aspects are considered with the purpose of minimizing or maximizing them over the spectrum of design variables and operation parameters under study. Thus, the optimization process involves the inclusion of two sets, each consisting of two objectives.

The first set of considerations focuses on the capital cost and the cost of exergy destruction as its key functions. It is imperative to minimize both the cost factors i.e., capital cost and the cost associated with exergy destruction. The reduced costs can be

attributed to an optimum compromise among different design variables. The design variables encompass the isentropic efficiencies, the effectiveness of heat exchangers, and losses associated with various components inside the CCPP system. The design variables are varied from the actual conditions (as per the real cycle) to the maximum attainable conditions (referred to as the unavoidable cycle) for the purpose of optimization, as depicted in Table 5. 9. Another set of optimization involves maximizing the modified exergetic efficiency and minimizing the total unavoidable cost per unit of work production ($/h.MW) for the CCPP system as two distinct objectives. When analysing the advanced exergoeconomics of an energy system, it is crucial to optimize the modified exergetic efficiency, which is dependent on advanced exergy components. Another cost aspect that needs to be minimized is the unavoidable cost per unit of work creation. If the cost that cannot be avoided is lower, then the portion that can be avoided will be higher, resulting in a greater potential for improvement in terms of exergy. Also, this optimization method provides insight into the utilization of various sets of operational parameters, such as TIT, PR, and DOC from an application perspective.

Therefore, the correlations for capital cost and exergy destruction cost are developed as the functions of only previously mentioned design variables (and keeping other parameters unchanged) with the help of Design Expert software. Similarly, additional correlations are established between total unavoidable cost per unit of work output and modified exergetic efficiency as functions of TIT, PR, and DOC, while holding all other variables constant.

The different types of correlations of costs (which are the functions of aforementioned efficiencies, effectiveness, and losses) were developed using the regression models under the statistical analysis of computed results from the MATLAB program. This problem is then addressed through the application of multi-objective optimization utilizing the genetic algorithm (MOGA). Consequently, every set has achieved Pareto optimality. During the execution of the genetic algorithm, the parameters selected were as follows: a population size of 200, a Pareto front population of 0.35, and a crossover fraction of 0.8. Moreover, the "tournament" is considered a selection function with a cardinality of 2, while "intermediate" is classified as a crossover function.

Fig. 5. 26 illustrates the Pareto optimal front, which represents the trade-off between the cost of exergy destruction and capital cost, for a given range of design variables as specified in the table. Given that both cost factors are bound to be minimized, the solution space is positioned to the left and underneath the Pareto optimal front. Three arbitrary points, labelled as 'A', 'B', and 'C', are positioned on the Pareto front to evaluate the optimized combination of design variables and other performance aspects, specifically exergetic efficiency (n_{ex}) and the total cost rate. Points 'A' and 'C' represent the two opposite ends, whereas 'B' serves as an intermediate point. At point 'A', the capital cost is at its highest while the cost of exergy destruction is at its lowest. However, as moving towards point 'C', the situation gets completely reversed. However, while the capital cost at point 'A' is at its highest, both the values of n_{ex} and total cost also appears to be at their maximum. Both of these parameters decrease as one moves towards point 'C'. At point 'B', the total cost is minimum, resulting in a reduction of 18.14% compared to the same at point 'A'. However, n_{ex} at point 'B' is also lower, with a decrease of just 4.45% compared to point 'A'. The result clearly indicates that the solutions in the vicinity of Point 'B' offer a more favourable balance between the two costs. However, at Point 'C', the total cost is higher and $n_{ex}$is lower compared to Point 'B', which is unfavourable from a design standpoint.

Furthermore, another investigation has been conducted on the values of design variables, as presented in Table 5. 9. It is noteworthy that among the nine design variables considered in this study, six design variables exhibit a narrow spectrum of variation rather than spanning over the complete range. These variables are $\eta_{is,comp}$, η_{CC}, ε_{sh}, ΔP_{CC}, ε_{cond}, and $\eta_{is,pump}$. These design variables have the following optimized ranges: 87.52–88.43%, 98.59–98.99%, 91.65–92.71%, 3.69–4.77%, 92.57-94.41%, and 89.80–92.97%.

Given that Point 'B' provides a favourable compromise between two cost rates, the suggested values of several design variables can be approximated as follows: $\eta_{is,comp}$ = 87.83%, $\eta_{is,gt}$ = 89.78%, $\eta_{is,st}$ = 92.60%, ε_{sh} = 91.97%, ΔP_{CC}= 4.31%, and $\eta_{is,pump}$= 92.24%. The remaining three design variables are optimized close to the upper limit of the range provided.

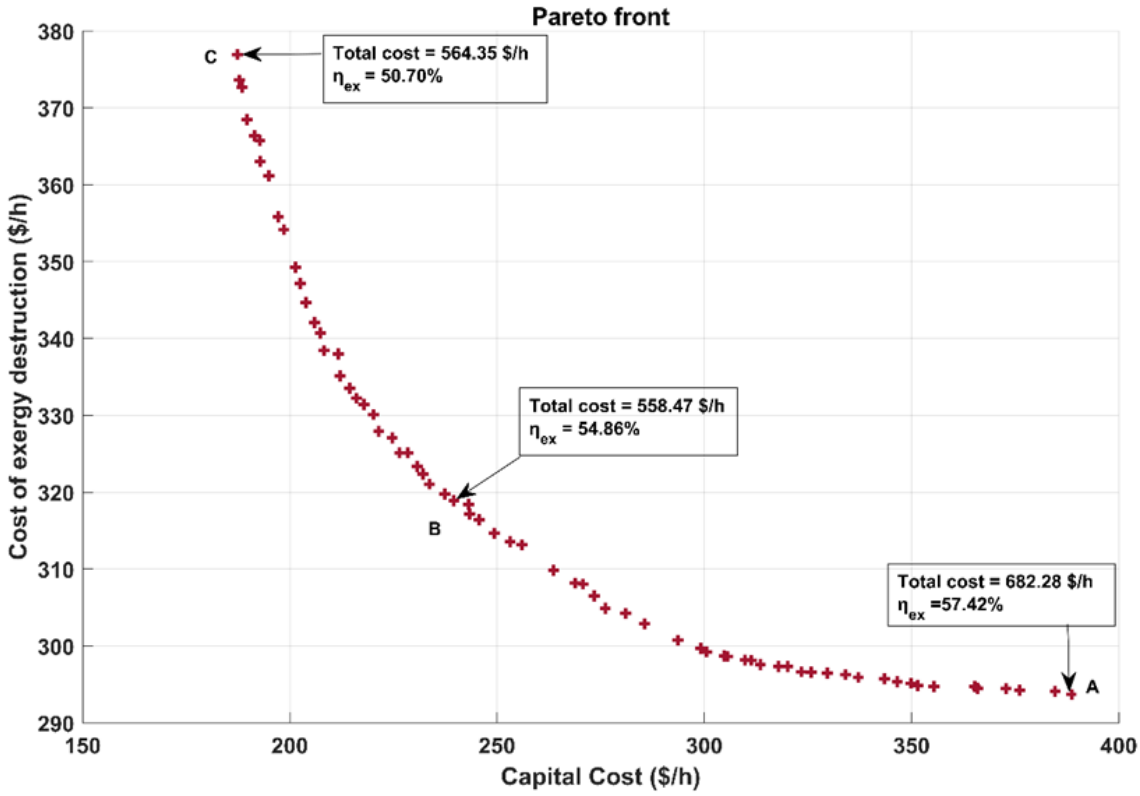

Fig. 5. 26 Pareto optimality between capital cost and cost of exergy destruction

Table 5. 9 Values of design variables on points 'A', 'B', and 'C'

Parameter	Range considered for optimization	Point 'A'	Point 'B'	Point 'C'
$\eta_{is,comp}$	86-94%	88.43%	87.83%	87.52%
$\eta_{is,gt}$	88-94%	93.78%	89.78%	89.09%
$\eta_{is,st}$	87-95%	94.96%	92.60%	88.52%
η_{cc}	95-99%	98.99%	98.91%	98.59%
ε_{sh}	90-95%	91.65%	91.97%	92.71%
ΔP_{CC}	1-7%	3.69%	4.31%	4.77%
ε_{cond}	90-95%	94.41%	94.91%	92.57%
η_{boiler}	85-95%	94.98%	94.74%	85.84%
$\eta_{is,pump}$	85-95%	92.87%	92.24%	89.80%

Over the range of TIT, PR, and DOC, Fig. 5. 27 depicts the Pareto optimality between modified exergetic efficiency (to be maximized) and total unavoidable cost per unit of work produced (to be minimized) by the CCPP system. The optimization ranges under consideration for the following operational parameters: TIT (1400K-1600K), PR (11-

14), and DOC (0-18K). The solution space for this optimization is located directly below and to the right of the Pareto front. Points 'A', 'B', and 'C' are considered on the Pareto optimum front to assess the trade-offs among all the given operational parameters. It is worth noting that the variation of PR and DOC has been spanned over the entire specified range, whereas TIT has been optimized within a narrow range of 1548.17K to 1597.71K, which is near the upper limit. At point 'A', the unavoidable cost per unit power output is minimized, while the value of $n_{ex,mod}$ is also minimized. Furthermore, the DOC value is 0.13K, indicating a negligible level of cooling. Moreover, as one progresses from point 'A' to point 'C', the PR also ascends to its highest value in the specified range. The increase in $n_{ex,mod}$ and the unavoidable cost per unit work output at point 'C' has been determined to be 5.05% and 6.02% with respect to point 'A'. Similarly, the calculated rise in both parameters at point 'B' is 2.63% and 2.79%.

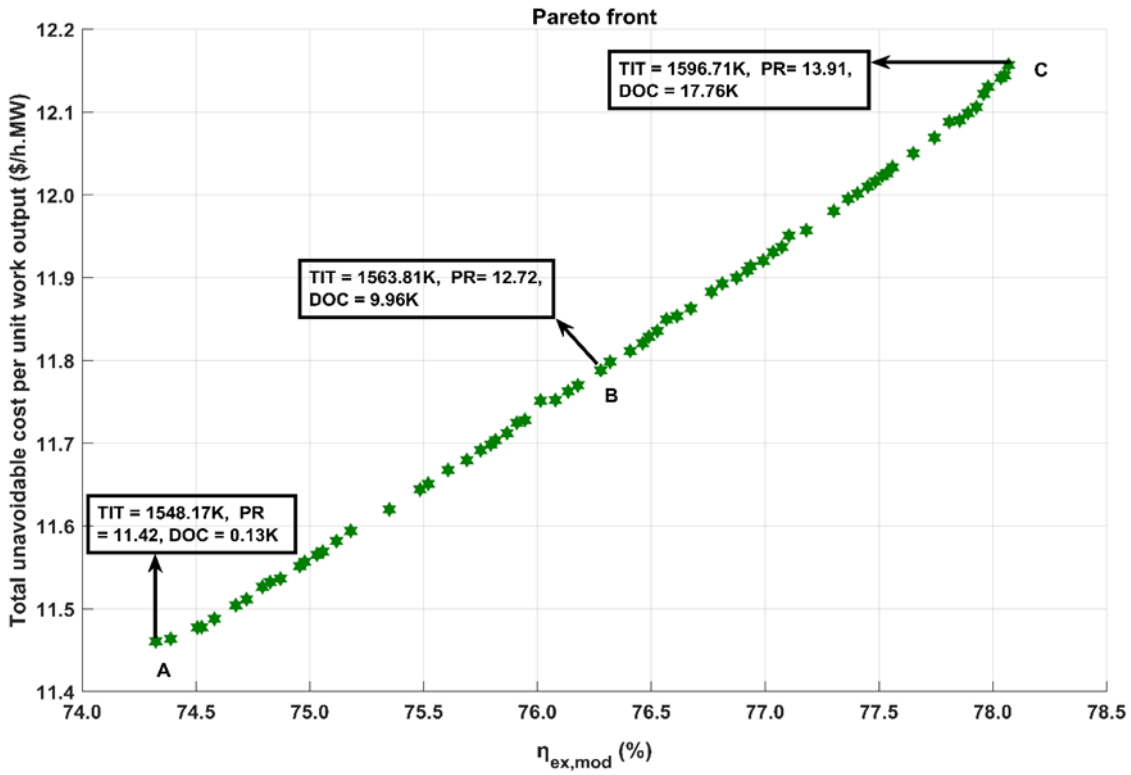

Fig. 5. 27 Pareto front between modified exergetic efficiency and total unavoidable cost per unit work output of CCPP plant

CHAPTER 6

CONCLUSIONS AND SCOPE FOR FUTURE RESEARCH

6.1 Introduction

This chapter demonstrates the concluding remarks perceived from the several analyses conducted on the CCPP system.

6.2 Double-effect VARS-integrated CCPP

The CCPP plant has undergone an analysis involving the implementation of inlet air cooling. This process is achieved through the integration of a water-LiBr based double-effect VARS. The analysis of the system has been conducted using energy, exergy, and exergy-based sustainability indicators. The conclusions that can be inferred from this study are summarized as follows:

- The integration of a double-effect vapour absorption refrigeration system with the CCPP enables an increase in specific work output and thermal efficiency by a maximum of 5.04% and 1.64%, respectively.
- To keep CIT at 288K, the VARS absorbs more heat from the HRSG's exit, as the COP of the VARS reduces with the rise in ambient temperature. Consequently, a reduction in the steam generation rate has been observed in the bottoming cycle.
- The combustion chamber is the dominant contributor to irreversibility, accounting for ≥60.32% of total irreversibility. The CCPP system with inlet air cooling is 1.23%–1.64% more exergetically efficient than a standalone CCPP plant.
- After using inlet air cooling, the fuel depletion ratio and exergetic improvement potential are found to be reduced by a maximum of 1.38% and 3.07%, respectively.
- The environmental effect factor for VARS-integrated CCPP (i.e., CCPPV) has been observed to decrease by 2.92% to 3.40%. Thus, the environmental sustainability index is found to be enhanced.
- In order to maximize the exergetic efficiency and total work output of CCPPV, the suitable degree of inlet air cooling ranges from 8 K to 18 K.

- Improved exergetic efficiency reduces the adverse environmental effect and promotes the system's sustainability as a result of efficient utilization of fuel.

6.3 Component-wise parametric investigation and Multi-objective optimization

An exergy-based parametric investigation is conducted on the CCPP and its components, followed by sensitivity analysis. Subsequently, multi-objective optimization of the simulated model utilizing a genetic algorithm is used to obtain the optimal value of selected parameters. The following are several conclusions outlined from this study:

- Though a drop in compressor inlet temperature improves the energy performance of the gas cycle, doing so with external cooling creates more irreversibilities than when the ambient temperature naturally drops. However, the variation in the exergetic efficiency of the gas cycle is regulated by the pressure ratio and TIT but the degree of cooling.
- High HRSG pressure (≥110 bar) improves the exergetic efficiency of HRSG when associated with increasing TIT. Moreover, the rate of irreversibility generation in HRSG is higher at high ambient temperatures.
- The exergetic efficiency of CCPP during inlet air cooling is equal to that of naturally cooled ambient air for the given range of pressure ratio. Considering exergy destruction, inlet air cooling in CCPP is more advantageous at higher TIT, attributable to a lesser increase in exergy destruction.
- According to the sensitivity analysis, increasing the TIT enhances the exergy of the CCPP as the efficiency defect decreases continuously within the specified range. Moreover, increasing the pressure ratio has an insignificant effect on the gas turbine cycle though it reduces the efficiency defect for CCPP, which relates to the preference for a higher-pressure ratio. This analysis also indicates that increasing the HRSG pressure is accompanied by a decreasing efficiency defect for the CCPP system. Even though the degree of cooling has minimal impact on the individual components of the CCPP, a very slight decrease in efficiency defect has been observed for the CCPP as a whole. The degree of cooling is a decisive factor because it influences the work output.

- Using a genetic algorithm for multi-objective optimization, the optimal values of design variables are determined and recommended. When the specific work output is maximized, the operating parameters DOC, pressure ratio, and TIT are 16.5 K, 12.2, and 1695.4 K, respectively, but the exergy destruction rate increases as well. If the price per unit of electricity is high, operating in this condition could be economically advantageous. But if this is not the case, the optimal compromise can be found by avoiding extremes on each Pareto front. Since there is always a loss in one objective function in return for a gain in another. A similar approach could be used to achieve an equilibrium between exergetic efficiency and destruction rate. Therefore, it can be attained at an intermediate point that tends to minimize the increase in exergy destruction while maximizing the increase in exergy efficiency.

6.4 Advanced Exergoeconomic assessment and Multi-objective optimization

This study involves conducting an exergy analysis on a CCPP system, followed by an exergy costing analysis. The exergy destruction of many components and the overall CCPP system is split into avoidable and unavoidable portions of exergy destruction. This split enables an assessment of the impact of different operational parameters on the corresponding cost factors. Furthermore, the CCPP system has undergone multi-objective optimization using GA, taking into account various objectives such as investment cost, cost of destruction, and thermodynamic performance factors. Additionally, the optimal fronts are acquired in order to evaluate the trade-offs that exist between operational parameters including TIT, PR, and DOC, and various design variables. Several noteworthy conclusions have been derived from the study, which are outlined below:

- The combustion chamber exhibits the largest potential for improvement, as it possesses the lowest exergetic efficiency of 74.77%, followed by the steam turbine with an exergetic efficiency of 79.97%. Similarly, the cost of destruction is highest in the case of the combustion chamber.
- While the sum of the costs of investment and destruction is greatest for the combustion chamber, its capital cost reflects the lowest proportion of the total. The steam condenser constitutes the maximum proportion, followed by the HRSG.

- However, cooling the inlet air increases the total investment cost (which includes both the capital cost and the cost of fuel) as well as the cost rate of work at all degrees of cooling, the latter increases at a significantly higher rate compared to the former. Thus, employing inlet air-cooling is economically beneficial.
- Under the standard settings, avoidable exergy destruction accounts for 25.02% of the overall exergy destruction. Additionally, the HRSG exhibits the highest potential to mitigate irreversibility generation, accounting for 91.53% of its overall irreversibility. In contrast, the combustion chamber has the lowest potential, contributing only 6.94% of its total irreversibility. Nonetheless, the steam turbine accounts for the largest proportion (31.68%) of the CCPP's total avoidable exergy destruction.
- Though, increasing the TIT increases the overall exergy destruction but its unavoidable component increases rapidly as compared to its avoidable component. Furthermore, when the TIT rises, the amount of avoidable exergy destruction in the gas turbine cycle reduces, while the same in the steam cycle increases.
- The total exergy destruction rate is decreased when the PR is increased, with the unavoidable portion experiencing a more substantial decrease than the avoidable portion. As PR rises, the gas turbine cycle's contribution to the total avoidable exergy destruction of CCPP increases, whereas the steam cycle's contribution decreases.
- The avoidable cost of destruction accounts for 35.84% of the total cost of destruction. Moreover, the combustion chamber is accountable for the highest overall unavoidable cost, which includes both capital and destruction costs, amounting to 49.3%. The overall cost rises in association with the increase in TIT. However, the cost of exergy destruction significantly influences this rise, rather than the capital cost.
- When optimizing the exergoeconomics of a CCPP system, the location around an intermediate point on the Pareto optimal front is the projected compromise between the exergetic efficiency and the total cost. The crucial design variables around this location approximated as $\eta_{is,comp}$ = 87.83%, $\eta_{is,gt}$ = 89.78%, $\eta_{is,st}$ = 92.60%, ε_{sh} = 91.97%, ΔP_{CC}= 4.31%, and $\eta_{is,pump}$= 92.24%.

- Based on the advanced exergoeconomic optimization of the CCPP system, the suggested set of optimal solutions approximates the PR of 13, DOC of 10K, and TIT of 1564K when the operational parameters are optimized to achieve improved modified exergetic efficiency and minimized unavoidable cost per unit of power generation.

6.5 Recommendations for future work

The findings of this study have the potential to inform the development of combined cycle power generation systems. These results may provide designers with guidance on how to integrate more energy-efficient systems. The analysis and optimization of CCPP systems featuring various integrations and configurations were the focus of this study. As outlined in the following section, the findings derived from this thesis research also indicate a number of potential avenues for future investigation:

- To enhance the performance of a CCPP system, warm ambient air to the compressor's inlet should be cooled.
- To utilize a waste heat-powered double-effect absorption refrigeration system instead of a mechanical refrigeration system and single effect absorption systems to cool the warm ambient air.
- To perform experimental research with the purpose of augmenting the corpus of knowledge.
- To conduct the analyses under varying climate conditions and inflation rates, while also examining the impact of associated parameters on the optimized values.
- To use advanced exergy end exergoeconomic analysis to understand the effect of the avoidable and unavoidable parts of exergy destruction in each component and optimize based on minimization of the avoidable exergy destruction in each component.
- To integrate the CCPP with several thermal systems like Organic Rankine cycles for better utilization of HRSG exhaust and enhanced power production efficiency.
- In order to achieve trade-offs, it is necessary to employ further optimisation techniques such as particle swarm optimisation and ant colony approaches, followed by a comparison.

References

[1] IEA, "Coal 2023," Paris, 2023. [Online]. Available: https://www.iea.org/reports/coal-2023, License: CC BY 4.0

[2] S. Ladage, M. Blumenberg, D. Franke, A. Bahr, R. Lutz, and S. Schmidt, "On the climate benefit of a coal-to-gas shift in Germany's electric power sector," *Scientific Reports*, vol. 11, no. 1, p. 11453, 2021/06/01 2021, doi: 10.1038/s41598-021-90839-7.

[3] IEA, " Tracking Clean Energy Progress 2023," Paris, 2023. [Online]. Available: https://www.iea.org/energy-system/fossil-fuels/natural-gas

[4] R. Kennedy, "Modern engines and power generators: a practical work on prime movers and the transmission of power steam, electric, water and hot air," *(No Title)*, 1905.

[5] T. Giampaolo, *Gas turbine handbook: principles and practice*. CRC press, 2020.

[6] R. Kurz and K. Brun, "Gas turbine performance," in *Asia Turbomachinery & Pump Symposium. 2016 Proceedings.*, 2016: Turbomachinery Laboratories, Texas A&M Engineering Experiment Station.

[7] J. H. Horlock, "Advanced gas turbine cycles: a brief review of power generation thermodynamics," 2013.

[8] P. P. Walsh and P. Fletcher, *Gas turbine performance*. John Wiley & Sons, 2004.

[9] Y. A. Cengel, M. A. Boles, and M. Kanoğlu, *Thermodynamics: an engineering approach*. McGraw-hill New York, 2011.

[10] A. Chaibakhsh and A. Ghaffari, "Steam turbine model," *Simulation Modelling Practice and Theory*, vol. 16, no. 9, pp. 1145-1162, 2008.

[11] T. Tanuma, *Advances in steam turbines for modern power plants*. Woodhead Publishing, 2022.

[12] A. S. Leyzerovich, *Steam turbines for modern fossil-fuel power plants*. Crc Press, 2021.

[13] P. Breeze, "Chapter 3 - Combined Heat and Power Principles and Technologies," in *Combined Heat and Power*, P. Breeze Ed.: Academic Press, 2018, pp. 21-32.

[14] J. Horlock, *Combined power plants: including combined cycle gas turbined CCGT plants*. Elsevier, 2013.

[15] T. k. Ibrahim *et al.*, "The optimum performance of the combined cycle power plant: A comprehensive review," *Renewable and Sustainable Energy Reviews*, vol. 79, pp. 459-474, 2017/11/01/ 2017, doi: https://doi.org/10.1016/j.rser.2017.05.060.

[16] M. A. Ehyaei, M. Tahani, P. Ahmadi, and M. Esfandiari, "Optimization of fog inlet air cooling system for combined cycle power plants using genetic algorithm," *Applied Thermal Engineering*, vol. 76, pp. 449-461, 2015/02/05/ 2015, doi: https://doi.org/10.1016/j.applthermaleng.2014.11.032.

[17] A. L. Polyzakis, C. Koroneos, and G. Xydis, "Optimum gas turbine cycle for combined cycle power plant," *Energy Conversion and Management*, vol. 49, no. 4, pp. 551-563, 2008/04/01/ 2008, doi: https://doi.org/10.1016/j.enconman.2007.08.002.

[18] M.-N. Dumont and G. Heyen, "Mathematical modelling and design of an advanced once-through heat recovery steam generator," *Computers & chemical engineering*, vol. 28, no. 5, pp. 651-660, 2004.

[19] V. Ganapathy, "Heat-recovery steam generators: Understand the basics," *Chemical engineering progress*, vol. 92, no. 8, pp. 32-45, 1996.

[20] P. Dechamps, "Advanced combined cycle alternatives with the latest gas turbines," 1998.

[21] I. Dincer and C. Zamfirescu, "Renewable-energy-based multigeneration systems," *International Journal of Energy Research*, vol. 36, no. 15, pp. 1403-1415, 2012.

[22] P. Ahmadi, M. A. Rosen, and I. Dincer, "Multi-objective exergy-based optimization of a polygeneration energy system using an evolutionary algorithm," *Energy*, vol. 46, no. 1, pp. 21-31, 2012.

[23] C. Vandervort, D. Leach, D. Walker, and J. Sasser, "Commercialization and Fleet Experience of the 7/9HA Gas Turbine Combined Cycle," in *ASME Turbo Expo 2019: Turbomachinery Technical Conference and Exposition*, 2019, vol. Volume 3: Coal, Biomass, Hydrogen, and Alternative Fuels; Cycle Innovations; Electric Power; Industrial and Cogeneration; Organic Rankine Cycle Power Systems, V003T08A006, doi: 10.1115/gt2019-91594. [Online]. Available: https://doi.org/10.1115/GT2019-91594

[24] J. Kotowicz and M. Brzęczek, "Analysis of increasing efficiency of modern combined cycle power plant: A case study," *Energy*, vol. 153, pp. 90-99, 2018.

[25] S. Adibhatla and S. Kaushik, "Energy, exergy and economic (3E) analysis of integrated solar direct steam generation combined cycle power plant," *Sustainable energy technologies and assessments*, vol. 20, pp. 88-97, 2017.

[26] A. Bejan, *Advanced engineering thermodynamics*. John Wiley & Sons, 2016.

[27] I. Dincer and M. A. Rosen, *Exergy: energy, environment and sustainable development*. Newnes, 2012.

[28] A. Bejan, G. Tsatsaronis, and M. J. Moran, *Thermal design and optimization*. John Wiley & Sons, 1995.

[29] P. Ahmadi and I. Dincer, "Thermodynamic and exergoenvironmental analyses, and multi-objective optimization of a gas turbine power plant," *Applied Thermal Engineering*, vol. 31, no. 14-15, pp. 2529-2540, 2011.

[30] P. Ahmadi, "Modeling, analysis and optimization of integrated energy systems for multigeneration purposes," 2013.

[31] M. A. Rosen and I. Dincer, "Exergoeconomic analysis of power plants operating on various fuels," *Applied Thermal Engineering*, vol. 23, no. 6, pp. 643-658, 2003/04/01/ 2003, doi: https://doi.org/10.1016/S1359-4311(02)00244-2.

[32] A. De Sa and S. Al Zubaidy, "Gas turbine performance at varying ambient temperature," *Applied Thermal Engineering*, vol. 31, no. 14-15, pp. 2735-2739, 2011.

[33] H. O. Egware and O. O. Ighodaro, "Evaluating the effect of ambient air temperature on the exergy sustainability of a 153MW gas turbine power plant," *International Journal of Thermofluids*, vol. 18, p. 100375, 2023/05/01/ 2023, doi: https://doi.org/10.1016/j.ijft.2023.100375.

[34] Y. Zhang, P. Liu, and Z. Li, "Gas turbine off-design behavior modelling and operation windows analysis under different ambient conditions," *Energy*, vol. 262, p. 125348, 2023/01/01/ 2023, doi: https://doi.org/10.1016/j.energy.2022.125348.

[35] R. Hosseini, A. Beshkani, and M. Soltani, "Performance improvement of gas turbines of Fars (Iran) combined cycle power plant by intake air cooling using a media evaporative cooler," *Energy Conversion and Management*, vol. 48, no. 4, pp. 1055-1064, 2007/04/01/ 2007, doi: https://doi.org/10.1016/j.enconman.2006.10.015.

[36] G. Şen *et al.*, "The effect of ambient temperature on electric power generation in natural gas combined cycle power plant—A case study," *Energy Reports*, vol. 4, pp. 682-690, 2018/11/01/ 2018, doi: https://doi.org/10.1016/j.egyr.2018.10.009.

[37] A. González-Díaz, A. M. Alcaráz-Calderón, M. O. González-Díaz, Á. Méndez-Aranda, M. Lucquiaud, and J. M. González-Santaló, "Effect of the ambient conditions on gas turbine combined cycle power plants with post-combustion CO2 capture," *Energy*, vol. 134, pp. 221-233, 2017/09/01/ 2017, doi: https://doi.org/10.1016/j.energy.2017.05.020.

[38] G. Barigozzi, A. Perdichizzi, C. Gritti, and I. Guaiatelli, "Techno-economic analysis of gas turbine inlet air cooling for combined cycle power plant for different climatic conditions," *Applied Thermal Engineering*, vol. 82, pp. 57-67, 2015/05/05/ 2015, doi: https://doi.org/10.1016/j.applthermaleng.2015.02.049.

[39] A. K. Mohapatra and Sanjay, "Exergetic evaluation of gas-turbine based combined cycle system with vapor absorption inlet cooling," *Applied Thermal Engineering*, vol. 136, pp. 431-443, 2018/05/25/ 2018, doi: https://doi.org/10.1016/j.applthermaleng.2018.03.023.

[40] A. Mishra, B. B. Arora, and A. Arora, "Multi-Objective Optimization of an Inlet Air-Cooled Combined Cycle Power Plant," *Journal of Thermal Science and Engineering Applications*, vol. 15, no. 7, 2023, doi: 10.1115/1.4062210.

[41] M. F. Elberry, A. A. Elsayed, M. A. Teamah, A. A. Abdel-Rahman, and A. F. Elsafty, "Performance improvement of power plants using absorption cooling system," *Alexandria Engineering Journal*, vol. 57, no. 4, pp. 2679-2686, 2018/12/01/ 2018, doi: https://doi.org/10.1016/j.aej.2017.10.004.

[42] Y. N. Dabwan, L. Zhang, and G. Pei, "A novel inlet air cooling system to improve the performance of intercooled gas turbine combined cycle power plants in hot regions," *Energy*, vol. 283, p. 129075, 2023/11/15/ 2023, doi: https://doi.org/10.1016/j.energy.2023.129075.

[43] J. F. Espinosa-Cristia *et al.*, "Exergy and environmental analysis of a novel turbine inlet air cooling technique for power augmentation in a CCPP based on waste energy," *Chemosphere*, vol. 338, p. 139402, 2023/10/01/ 2023, doi: https://doi.org/10.1016/j.chemosphere.2023.139402.

[44] M. R. Majdi Yazdi, F. Ommi, M. A. Ehyaei, and M. A. Rosen, "Comparison of gas turbine inlet air cooling systems for several climates in Iran using energy, exergy, economic, and environmental (4E) analyses," *Energy Conversion and Management*, vol. 216, p. 112944, 2020/07/15/ 2020, doi: https://doi.org/10.1016/j.enconman.2020.112944.

[45] S. S. Baakeem, J. Orfi, and H. Al-Ansary, "Performance improvement of gas turbine power plants by utilizing turbine inlet air-cooling (TIAC) technologies in Riyadh, Saudi Arabia," *Applied Thermal Engineering*, vol. 138, pp. 417-432, 2018/06/25/ 2018, doi: https://doi.org/10.1016/j.applthermaleng.2018.04.018.

[46] C. Deng *et al.*, "Air cooling techniques and corresponding impacts on combined cycle power plant (CCPP) performance: A review," *International Journal of Refrigeration*, vol. 120, pp. 161-177, 2020/12/01/ 2020, doi: https://doi.org/10.1016/j.ijrefrig.2020.08.008.

[47] V. Zare, "Performance improvement of biomass-fueled closed cycle gas turbine via compressor inlet cooling using absorption refrigeration; thermoeconomic analysis and multi-objective optimization," *Energy Conversion and Management*, vol. 215, p. 112946, 2020/07/01/ 2020, doi: https://doi.org/10.1016/j.enconman.2020.112946.

[48] E. Matjanov, "Gas turbine efficiency enhancement using absorption chiller. Case study for Tashkent CHP," *Energy*, vol. 192, p. 116625, 2020/02/01/ 2020, doi: https://doi.org/10.1016/j.energy.2019.116625.

[49] O. K. Singh, "Performance enhancement of combined cycle power plant using inlet air cooling by exhaust heat operated ammonia-water absorption refrigeration system," *Applied Energy*, vol. 180, pp. 867-879, 2016/10/15/ 2016, doi: https://doi.org/10.1016/j.apenergy.2016.08.042.

[50] S. Sahu, D. Thatoi, and A. Mohapatra, "Analysis of Techniques to Improve Sustainable Performance of Gas-Turbine Based Combined Cycle System," 2023. [Online]. Available: https://doi.org/10.4271/2023-01-0943.

[51] S. Pourhedayat, E. Hu, and L. Chen, "A comparative and critical review on gas turbine intake air pre-cooling strategies," *Thermal Science and Engineering Progress*, vol. 41, p. 101828, 2023/06/01/ 2023, doi: https://doi.org/10.1016/j.tsep.2023.101828.

[52] T. K. Ibrahim and M. Rahman, "Effect of compression ratio on performance of combined cycle gas turbine," *International journal of energy engineering*, vol. 2, no. 1, pp. 9-14, 2012.

[53] M. R. Almajali and O. A. S. Quran, "Parametric Study on the Performance of Combined Power Plant of Steam and Gas Turbines," *Journal of Thermal Science and Engineering Applications*, vol. 13, no. 5, 2021, doi: 10.1115/1.4049753.

[54] L. T. Shireef and T. K. Ibrahim, "Influence of operating parameters on the performance of combined cycle based on exergy analysis," *Case Studies in Thermal Engineering*, vol. 40, p. 102506, 2022/12/01/ 2022, doi: https://doi.org/10.1016/j.csite.2022.102506.

[55] N. Dev and R. Attri, "Performance analysis of combined cycle power plant," *Frontiers in Energy*, vol. 9, no. 4, pp. 371-386, 2015/12/01 2015, doi: 10.1007/s11708-015-0371-9.

[56] A. Ahmed, K. K. Esmaeil, M. A. Irfan, and F. A. Al-Mufadi, "Design methodology of heat recovery steam generator in electric utility for waste heat recovery," *International Journal of Low-Carbon Technologies*, vol. 13, no. 4, pp. 369-379, 2018, doi: 10.1093/ijlct/cty045.

[57] T.-D. Hoang and D. K. Pawluskiewicz, "The efficiency analysis of different combined cycle power plants based on the impact of selected parameters," *International Journal of Smart Grid and Clean Energy*, vol. 5, no. 2, pp. 77-85, 2016.

[58] O. Mahian, M. R. Mirzaie, A. Kasaeian, and S. H. Mousavi, "Exergy analysis in combined heat and power systems: A review," *Energy Conversion and Management*, vol. 226, p. 113467, 2020/12/15/ 2020, doi: https://doi.org/10.1016/j.enconman.2020.113467.

[59] M. S. Ali, Q. N. Shafique, D. Kumar, S. Kumar, and S. Kumar, "Energy and exergy analysis of a 747-MW combined cycle power plant Guddu," *International Journal of Ambient Energy*, vol. 41, no. 13, pp. 1495-1504, 2020/11/09 2020, doi: 10.1080/01430750.2018.1517680.

[60] M. Babaei Jamnani and A. Kardgar, "Energy-exergy performance assessment with optimization guidance for the components of the 396-MW combined-cycle power plant," *Energy Science & Engineering*, vol. 8, no. 10, pp. 3561-3574, 2020, doi: https://doi.org/10.1002/ese3.764.

[61] A. Z. Sahin, A. Al-Sharafi, B. S. Yilbas, and A. Khaliq, "Overall performance assessment of a combined cycle power plant: An exergo-economic analysis," *Energy Conversion and Management*, vol. 116, pp. 91-100, 2016/05/15/ 2016, doi: https://doi.org/10.1016/j.enconman.2016.02.079.

[62] H. Gu, X. Cui, H. Zhu, F. Si, and Y. Kong, "Multi-objective optimization analysis on gas-steam combined cycle system with exergy theory," *Journal of Cleaner Production*, vol. 278, p. 123939, 2021/01/01/ 2021, doi: https://doi.org/10.1016/j.jclepro.2020.123939.

[63] A. G. Memon, R. A. Memon, K. Harijan, and M. A. Uqaili, "Parametric based thermo-environmental and exergoeconomic analyses of a combined cycle power plant with regression analysis and optimization," *Energy Conversion and Management*, vol. 92, pp. 19-35, 2015/03/01/ 2015, doi: https://doi.org/10.1016/j.enconman.2014.12.033.

[64] A. Ganjehkaviri, M. N. Mohd Jaafar, P. Ahmadi, and H. Barzegaravval, "Modelling and optimization of combined cycle power plant based on exergoeconomic and environmental analyses," *Applied Thermal Engineering*, vol. 67, no. 1, pp. 566-578, 2014/06/01/ 2014, doi: https://doi.org/10.1016/j.applthermaleng.2014.03.018.

[65] A. Bolatturk, A. Coskun, and C. Geredelioglu, "Thermodynamic and exergoeconomic analysis of Çayırhan thermal power plant," *Energy Conversion and Management*, vol. 101, pp. 371-378, 2015/09/01/ 2015, doi: https://doi.org/10.1016/j.enconman.2015.05.072.

[66] M. Awaludin, N. I. Rivai, R. D. Amir, and Nasruddin, "Exergoeconomic Analysis of 21.6 MW Gas Turbine Power Plant in Riau, Indonesia," *Journal of Advanced Research in Fluid Mechanics and Thermal Sciences*, vol. 84, no. 1, pp. 126-134, 07/02 2021, doi: 10.37934/arfmts.84.1.126134.

[67] F. Unal and D. B. Ozkan, "Application of exergoeconomic analysis for power plants," *Thermal Science*, vol. 22, no. 6 Part A, pp. 2653-2666, 2018.

[68] A. G. Kaviri, M. N. M. Jaafar, and T. M. Lazim, "Modeling and multi-objective exergy based optimization of a combined cycle power plant using a genetic algorithm," *Energy Conversion and Management*, vol. 58, pp. 94-103, 2012/06/01/ 2012, doi: https://doi.org/10.1016/j.enconman.2012.01.002.

[69] S. K. Bakhshmand, R. K. Saray, K. Bahlouli, H. Eftekhari, and A. Ebrahimi, "Exergoeconomic analysis and optimization of a triple-pressure combined cycle plant using evolutionary algorithm," *Energy*, vol. 93, pp. 555-567, 2015/12/15/ 2015, doi: https://doi.org/10.1016/j.energy.2015.09.073.

[70] M. A. Javadi, S. Hoseinzadeh, M. Khalaji, and R. Ghasemiasl, "Optimization and analysis of exergy, economic, and environmental of a combined cycle power plant," *Sādhanā,* vol. 44, no. 5, p. 121, 2019/04/23 2019, doi: 10.1007/s12046-019-1102-4.

[71] T. Morosuk and G. Tsatsaronis, "Advanced exergy-based methods used to understand and improve energy-conversion systems," *Energy*, vol. 169, pp. 238-246, 2019/02/15/ 2019, doi: https://doi.org/10.1016/j.energy.2018.11.123.

[72] A. K. Mossi Idrissa and K. Goni Boulama, "Advanced exergy analysis of a combined Brayton/Brayton power cycle," *Energy*, vol. 166, pp. 724-737, 2019/01/01/ 2019, doi: https://doi.org/10.1016/j.energy.2018.10.117.

[73] T. Koroglu and O. S. Sogut, "Conventional and advanced exergy analyses of a marine steam power plant," *Energy*, vol. 163, pp. 392-403, 2018/11/15/ 2018, doi: https://doi.org/10.1016/j.energy.2018.08.119.

[74] D. Barreto, J. Fajardo, G. C. Caballero, and Y. C. Escorcia, "Advanced Exergy and Exergoeconomic Analysis of a Gas Power System with Steam Injection and Air Cooling with a Compression Refrigeration Machine," *Energy Technology*, vol. 9, no. 5, p. 2000993, 2021, doi: https://doi.org/10.1002/ente.202000993.

[75] E. Açıkkalp, H. Caliskan, O. Altuntas, and A. Hepbasli, "Novel combined extended-advanced exergy analysis methodology as a new tool to assess thermodynamic systems," *Energy Conversion and Management*, vol. 236, p. 114019, 2021/05/15/ 2021, doi: https://doi.org/10.1016/j.enconman.2021.114019.

[76] C. Uysal and A. Keçebaş, "Advanced exergoeconomic analysis with using modified productive structure analysis: An application for a real gas turbine cycle," *Energy*, vol. 223, p. 120085, 2021/05/15/ 2021, doi: https://doi.org/10.1016/j.energy.2021.120085.

[77] H. Caglayan and H. Caliskan, "Advanced exergy analyses and optimization of a cogeneration system for ceramic industry by considering endogenous, exogenous, avoidable and unavoidable exergies under different environmental conditions," *Renewable and Sustainable Energy Reviews*, vol. 140, p. 110730, 2021/04/01/ 2021, doi: https://doi.org/10.1016/j.rser.2021.110730.

[78] P. Nag, "Engineering thermodynamics," *New Delhi*, 2008.

[79] T. J. Kotas, *The exergy method of thermal plant analysis*. Paragon Publishing, 2012.

[80] S. Kaushik, V. S. Reddy, and S. Tyagi, "Energy and exergy analyses of thermal power plants: A review," *Renewable and Sustainable energy reviews*, vol. 15, no. 4, pp. 1857-1872, 2011.

[81] P. Ahmadi, I. Dincer, and M. A. Rosen, "Exergy, exergoeconomic and environmental analyses and evolutionary algorithm based multi-objective optimization of combined cycle power plants," *Energy*, vol. 36, no. 10, pp. 5886-5898, 2011/10/01/ 2011, doi: https://doi.org/10.1016/j.energy.2011.08.034.

[82] M. Ameri, P. Ahmadi, and A. Hamidi, "Energy, exergy and exergoeconomic analysis of a steam power plant: A case study," *International Journal of energy research*, vol. 33, no. 5, pp. 499-512, 2009.

[83] P. Nag, *Power plant engineering*. Tata McGraw-Hill New Delhi, India, 2008.

[84] M. Ameri, H. Mokhtari, and M. Mostafavi Sani, "4E analyses and multi-objective optimization of different fuels application for a large combined cycle power plant," *Energy*, vol. 156, pp. 371-386, 2018/08/01/ 2018, doi: https://doi.org/10.1016/j.energy.2018.05.039.

[85] I. Dincer and Y. A. J. E. Cengel, "Energy, entropy and exergy concepts and their roles in thermal engineering," vol. 3, no. 3, pp. 116-149, 2001.

[86] A. Fazeli, S. Zandi, K. Golbaten Mofrad, G. Salehi, M. H. Khoshgoftar Manesh, and R. Shirmohammadi, "Comparative thermoeconomic optimization and exergoenvironmental analysis of an ejector refrigeration cycle integrated with a cogeneration system utilizing waste exhaust heat recovery," *Environmental Progress & Sustainable Energy*, vol. 41, no. 6, p. e13875, 2022, doi: https://doi.org/10.1002/ep.13875.

[87] A. Midilli and I. Dincer, "Development of some exergetic parameters for PEM fuel cells for measuring environmental impact and sustainability," *International Journal of Hydrogen Energy*, vol. 34, no. 9, pp. 3858-3872, 2009/05/01/ 2009, doi: https://doi.org/10.1016/j.ijhydene.2009.02.066.

[88] A. A. Sinha *et al.*, "A novel comparison of energy-exergy, and sustainability analysis for biomass-fueled solid oxide fuel cell integrated gas turbine hybrid configuration," *Energy Conversion and Management*, vol. 283, p. 116923, 2023/05/01/ 2023, doi: https://doi.org/10.1016/j.enconman.2023.116923.

[89] A. A. Sinha, T. Choudhary, M. Z. Ansari, and Sanjay, "Estimation of exergy-based sustainability index and performance evaluation of a novel intercooled hybrid gas turbine system," *International Journal of Hydrogen Energy*, vol. 48, no. 23, pp. 8629-8644, 2023/03/15/ 2023, doi: https://doi.org/10.1016/j.ijhydene.2022.10.260.

[90] G. Tsatsaronis and T. Morosuk, "Exergy-based methods for computer-aided design of energy conversion systems," in *Computer Aided Chemical Engineering*, vol. 29, E. N. Pistikopoulos, M. C. Georgiadis, and A. C. Kokossis Eds.: Elsevier, 2011, pp. 1949-1953.

[91] G. Tsatsaronis and M.-H. Park, "On avoidable and unavoidable exergy destructions and investment costs in thermal systems," *Energy conversion and management*, vol. 43, no. 9-12, pp. 1259-1270, 2002.

[92] S. S. Rao, *Engineering optimization: theory and practice*. John Wiley & Sons, 2019.

[93] U. M. Diwekar, *Introduction to applied optimization*. Springer Nature, 2020.

[94] A. A. Bazmi and G. Zahedi, "Sustainable energy systems: Role of optimization modeling techniques in power generation and supply—A review," *Renewable and sustainable energy reviews,* vol. 15, no. 8, pp. 3480-3500, 2011.

[95] Z. N. Pintarič and Z. Kravanja, "Suitable Process Modelling for Proper Multi-Objective Optimization of Process Flow Sheets," in *Computer Aided Chemical Engineering*, vol. 33, J. J. Klemeš, P. S. Varbanov, and P. Y. Liew Eds.: Elsevier, 2014, pp. 1387-1392.

[96] W. Forst and D. Hoffmann, *Optimization—theory and practice*. Springer Science & Business Media, 2010.

[97] J. Nocedal and S. J. Wright, *Numerical optimization*. Springer, 1999.

[98] K. Deb, "Evolutionary algorithms for multi-criterion optimization in engineering design," *Evolutionary algorithms in engineering and computer science,* vol. 2, pp. 135-161, 1999.

[99] A. Ghaffarizadeh, K. Ahmadi, and N. S. Flann, "Sorting unsigned permutations by reversals using multi-objective evolutionary algorithms with variable size individuals," in *2011 IEEE Congress of Evolutionary Computation (CEC)*, 2011: IEEE, pp. 292-295.

[100] D. E. Goldberg, "Optimization, and machine learning," *Genetic algorithms in Search,* 1989.

[101] K. Deb, K. Sindhya, and J. Hakanen, "Multi-objective optimization," in *Decision sciences*: CRC Press, 2016, pp. 161-200.

[102] N. Srinivas and K. Deb, "Muiltiobjective optimization using nondominated sorting in genetic algorithms," *Evolutionary computation,* vol. 2, no. 3, pp. 221-248, 1994.

[103] T. Korakianitis and D. Wilson, "Models for predicting the performance of Brayton-cycle engines," 1994.

[104] A. A. Sinha, Sanjay, M. Z. Ansari, A. K. Shukla, and T. Choudhary, "Comprehensive review on integration strategies and numerical modeling of fuel cell hybrid system for power & heat production," *International Journal of Hydrogen Energy,* vol. 48, no. 86, pp. 33669-33704, 2023/10/22/ 2023, doi: https://doi.org/10.1016/j.ijhydene.2023.05.097.

[105] Y. S. Touloukian, Tadash, M. *Thermo-physical Properties of Matter, Vol. 6*.

[106] M. Sharma and O. Singh, "Exergy analysis of the dual pressure HRSG for varying physical parameters," *Applied Thermal Engineering,* vol. 114, pp. 993-1001, 2017.

[107] S. Naemi, M. Saffar-Avval, S. B. Kalhori, and Z. Mansoori, "Optimum design of dual pressure heat recovery steam generator using non-dimensional parameters based on thermodynamic and thermoeconomic approaches," *Applied Thermal Engineering,* vol. 52, no. 2, pp. 371-384, 2013.

[108] S. Kumar and O. Singh, "Performance Evaluation of Gas-Steam Combined Cycle Having Transpiration Cooled Gas Turbine," *Distributed Generation & Alternative Energy Journal,* vol. 28, no. 2, pp. 43-60, 2013/04/01 2013, doi: 10.1080/21563306.2013.10677550.

[109] A. K. Shukla and O. Singh, "Thermodynamic investigation of parameters affecting the execution of steam injected cooled gas turbine based combined cycle power plant with vapor absorption inlet air cooling," *Applied Thermal Engineering*, vol. 122, pp. 380-388, 2017/07/25/ 2017, doi: https://doi.org/10.1016/j.applthermaleng.2017.05.034.

[110] R. Gomri and R. Hakimi, "Second law analysis of double effect vapour absorption cooler system," *Energy Conversion and Management*, vol. 49, no. 11, pp. 3343-3348, 2008/11/01/ 2008, doi: https://doi.org/10.1016/j.enconman.2007.09.033.

[111] J. Pátek and J. Klomfar, "A computationally effective formulation of the thermodynamic properties of LiBr–H2O solutions from 273 to 500K over full composition range," *International Journal of Refrigeration*, vol. 29, no. 4, pp. 566-578, 2006/06/01/ 2006, doi: https://doi.org/10.1016/j.ijrefrig.2005.10.007.

[112] F. J. J. P. L. Lansing, California Institute of Technology, Pasadena, CA, Deep Space Network Progress Report, "Computer modeling of a single-stage lithium bromide/water absorption refrigeration unit," vol. 42, pp. 247-257, 1976.

[113] S. I.-u.-H. Gilani and M. S. M. S. Ahmed, "Solution Crystallization Detection for Double-effect LiBr-H2O Steam Absorption Chiller," *Energy Procedia*, vol. 75, pp. 1522-1528, 2015/08/01/ 2015, doi: https://doi.org/10.1016/j.egypro.2015.07.304.

[114] G. Tsatsaronis, L. Lin, and J. Pisa, "Exergy costing in exergoeconomics," 1993.

[115] P. Roosen, S. Uhlenbruck, and K. Lucas, "Pareto optimization of a combined cycle power system as a decision support tool for trading off investment vs. operating costs," *International Journal of Thermal Sciences*, vol. 42, no. 6, pp. 553-560, 2003.

[116] E. Açıkkalp, H. Aras, and A. Hepbasli, "Advanced exergy analysis of an electricity-generating facility using natural gas," *Energy conversion and management*, vol. 82, pp. 146-153, 2014.

[117] F. Petrakopoulou, G. Tsatsaronis, T. Morosuk, and A. Carassai, "Conventional and advanced exergetic analyses applied to a combined cycle power plant," *Energy*, vol. 41, no. 1, pp. 146-152, 2012.

[118] N. Hasan, J. N. Rai, and B. B. Arora, "Optimization of CCGT power plant and performance analysis using MATLAB/Simulink with actual operational data," *SpringerPlus*, vol. 3, no. 1, p. 275, 2014/06/01 2014, doi: 10.1186/2193-1801-3-275.

[119] H. Yin, M. Qu, and D. H. Archer, "Model based experimental performance analysis of a microscale LiBr–H2O steam-driven double-effect absorption Chiller," *Applied Thermal Engineering*, vol. 30, no. 13, pp. 1741-1750, 2010/09/01/ 2010, doi: https://doi.org/10.1016/j.applthermaleng.2010.04.004.

LIST OF PUBLICATIONS

1. Mishra, A., Arora, B. B., and Arora, A. "Multi-Objective Optimization of an Inlet Air-Cooled Combined Cycle Power Plant." ASME. J. Thermal Sci. Eng. Appl. July 2023; 15(7): 071005. (SCIE)
2. Mishra, A., Arora, B.B. & Arora, A. "Exergy-based sustainability analysis of combined cycle gas turbine plant integrated with double-effect vapor absorption refrigeration system." J Braz. Soc. Mech. Sci. Eng. 46, 20 (2024). (SCIE)
3. Mishra, A., Arora, B.B. & Arora, A. "Exergoeconomic analysis of a Combined cycle Gas Turbine plant based on several operational parameters." Recent Advances in Mechanical Engineering, Volume 1, ICMech-REC 2023, Lecture Notes in Mechanical Engineering, Springer, Singapore (SCOPUS)

LIST OF INTERNATIONAL CONFERENCES

1. Mishra, A., Arora, B. B., and Arora, A. "Advanced exergy analysis-based performance assessment of a combined cycle gas turbine plant", ICERTSD – 2023, IIEST Shibpur, India, 27-28th April, 2023.
2. Mishra, A., Arora, B. B., and Arora, A. "Exergoeconomic analysis of a Combined cycle Gas Turbine plant based on several operational parameters", (ICMech- REC - 2023), NIT Warangal, India, 23-25th June, 2023.

AUTHOR'S BIODATA

Ashutosh Mishra, a graduate in Mechanical Engineering from Uttar Pradesh Technical University and an M. Tech holder in Thermal Engineering from Delhi Technological University (2017), is dedicated to advancing sustainable energy systems. With a focus on energy conversion, environmental sustainability, optimization, and clean energy production, his research addresses global energy challenges through innovative and interdisciplinary approaches. He authored several prestigious SCIE-indexed publications. For which he has also received the Research Excellence Award. He has also presented his work at several International conferences. Known for his perseverance and collaborative spirit, his work reflects a commitment to aligning energy advancements with environmental conservation.